DOCUMENT RESUME

ED 094 761 IR 000 961

AUTHOR	Risch, Craig O.; And Others
TITLE	Design of a 12 Channel FM Microwave Receiver.
INSTITUTION	Washington Univ., St. Louis, Mo. Center for Development Technology.
SPONS AGENCY	National Aeronautics and Space Administration, Washington, D.C.
REPORT NO	R-T-74-2
PUB DATE	Jul 74
NOTE	166p.
EDRS PRICE	MF-$0.75 HC-$7.80 PLUS POSTAGE
DESCRIPTORS	Branching; *Broadcast Reception Equipment; Color Television; *Communication Satellites; *Electronic Equipment; Equipment Utilization; *Television; Video Equipment
IDENTIFIERS	Ground Station Receivers; Program Application Communication Satellites Educa; Washington University

ABSTRACT

The design, fabrication, and performance of elements of a low cost FM microwave satellite ground station receiver are described. It is capable of accepting 12 contiguous color television equivalent bandwidth channels in the 11.72 to 12.2 GHz band. Each channel is 40 MHz wide and incorporates a 4MHz guard band. The modulation format is wideband FM, and the channels are frequency division multiplexed. Twelve independent CATV compatible baseband outputs are provided. The overall system specifications are first discussed, then consideration is given to the receiver subsystems and the signal branching network. (Author/WCM)

ED 094761

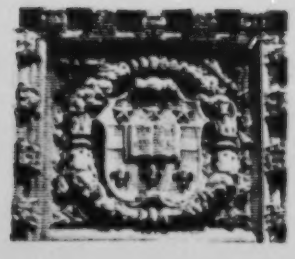

WASHINGTON UNIVERSITY

CENTER FOR DEVELOPMENT TECHNOLOGY
COMMUNICATIONS GROUP

REPORT No. R(T)-74/2 JULY, 1974

DESIGN OF A 12 CHANNEL FM MICROWAVE RECEIVER

CRAIG O. RISCH
FRED J. ROSENBAUM
ROBERT O. GREGORY

IR 000 961

WASHINGTON UNIVERSITY / ST. LOUIS / MISSOURI 63130

ED 094761

PROGRAM ON APPLICATION OF COMMUNICATIONS SATELLITES
TO EDUCATIONAL DEVELOPMENT

Center for Development Technology
(Communications Group)

Washington University

Report No. R(T)-74/2

July, 1974

DESIGN OF A 12 CHANNEL FM MICROWAVE RECEIVER

CRAIG O. RISCH

FRED J. ROSENBAUM

ROBERT O. GREGORY

U.S. DEPARTMENT OF HEALTH,
EDUCATION & WELFARE
NATIONAL INSTITUTE OF
EDUCATION
THIS DOCUMENT HAS BEEN REPRODUCED EXACTLY AS RECEIVED FROM THE PERSON OR ORGANIZATION ORIGINATING IT. POINTS OF VIEW OR OPINIONS STATED DO NOT NECESSARILY REPRESENT OFFICIAL NATIONAL INSTITUTE OF EDUCATION POSITION OR POLICY

This study was supported by the National Aeronautics and Space Administration under Grant No. NGR-26-008-054. The views expressed in this memorandum are those of the author and do not necessarily represent those of the Center for Development Technology, Washington University, or the sponsoring agency.

DESIGN OF A 12 CHANNEL FM MICROWAVE RECEIVER

Abstract

The design, fabrication, and performance of elements of a low cost FM microwave satellite ground station receiver is described. It is capable of accepting 12 contiguous color television equivalent bandwidth channels in the 11.72 to 12.2 GHz band. Each channel is 40 MHz wide and incorporates a 4 MHz guard band. The modulation format is wideband FM and the channels are frequency division multiplexed. Twelve independent CATV compatible baseband outputs are provided. The overall system specifications are first discussed, then consideration is given to the receiver subsystems and the signal branching network.

TABLE OF CONTENTS

No.		Page
1.	Introduction	1
	1.1 Background	1
	1.2 Previous Results	3
	1.3 System Considerations	4
	1.4 Scope	11
2.	Mixer, IF Amplifier and Band-Pass Filters	13
	2.1 Introduction	13
	2.2 Pre-Amplifier Design	14
	2.3 Power Amplifier Design	18
	2.4 First Band-Pass Filter	19
	2.4.1 Design and Analysis	19
	2.4.2 Performance	21
	2.5 Second Band-Pass Filter	21
	2.5.1 Design and Analysis	21
	2.5.2 Performance	22
	2.6 Mixer Description	25
	2.7 Overall Performance of the IF Amplifier	25
3.	Demodulator and Output Amplifier	36
	3.1 Introduction	36
	3.2 Wideband Limiter	36
	3.2.1 Design and Analysis	36
	3.2.2 Single Stage Prototype	40
	3.2.3 Construction of a Two Stage Limiter	42
	3.2.4 Performance	44
	3.3 Low-Pass Filter	44
	3.3.1 Specifications	44
	3.3.2 Design and Analysis	45
	3.3.3 Performance	49

TABLE OF CONTENTS
(continued)

No.		Page
3.4	Wideband Discriminator	54
3.4.1	Design and Analysis	54
3.4.2	Performance	60
3.4.3	Performance of 300Ω Discriminator	60
3.5	Overall Performance	61
3.6	Base Band Output Amplifier	68
3.6.1	Design and Analysis	68
3.6.2	Performance	71
4.	Branching Network	76
4.1	Introduction	76
4.2	Channel Dropping Filter Design and Theoretical Performance	77
4.3	Prototype Filter Performance	88
4.4	Manifold Design and Prototype Performance	89
5.	Conclusions	99
5.1	Principal Results	99
5.2	Future Work	101
6.	Acknowledgement	108
7.	Appendices	109
7.1	Filter Design	110
7.1.1	Introduction	110
7.1.2	Prototype Equations and Low-Pass Design	110
7.1.3	Band-Pass Filter Design	119
7.1.4	High-Pass Filter Design	127
7.2	Voltage Controlled Oscillator	136
7.3	Lumped Element Quarter Wavelength Transformer	141
7.4	Fourier Analysis of a Trapezoidal Wave	143
7.5	Measurement Techniques	146

TABLE OF CONTENTS
(continued)

No.		Page
7.5.1	Measurement of Limiter Harmonics.	146
7.5.2	Measurement of Inductance with Hewlett-Packard Automatic Network Analyzer.	146
7.6	Determination of Parallel Line $\lambda/4$ Coupled Filter Dimensions Using a Fibonacci Search.	149
8.	Bibliography.	153

LIST OF TABLES

No.		Page
1.1	Satellite Ground-Terminal Characteristics	8
2.1	Element Values for First Band-Pass Filter	20
2.2	Element Values for Second Band-Pass Filter	24
2.3	Mixer Performance Specifications	26
3.1	Power Levels of Harmonics in Limiter Output	47
4.1	Dimensions of Parallel Strips Normalized to B = 1/8 inch	82
4.2	Line Lengths for Manifold	95
5.1	Performance Specifications of Baseband Channel	104
5.2	Cost Estimate for One Baseband Channel	105
5.3	Estimated Cost of the Branching Network	106
5.4	Estimated Delivered Cost of the Entire Ground Station	107

LIST OF FIGURES

No.		Page
1.1	Constitution of the Baseband Signal	6
1.2	Block Diagram of 12 Channel Receiver.	9
2.1	Schematic Diagram of MC1590G Package.	16
2.2	Schematic Diagram of Mixer and IF Amplifier	17
2.3	Comparison of Amplitude Responses of Branching Network, First BPF, and Second BPF and Resultant Response.	23
2.4	Basic Mixer Schematic	27
2.5	Isolation Between LO and RF Port in dB as a Function of Frequency	28
2.6	Return Loss of Mixer Input as a Function of Frequency . . .	29
2.7	Input Impedance to Mixer Over the Frequency Range of 1.0 to 1.4 GHz Normalized to 50Ω.	30
2.8	IF Amplifier Output Power as a Function of Input Power. . .	32
2.9	Intermodulation Product Levels Relative to f_{mb} as a Function of Frequency for Different Levels of f_{int} and f_{mb}	33
2.10	IF Amplifier Frequency Response and Response of Diode Detector.	34
3.1	Basic Limiter Configuration	37
3.2	Limiter Input (Dotted Line) and Output (Solid Line) as a Function of θ for One Period.	39
3.3	Change in Output Power as a Function of the Change in Input Power for Single Stage Limiter.	41
3.4	Limiter Amplifier Schematic	43
3.5	Change in Output Power as a Function of the Change in Input Power for a Two-Stage Limiter	46
3.6	Photograph of Limiter Output at 80 MHz.	48
3.7	Experimental and Theoretical Responses for Limiter Low-Pass Filter.	51

LIST OF FIGURES
(continued)

No.		Page
3.8	Output Power as a Function of Input Power for Three Different Frequencies	52
3.9	Frequency Response of Limiter	53
3.10	Basic Discriminator Configuration	55
3.11	Open Circuit and Short Circuit Transmission Line Equivalent Circuits.	57
3.12	Normalized Discriminator Output as a Function of Input Frequency	58
3.13	Prototype Discriminator Output as a Function of Input Frequency	62
3.14	Voltage Output as a Function of Input Frequency for the Open and Short Circuit Line Equivalents	63
3.15	System Response at the Output of the Limiter-Filter	65
3.16	System Response After Tuning Limiter-Filter	66
3.17	Discriminator Output as a Function of Frequency When Connected to Limiter Output	67
3.18	Discriminator Output for Various Input Levels	69
3.19	Output Amplifier Schematic.	70
3.20	Overall Schematic of Demodulator and Output Amplifier	72
3.21	Output of Final Amplifier as a Function of Input Frequency Deviation	74
3.22	Final Amplifier Output Voltage as a Function of Input Frequency Deviation for Differing Input Power Levels.	75
4.1	Power Levels and Frequencies of LO Relative to the Signal Channels, Dotted Lines are LO Power Level Before Isolation, Solid Lines Indicate Level After Isolation	78

LIST OF FIGURES
(continued)

No.		Page
4.2	Five Resonator Parallel Coupled Resonator Filter.	80
4.3	Filter Amplifier Schematic.	83
4.4	Filter Amplifier Gain and Reverse Isolation Over the Range of 1.0 to 1.4 GHz	84
4.5	Input and Output Return Loss Swept Over the Range of 1.0 - 1.4 GHz with Upper Trace Showing 0 dB Reference . . .	85
4.6	Forward Isolation:Frequency Swept from 1.0 to 1.4 GHz with Top Trace or 0 dB Reference and Vertical Scale of 2 dB/cm.	86
4.7	Theoretical Prototype Channel Dropping Filter Performance	87
4.8	Experimental and Theoretical Responses for Prototype Channel Dropping Filter	90
4.9	Branching Network	93
4.10	Branching Network Insertion Loss (Solid Line) and Return Loss (Dotted Line)as a function of Input Frequency	97
4.11	Passband Response of a Typical Filter	98
5.1	Baseband Channel Package.	103
Appendices:		
7.1.1	Focal Program for Determining the Number of Elements in a Low-Pass Filter.	112
7.1.2	Low-Pass Filter Configurations	113
7.1.3	Low-Pass Filter Frequency Response	114
7.1.4	FOCAL Program for Generating the g Values and Determining the Values of the Elements in a Low-Pass Filter.	117
7.1.5	Print Out of Low-Pass Filter Design Program.	118
7.1.6	Low-Pass Limiter Filter.	120
7.1.7	Frequency Response of a Band-Pass Filter	121

LIST OF FIGURES
(continued)

No.		Page
7.1.8	FOCAL Program to Determine the Number of Elements for a Band-Pass Filter.	122
7.1.9	Possible Band-Pass Filter Configurations.	123
7.1.10	Band-Pass Design Program.	126
7.1.11	Print Out for Band-Pass Design Program.	128
7.1.12	Input Band-Pass Filter.	129
7.1.13	Frequency Response of a High-Pass Filter.	131
7.1.14	FOCAL Program for Determining the Number of Elements in a High-Pass Filter.	132
7.1.15	High-Pass Design Program.	133
7.1.16	Possible High Pass Configurations	134
7.1.17	Print Out of High-Pass Design Program	135
7.1.18	High-Pass Filter Design Example	137
7.2.1	Voltage Controlled Oscillator	138
7.2.2	VCO Output Frequency as a Function of Input Voltage to the Varactor.	139
7.2.3	VCO Output Power as a Function of Output Frequency.	140
7.3.1	$\lambda/4$ Transmission Line and Equivalent Circuit.	142
7.3.2	Magnitude of Reflection Coefficient as a Function of Frequency for $\lambda/4$ Transformer	144
7.5.1	Experimental Set-Up Used to Measure Harmonic Content of the Limiter	147
7.5.2	Set-Up for Inductance Measurement	148
7.6.1	Part I of Search Program.	151
7.6.2	Part II of Search Program	152

DESIGN OF A 12 CHANNEL FM MICROWAVE RECEIVER

1 INTRODUCTION

1.1 BACKGROUND

The communication satellite is being seen as an evermore viable means of providing an educational communication system. (1)* If a multi-carrier satellite transponder having a large number of TV-equivalent bandwidth channels were used in conjunction with a CATV system it would be possible to economically disseminate large amounts of information to many subscribers. In order to implement such a system with many points of reception, low cost terminal equipment is required. Newman et. al. (2) have suggested the use of multi-channel, multicarrier ground station receivers to provide the necessary satellite to CATV interconnection using one RF carrier per channel.

Although it is intended for use in an educational satellite network, low cost ground receivers such as the one described here could be used for commercial purposes as well.

This report is concerned with the implementation of a low cost microwave receiver. This receiver is designed to accept 12 contiguous

*The numbers in parentheses in the text indicate references in the Bibliography.

color television equivalent bandwidth channels in the 11.72 to 12.2 GHz band using a wideband FM format and frequency division multiplexing (FDM) of the channels. Each individual channel is to have a usable bandwidth of 36 MHz and a guard band of 4 MHz. The receiver provides an output for each channel compatible with standard video signals suitable for use with a CATV headend.

As it is our intention that these receivers find widespread usage, both in education and commercial systems, a low cost (less than $10,000) is a major design consideration. For example, a double conversion scheme is used which allows construction of the channel dropping filters at L-band, utilizing stripline techniques which are more economical than the use of wave guide or coaxial filters as required at higher frequencies. Beyond the channel separation filters, i.e. branching network, the design of each channel is identical. Straightforward, yet innovative designs were attempted which use standard components. Identical components have been used as much as possible to obtain economies of scale. The use of tunable elements has been avoided wherever possible to eliminate the need for complicated testing and alignment procedures.

The main emphasis of this report will be on the design of the branching network and baseband channels along with some discussion on the front-end design of the receiver. Theoretical performance characteristics based on overall system requirements are determined for each subsystem. The performance of each subsystem is evaluated to see how well the specifications are met. In order to lend some perspective to the work reported here let us first examine some other work done in the area of ground station receiver design.

1.2 PREVIOUS RESULTS

General Electric has reported a single conversion, single channel receiver (3) (4). Use of the appropriate converter at the front end allows for either 2.5 GHz or 12 GHz recention. The converter feeds a 7 stage transistor IF amplifier having a center frequency of 120 MHz with a bandwidth of 40 MHz and an overall gain of 45 dB. Following the IF amplifier is the limiter which is a single stage differential amplifier with a low-pass filter at the output. The discriminator uses open and short circuited $\lambda/8$ transmission lines with S-band Schottky diodes as the detectors. The baseband amplifier is DC coupled to the discriminator to produce the necessary video output of 1Vpp into 75Ω.

Lusignan, et. al. (5) report another single channel, single conversion system for use at 2.62 GHz. The front-end down converter for this system provides an IF of 120 MHz. The IF Amplifier has a 25.2 MHz bandwidth and a gain of 60 dB. It is implemented by a cascade of four transistor stages with an FET input. All stages are transformer coupled. The limiter, which is coupled to the output of the IF Amplifier through a 3-pole filter, is merely a two stage differential amplifier running in saturation. The limiter has a 5 dB dynamic range. The discriminator which is directly coupled to the limiter uses a single $3\lambda/8$ short circuited transmission line and one detector diode. The resulting output suffers at most a 2% deviation from linearity over a 25 MHz bandwidth centered at 120 MHz.

Another single channel, single conversion system has been reported by NASA (6). The front-end converter is designed to work

at 845 to 875 MHz and to provide a 70 MHz IF. The IF amplifier consists of four cascaded transistor stages capacitively coupled. It has a voltage gain of 75 dB, provides a nominal output of 0 dBm into 75Ω and must accept -60 to -30 dBm, 75Ω inputs. The dynamic range is 20 dB and the 1 dB bandwidth is 30 MHz. The limiter is a three stage transistor amplifier employing signal biased back-to-back diodes at the output of the last two stages. Its operating input level is 0 dBm at 75Ω. The dynamic range is 15 dB and the 0.5 dB bandwidth is 30 MHz. Two transistors turn the single ended output of the limiter into a balanced output which drives a Foster-Seely type discriminator which has an output linearity of 3% over the 30 MHz band. A three stage FET amplifier provides a standard video signal of 1 Vpp into 75Ω.

RCA (7) has reported the design of a 24 channel spaceborne transponder for operation at 5925 to 6425 MHz in the receiver mode and 3700 to 4200 MHz in the transmit mode. The bandwidth of each of the baseband channels is 36 MHz.

1.3 SYSTEM CONSIDERATIONS

Based on a report of the results of the 1971 World Administrative Radio Conference (8) and the existing usage of the various services discussed in that report, operation in the 12 GHz region is indicated for television broadcasting from satellites. The receiver we have designed is to be used in a multicarrier system where individual TV channels are Frequency Division Multiplexed (FDM) together in a 11.72 - 12.20 GHz band. Such a system has several important advantages over a single carrier system. First, it allows individual TV channels to originate simultaneously from different

programming centers. It also permits channelization in the satellite transponder design so that one can limit certain failures in the transponder to individual channels. The need for tight phase and amplitude requirements over broad bandwidth in the various subsystems of the transponder and earth terminal is reduced by a multicarrier approach.

The constitution of the baseband signal is shown in Figure 1.1. In addition to the standard video signal, the system must handle two 15 KHz aural signals. The two aural channels are handled by FM modulating two subcarriers, one at 4.7 MHz and the other at 5.8 MHz, and then frequency division multiplexing them with the video baseband.

In any satellite to earth communication system there is a optimum balance between the amount of Effective Radiated Power (ERP) produced by the satellite and the needed sensitivity or "Figure of Merit (G/T)" for the earth station receiver. In general, G/T is defined as the ratio of antenna gain to overall system noise temperature and is expressed in dB/°K. The optimum G/T which produces the best overall system economy depends on the user, system requirements, launch vehicle constraints, etc. Computer aided satellite system analysis and utilization studies carried out by Stagl et. al. (9) at Washington University indicate 18-22 dB/°K to be the optimum range for G/T for a community reception type satellite television broadcast system in the U.S. for near term educational program delivery via interconnection of institutional and commercial CATV headends. Based on satellite television broadcasting system optimization studies, (9) (10) we have opted for G/T of 17.5 dB/°K for our receiver. This G/T is to be achieved with a 10 ft. parabolic antenna which has 49 dB gain at

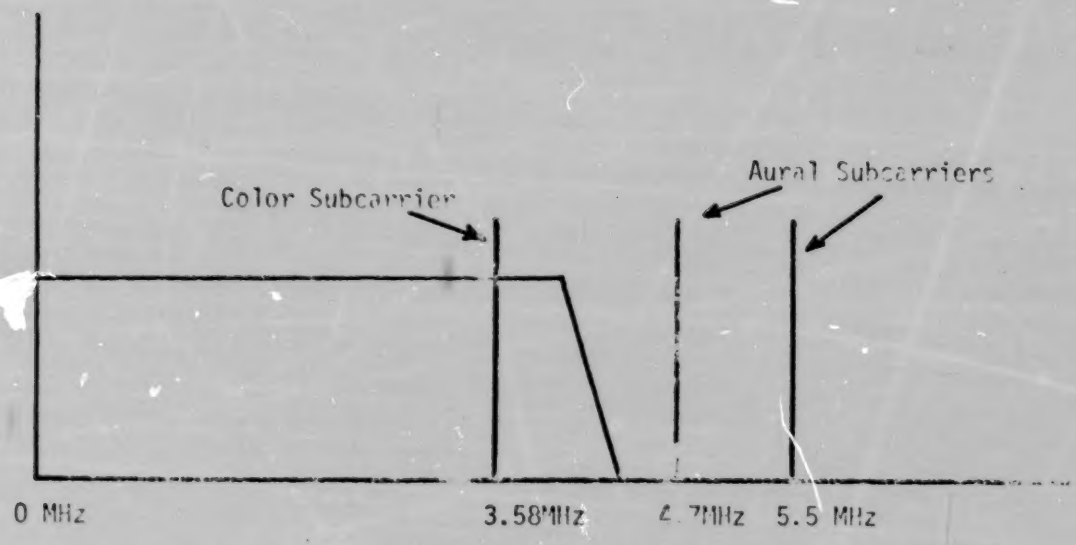

Fig. 1.1 - Constitution of the Baseband Signal

12 GHz and a receiving system noise temperature of 1400°K of which 200°K is attributed to antenna noise and the remainder to the receiver. This 10 ft. disk should have limited steering capabilities and a 3 dB beamwidth of .55° - .60° which is adequate to accomodate wind caused deviations from the set axis and the satellite movements provided that the spacecraft has a ±0.' East-West as well as North-South station keeping ability.

With an ERP of 56 dBW per TV channel and a 36 MHz RF channel bandwidth, the proposed terminal with a G/T of 17.5 dB/°K will be able to deliver a peak video signal power to weighted r.m.s. noise ratio $[S/N]_{p,w}$ of 53 dB for 99.8 percent of time in a region with rain statistics similar to that of New Jersey. (2) With the satellite uplink, downlink and the farthest route in the cable-television distribution plant peak weighted signal to noise ratio $[S/N]_{p.w}$ being 67 dB, 53 dB and 53 dB respectively, the user served by the farthest drop cable facility would have the potential of receiving a $[S/N]_{p,w}$ of 49 dB or a TV picture equivalent to TASO Grade I. (2)

The desired characteristics of the ground terminal are summarized in Table 1.1 and the resulting receiver block diagram is given in Figure 1.2. The expected input power level is -74 dBm per channel. Allowance is made for a 15 dB fade margin. In order to eliminate the need for a balanced mixer configuration at the input and to more easily facilitate separation of the channels, we have opted for a double conversion scheme.

The front-end down converter which frequency shifts the information from 11.72 - 12.2 GHz to 1.02 - 1.5 GHz was built by Westinghouse

TABLE 1.1

SATELLITE GROUND-TERMINAL CHARACTERISTICS

Ground Terminal Type	Receive Only
Antenna	10-ft. parabolic dish Limited manual steering
Antenna Gain	48.98 dB at 12-GHz 54 percent efficiency.
Antenna Polarization	Linear
Antenna Noise Temperature [T_A]	200°K (Maximum)
Low Noise Receiver	Double Conversion - First IF at 1 GHz and the second at 80 MHz Channel Separation after 1st IF.
Receiver Noise Temperature [T_R]	1,200°K (Maximum)
Receiver Bandwidth	11.700 - 12.200 GHz
Individual RF Carrier Bandwidth (Per TV Channel)	36 MHz
Modulation	Frequency Modulation
Demodulator	Discriminator (12 dB threshold)
Receiving System Noise Temperature [$T_S=T_A+T_R$]	1,400°K
Receiving System [G/T] [Antenna Gain to System Noise Temperature Ratio]	17.52 dB/°K

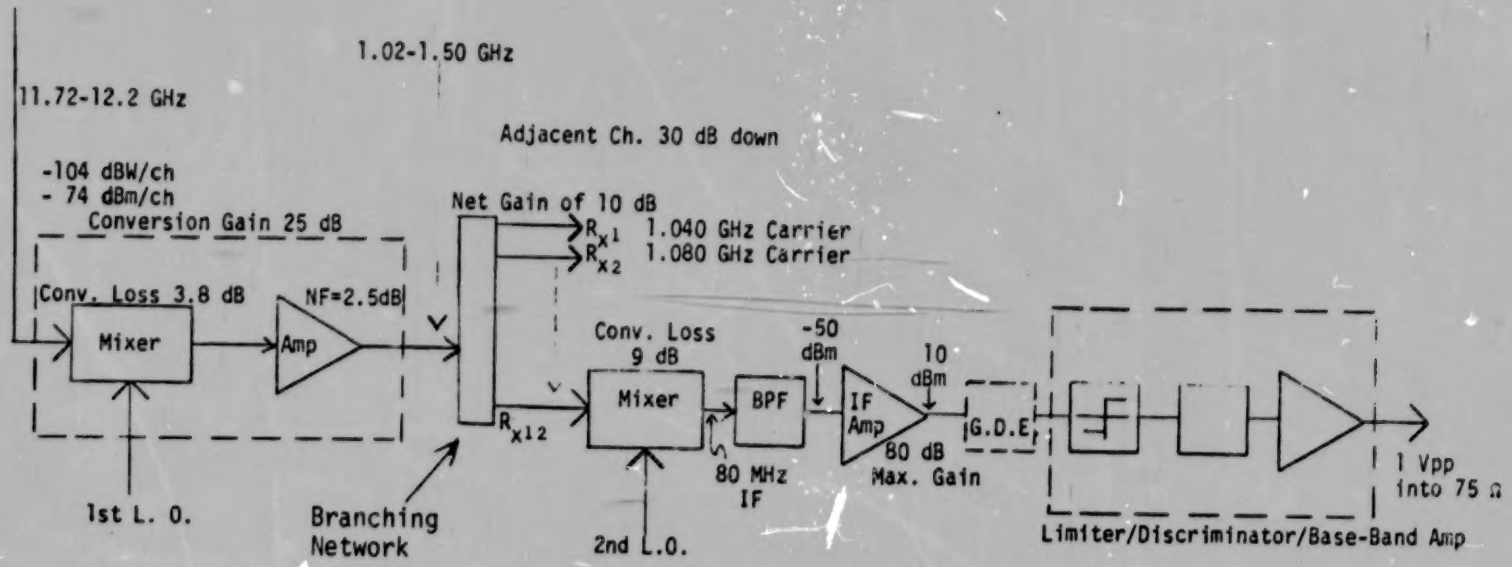

Figure 1.2 Block Diagram of 12 Channel Receiver

(11). It consists of a single ended (single diode) mixer employing image and sum frequency enhancement techniques to achieve a midband insertion loss of 3.8 dB, and a three stage IF amplifier having a noise figure of 2.5 dB. The overall conversion results is a gain of 25 dB.

The branching network used in the present effort consists of a set of 12 doubly terminated Tchebycheff filters appropriately spaced along a distribution network. To help make up for distributed losses and to allow for an additional measure of isolation against leakage from the second local oscillator (LO) into adjacent channels, a single transistor amplifier is implemented at the output of each filter.

After branching, the 12 individual channels are now available to the inputs of 12 identical individual baseband channels at a maximum level of -40 dBm. As seen in Figure 1.2, each baseband channel consists of a mixer, bandpass filter (BPF), IF amplifier, group delay equalizers (G.D.E.), limiter, discriminator and baseband amplifier. The mixer at the input to each of these channels converts to the second intermediate frequency of 80 MHz. Preliminary calculations showed that this frequency would most easily facilitate the synthesis of the required set of 12 local oscillator frequencies. An appropriate bandpass filter having a bandwidth of 36 MHz filters the output of the mixer and provides some additional channel selectivity. The IF amplifier should be able to provide a nominal 10 dBm level for a minimum input of -70 dBm, to drive the limiter and discriminator. The limiter must be wideband (40 MHz) and have a minimum 10 dB dynamic range. The discriminator must provide an extremely linear output (<3% deviation)

from linearity, based on previous work (5) (6), to prevent phase distortion of the signal. The final amplifier provides a 1 Vpp composite video signal into 75Ω which is compatible with typical CATV remodulators for local distribution. Provision is made for group delay equalizers to adjust the channel's delay characteristics.

It is planned that the 12 local oscillator frequencies for the baseband channels plus the X-band LO for the front end will be synthesized from one 10 MHz crystal used in conjunction with appropriate harmonic generators mixers, and filters.

1.4 SCOPE

Chapter 2 is concerned with the design, construction, and performance of the IF amplifier. Included in this section is a discussion on the specification of the bandpass filters and their design. The performance of a commercially made mixer is also discussed. The section concludes with some data taken on the overall IF amplifier performance when driven by the mixer.

Chapter 3 is devoted to the limiter and discriminator. The design of a simple limiter configuration and its performance are first considered. This is followed by a discussion on the design of a low-pass filter to remove the higher order harmonics in the limiter's output to the discriminator. The design of a modified transmission line discriminator then follows along with a discussion on the conversion from a distributed parameter to a lumped parameter system. This chapter concludes with performance results for the entire baseband channel from the input of the mixer to the output of the baseband amplifier.

Chapter 4 discusses the design criteria for the branching networks. Theoretical performance is considered along with the performance of a first cut prototype filter design.

A final discussion and summarized results are given in Chapter 5.

2. MIXER, IF AMPLIFIER AND BAND-PASS FILTERS

2.1 INTRODUCTION

This chapter describes the design, construction, and performance of the IF amplifier and its accompanying band-pass filters. Also discussed is the performance of a small commercially produced flat pack mixer used to down convert from X-band to the 80 MHz IF. The specifications for the amplifier are discussed first. These include determining input and output power and impedance levels, overall gain requirements, bandwidth, and selectivity. Then consideration is given to implementing a design and evaluation prototype performance. Finally, the overall performance of the IF amplifier with the mixer driving it is reported.

The preliminary operating specifications for the IF amplifier are specified by Newman et. al. (2). Final specifications evolved during the design phase. Based on the input impedance level and power requirements of the limiter, the IF amplifier should have an output impedance level of 300Ω and be able to provide about 6 V_{pp}. This corresponds to an output power of approximately 12 dBm. Its input impedance should match the mixer's output impedance of 50Ω and it should be able to amplify a minimum signal of -70 dBm. Hence, the amplifier must have a maximum gain of 80 dB over the frequency range of 60 to 100 MHz. In order to eliminate the need for an AGC loop and to provide additional limiting we will consider operating the amplifier near or in saturation, provided that its intermodulation characteristics do not adversely affect the system performance.

The band pass specifications and selectivity of each channel are now considered. The selectivity requirement chosen is based on that

used for the microwave receivers of the Bell System's TH-3 telephone communication system (12): at least 30 dB suppression of the adjacent channel band edges. Based on Carson's rule, at least 36 MHz is needed for the desired FM format. Allowing a 4 MHz guard band, 40 MHz of bandwidth per channel is available in our design. Therefore the amplitude roll-off can start at 52 and 98 MHz, respectively, and be down 30 dB at 58 MHz and 102 MHz. Since the sharpest selectivities with the fewest number of elements are obtained with the Tchebycheff response, such filters are used in the design.

Before turning to the actual design, let us consider the configuration we intend to use for the amplifier. One can think of the IF amplifier as consisting of a pre-amplifier section and power amplifier section. The band pass filter is also implemented in two sections. One is at the input to the first pre-amplifier stage, the other following it. Although both filters serve the purpose of eliminating out-of-band signal components, the second band pass filter also helps eliminate high frequency noise in the amplifier. In addition, such an arrangement prevents the need for a multipole filter at the input to the IF Amplifier which might prove difficult to tune and have excessive insertion loss.

2.2 PRE-AMPLIFIER DESIGN

Most of the gain is to be developed in the pre-amplifier section. The easiest and most economical way of implementing this section is to use several high frequency, linear amplifier integrated circuits in cascade. The MC1590G integrated circuit presents acceptable characteristics for such use. According to its specifications, each package should be able to provide at least 20 dB of gain out to 100 MHz.

Figure 2.1 shows a schematic diagram of this package (13). By adjusting the size of the load resistors, R_L, through which bias is supplied to pins 5, 6, and 7, one can control the gain and resulting bandwidth. For R_L = 100 Ω, each package is able to develop a gain of between 20 and 25 dB. For this amount of gain however, the response starts to roll off above 80 MHz. By using inductive peaking on the output pins 5 and 6, it is possible to raise the response on the high end. To calculate the required inductance one first determines the input and output impedance of the package. From the data sheet, it is found that the output capacitance and resistance are $C_0 \cong 2$ pf and $R_0 \cong 2K\Omega$, respectively. For the input there is a capacitance $C_i \cong 8$ pf and resistance $R_i \cong 1K\Omega$. Maximally flat response out to at least 100 MHz requires (14):

$$1.54 = R_L \sqrt{\frac{C}{L}} \qquad (2.1)$$

where R_L = 100 Ω and $C = C_i + C_0$ = 10 pf. Solving equation 2.1, one finds that L = .04 μh.

The pre-amplifier stage was prototyped by cascading two packages in the same manner as I.C. 2 and 3 in Figure 2.2. For proper operation, DC bias must be applied to pins 5, 6, and 7. By supplying 22 volts to the 120 Ω resistor at the input to the biasing network it is possible to bias pins 5, 6, and 7 to their maximum rated level of 18 volts. This level results in the most gain per package. From the 32 volt level required to operate the limiter, the 22 volt level is obtained from the 2N2959 emitter follower and zener diode configuration indicated in Figure 2.2. For use in the prototype, pin 1 on the first package was terminated in 50 Ω to match the signal generator. Also,

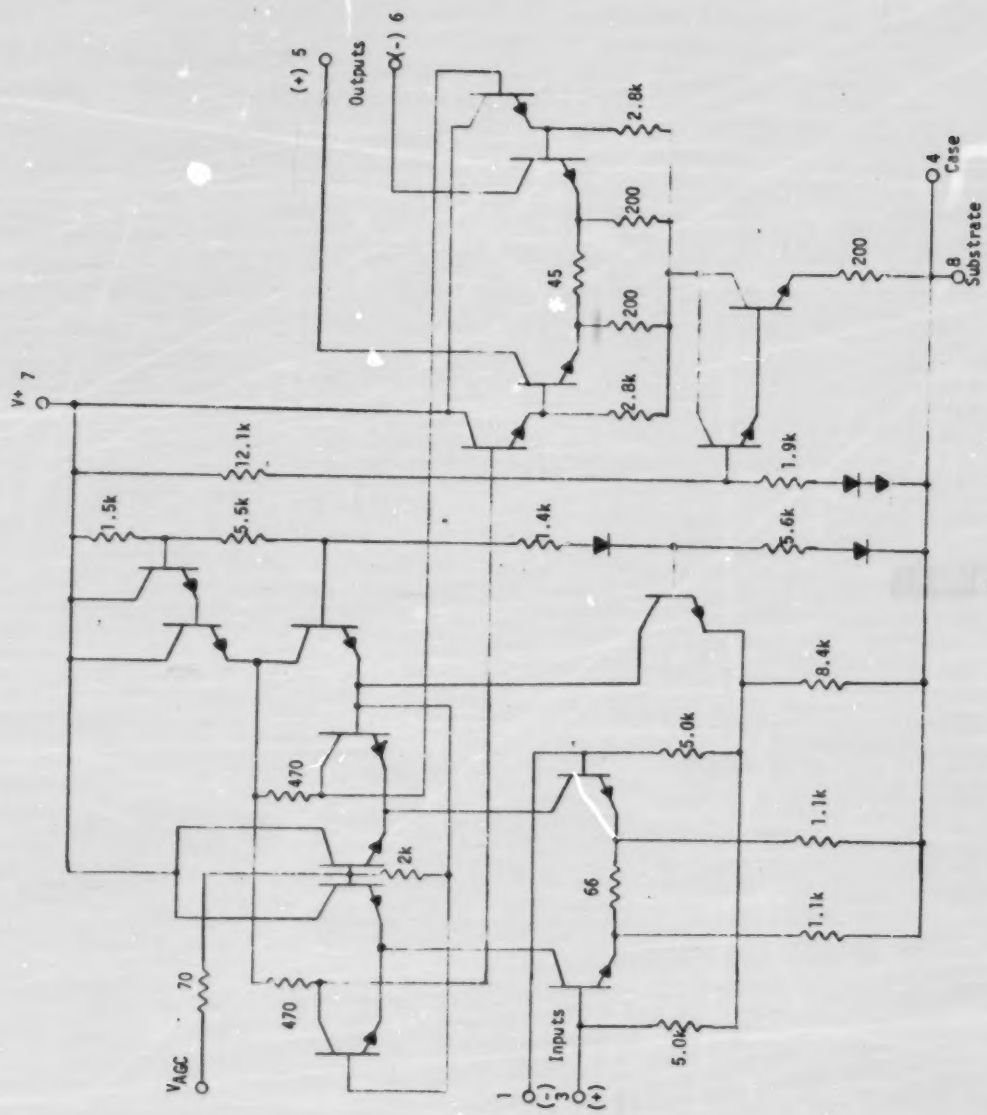

Figure 2.1 Schematic Diagram of MC1520R Package

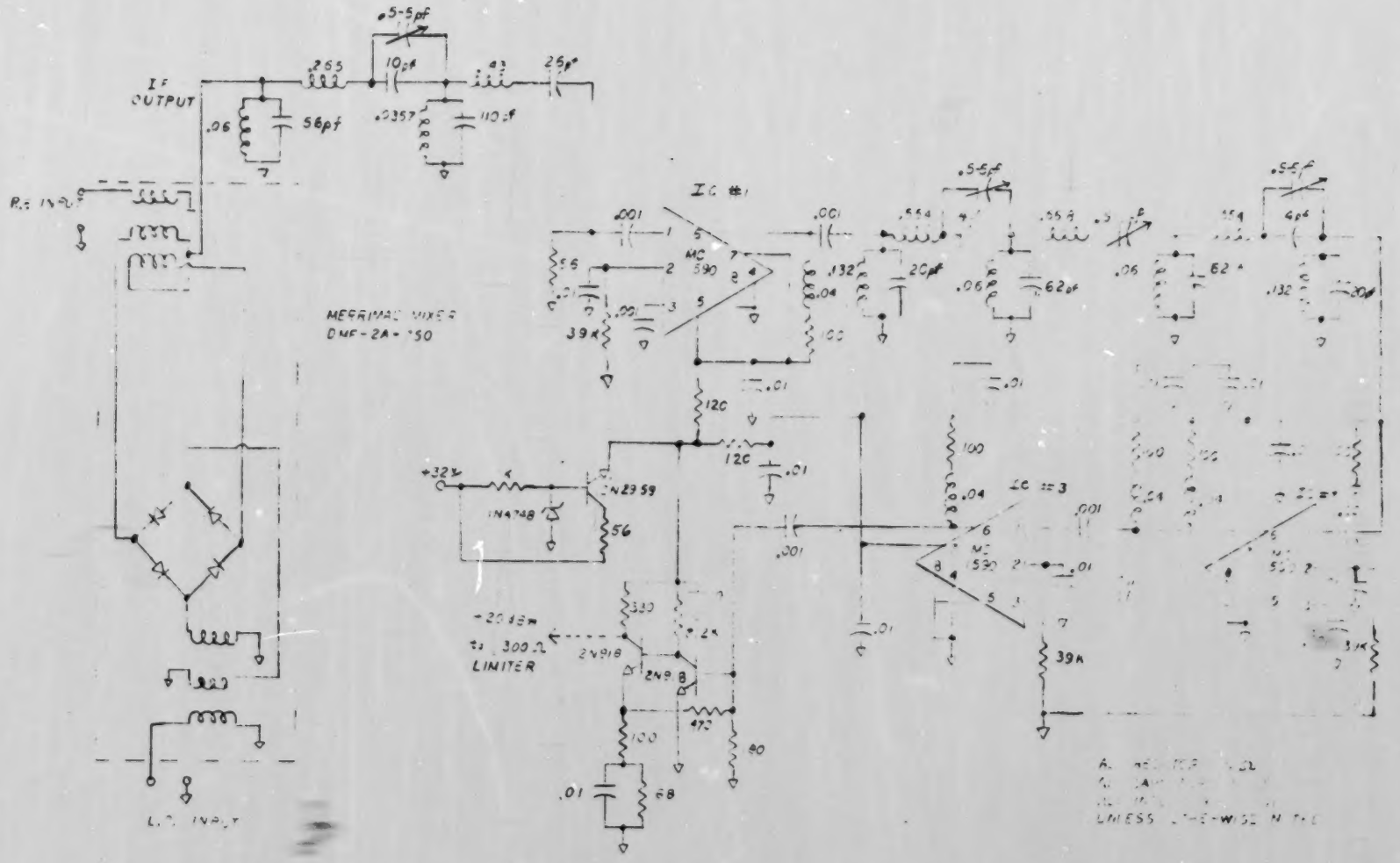

Figure 2.2 Schematic Diagram of Mixer and I.F. Amplifier

BEST COPY AVAILABLE

pin 5 on the second package had the same R-L arrangement as pin 6. Point by point measurements showed that there was a 2 dB variation in gain over the range of 60 - 100 MHz and a gain of approximately 23 dB per package with an input level of -50 dBm. A cascade of three of these packages is needed to adequately drive the power amplifier for inputs at -70 dBm.

2.3 POWER AMPLIFIER DESIGN

Preliminary considerations for this stage suggested that a push-pull arrangement would be desirable since both outputs of the MC1590G could be used. However, subsequent prototyping and testing of such an arrangement indicated that the necessary gain and required bandwidth could not be obtained. This was largely due to the problem of effectively fabricating transformers at these frequencies.

Instead of the push-pull arrangement, only pin 6 is used to drive a feed-back pair of 2N918 transistors in the arrangement shown in Figure 2.2. The design of such a stage is reasonably straightforward and can be easily developed experimentally as was done here. The 2.2KΩ resistor in the collector of the input transistor serves mainly as a bias resistor and its value is not overly critical. The value of 330 Ω in the collector of the output transistor was chosen to provide a 300 Ω output level for the limiter and the value of 180 Ω in the base of the input transistor provided the best match to the pre-amplifier output. It was found that providing some series feedback in the emitter in addition to the shunt feedback of a 470 Ω resistor provided the necessary power to drive the limiter over the frequency range of interest. It was found that this stage when

prototyped provided an additional 13 dB of gain to the signal appearing at the output of the preamplifier when biased at 22 volts as shown in Figure 2.2.

2.4 FIRST BAND-PASS FILTER

2.4.1 Design and Analysis

In order to arrive at a suitable design for the first band-pass filter, the following parameters must first be specified: selectivity, center frequency, upper and lower cut-off frequencies, acceptable passband ripple and impedance level. The selectivity is first determined. In order not to have too many elements and a high pass-band insertion loss, a specification of 30 dB attenuation at 120 MHz was chosen. It will be seen later that this taper along with the tapers of the branching network and second band-pass filter are adequate to provide the necessary 30 dB attenuation at adjacent band edges. The center frequency is 80 MHz and the upper and lower cut-off frequencies are 98 MHz and 62 MHz respectively. The passband ripple should be .01 dB to provide a smooth passband response and the impedance level is 50 Ω to match the mixer.

Applying the methods outlined in Appendix 7.1.3, it was determined that a filter having these specifications must have 4 resonators with the element values indicated in Table 2.1. This filter is shown schematically in Figure 7.1.12. It must be noted that a slight impedance transformation takes place, since the required terminating resistance is 55 Ω. This terminating resistance is realized in a 56 Ω resistor which is connected between pin 1 of IC number 1 and ground.

TABLE 2.1 Element Values for First Band-Pass Filter

Resonator No.	L μh	C pf
1	)6614	53.0316
2	.25634	5.7118
3	)3568	6.827
4	14316	29.1212

2.4.2 Performance

The filter was constructed using hand wound inductors and stock value silver mica capacitors. The inductors were fabricated with #30 wire using 22 MΩ 1/4 watt resistors as the form and applying the formulas of Grover (15) to determine the number of turns. The completed inductors were then tested on a phase meter according to the method shown in Appendix 7.5.2 and the turns spacing was adjusted to provide the required inductance. For the required capacitance values, parallel combinations of not more than two fixed capacitors were used to attempt to realize as closely as possible the values indicated in Table 2.1. In practice these values can be realized to an accurancy of 5%.

Subsequent swept measurements indicated that some trimming was needed to tune up the response. It was found that the best response was obtained using values shown in Figure 2.2. This arrangement gave a reasonably flat amplitude response with about a ± .5 dB ripple over the passband. At 62 and 98 MHz the response was down 1 dB. Due to the lack of sensitivity of our equipment we were unable to effectively measure out-of-band response. Although this response is somewhat different from the calculated response, one must consider that these filter designs are based on loss free considerations (i.e. infinite Q inductors and capacitors). Also, we are not able to realize the precise values of required inductance and capacitance. Furthermore, there are parasitic effects which are hard to account for.

2.5 SECOND BAND-PASS FILTER

2.5.1 Design and Analysis

The selectivity of this filter is specified by the performance of the branching network filters and first band pass filter. Together,

both of these filters provide 60 dB of attenuation at 120 MHz. A brief graphical analysis given in Figure 2.3 shows that if an attenuation of 30 dB at 110 MHz for the second band pass filter is specified, there will be a total of 30 dB of attenuation at 58 and 102 MHz as desired. The center frequency is 80 MHz with upper and lower cut-off frequencies of 100 and 60 MHz. The pass band ripple again is to be .01 dB and the impedance level is 100 Ω to match the biasing resistance on pin 6 of the IC package.

Applying the methods of Appendix 7.1.3, the number of resonators required is found to be 7. The required values of inductance and capacitance are found as outlined in Appendix 7.1.3, also. Assuming a configuration of the form shown in Figure 7.1.9, the resonators should have values of L and C as indicated in Table 2.2. On this structure, the input and output impedance are each 100 Ω.

2.5.2 Performance

This filter, like the first band-pass filter, was constructed with hand wound inductors and stock capacitors. Initial swept measurements indicated that some trimming of component values was necessary to tune up the response. By altering capacitor values as shown on Figure 2.2, an equi-ripple response of ± .5 dB between 62 and 98 MHz was obtained. Again, it was difficult to effectively measure the out-of-band response due to the lack of sensitivity of our equipment.

As before, the difference between the response predicted by the design equations and the actual response can be attributed to lossy elements, inability to obtain the exact required value for a given element and parasitic effects.

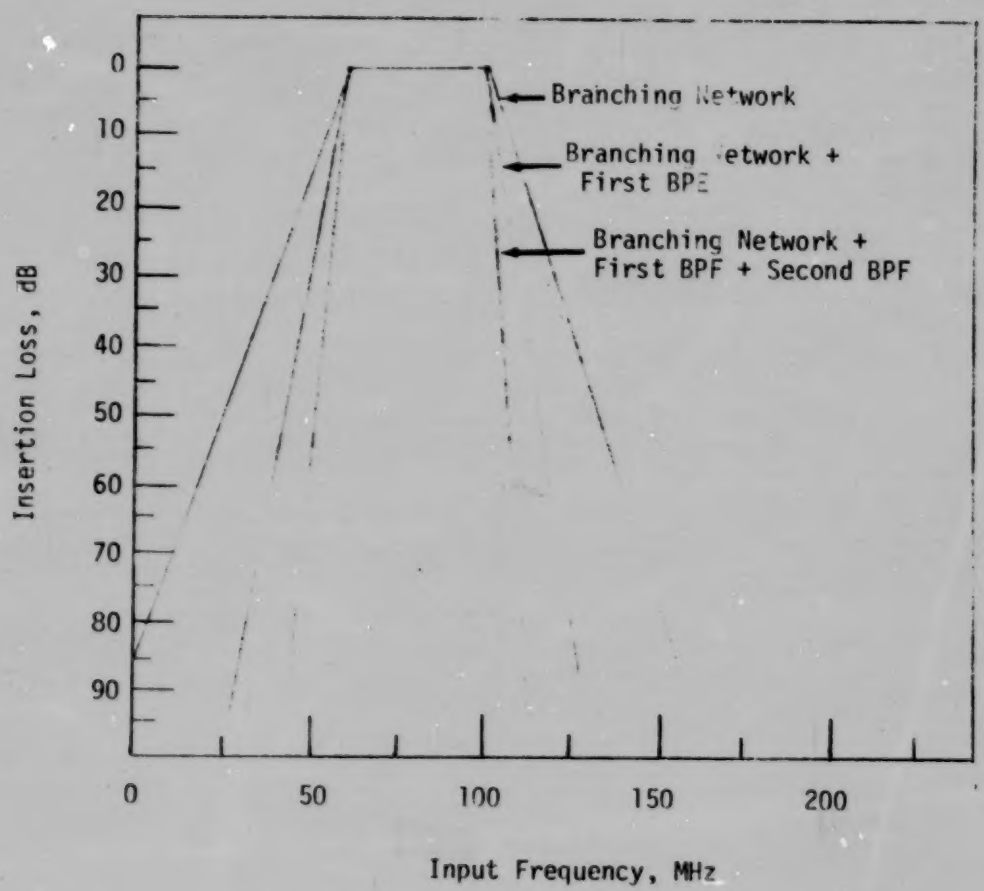

Figure 2.3 Comparison of Amplitude Responses of Branching Network, First BPF and Second BPF and Resultant Response

Table 2.2 Element Values for Second Band-Pass Filter

Resonator No.	L μh	C pf
1 and 7	.13314	31.7095
2 and 6	.55403	7.6200
3 and 5	.06070	69.5561
4	.64780	6.4969

2.6 MIXER DESCRIPTION

The mixer used to down convert from L-band to the 80 MHz IF is manufactured by Merrimac Research and Development Inc. It is their model DMF-2A-750 "Flat Pack" subminature mixer which has specifications as given in Table 2.3. The device measures .13 X .50 x .38 inches and has 8 pins, three of which serve as connections for the LO, RF, and IF respectively. The rest are connected to ground. Figure 2.4 shows the schematic diagram of this device as furnished by Merrimac. The hot carrier diodes are arranged in a monolithic IC quad.

Subsequent testing showed that the mixer was within its advertised specifications. Figure 2.5 shows a plot of LO to RF port isolation as a function of frequency.

2.7 OVERALL PERFORMANCE OF THE IF AMPLIFIER

Driving the IF amplifier from the output of the mixer, measurements were made on the input impedance to the mixer, minimum detectable signal, linear dynamic range, two tone intermodulation products, and the frequency response. All of these measurements are referenced to the input of the mixer. At the output of the amplifier, a 300 Ω to 50 Ω resistive L-pad was used to provide about 20 dB of attenuation and the appropriate impedance match to the 50 Ω measurement system.

The RF port to the mixer was matched experimentally with a 1 pf capacitor to ground across the RF input line to the mixer. This resulted in a return loss of more than 15 dB over the range of 1.0 to 1.4 GHz as shown in Figure 2.6. Figure 2.7 shows the Smith chart representation of the input impedance normalized to 50 Ω over the same

Table 2.3 Mixer Performance Specifications

Frequency Range	
RF and LO	50-1500 MHz
I.F	DC - 1000 MHz
Isolation	
LO - RF	25 dB 500-1500 MHz
LO - IF	20 dB 500-1500 MHz
RF - IF	15 dB 500-1000 MHz
Conversion Loss	9 dB
Compression (1 dB)	0 dBm
Impedance (Nominal)	50 Ω
Local Oscillator Drive	+10 dBm
Max. Input Power	+17 dBm
N.F.	9 dB ± 1 dB
Weight	2.8 grams

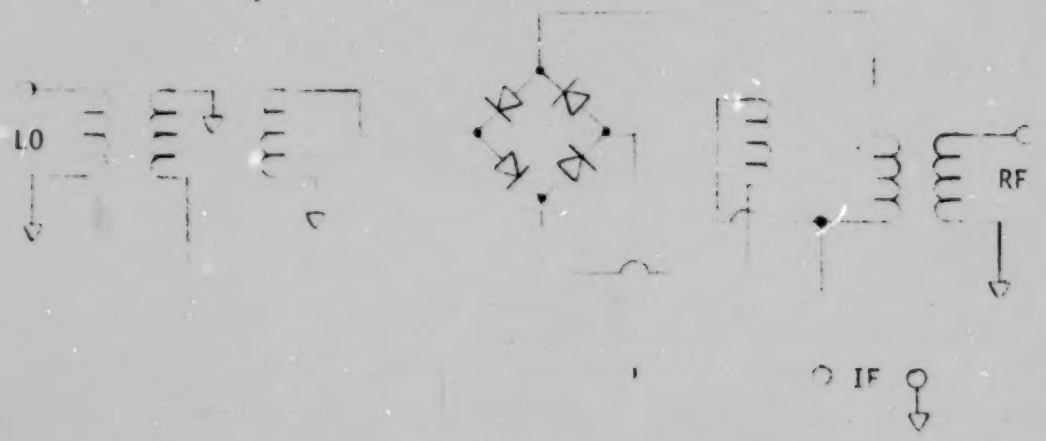

Figure 2.4 Basic Mixer Schematic

BEST COPY AVAILABLE

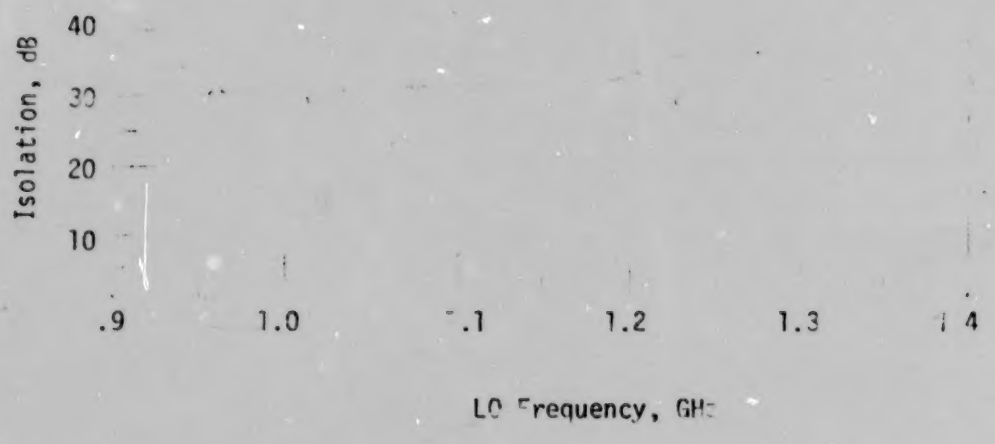

Figure 2.5 Isolation of Between LO and RF Port in dB as a Function of LO Frequency

BEST COPY AVAILABLE

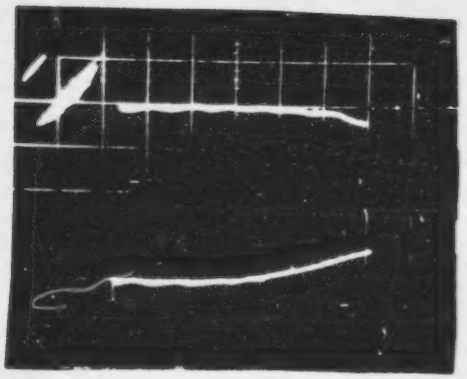

Upper Trac is 0 dB Reference

Vertical Scale: 5 dB/cm

Horizontal Scale: Trace Begins at 1.0 GHz and Ends at 1.4 GHz

Figure 2.6 Return Loss of Mixer Input as a Function of Frequency

BEST COPY AVAILABLE

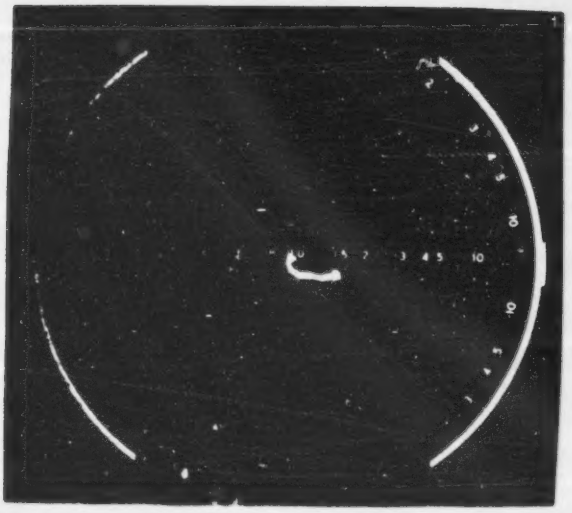

Figure 2.7 Input Impedance to Mixer Over the Frequency Range of 1.0 to 1.4 GHz Normalized to 50Ω

frequency range. As can be seen, the input impedance is nominally between 50 Ω and 75 Ω. At 1 GHz, the input is about perfectly matched to 50 Ω. In a similar manner, the LO port is matched by slightly widening the input line to obtain a nominal return loss of 10 dB.

The minimum detectable signal at the mixer's input was found to be approximately -86 dBm. A plot of output power as a function of input power as shown in Figure 2.8. Curve A is the measured response. The output wideband noise level is -2.67 dBm and affects the dynamic response at low levels. Curve B shows the equivalent linear dynamic range if no noise were present. From Curve A it is apparent that the range of linear operation is between -65 dBm and -52 dBm. Operation into the nonlinear range, as will be seen later, can result in higher intermodulation distortion than operation in the linear range.

In order to study the effects of intermodulation distortion, two signals (tones) were fed simultaneously into the RF port of the mixer. One tone, f_{mb}, at 1240 MHz, produces the desired 80 MHz IF while the other tone, f_{int}, was varied between 1220 MHz and 1260 MHz to produce interferring signals in the 60 to 100 MHz IF band. A spectrum analyzer was then used to measure the resulting spurious signals. Figure 2.9 shows the power levels of the resulting spurious signals relative to the level of f_{mb} plotted as a function of their frequency for three different levels of f_{int}. The desired signal f_{mb} is at a level of -50 dBm, the point at which the amplifier begins to saturate. The level of f_{mb} was then lowered to -55 dBm. It was found that spurious signals are not detectable if f_{int} were much below -55 dBm, as is shown in Figure 2.9. As can be seen, operation

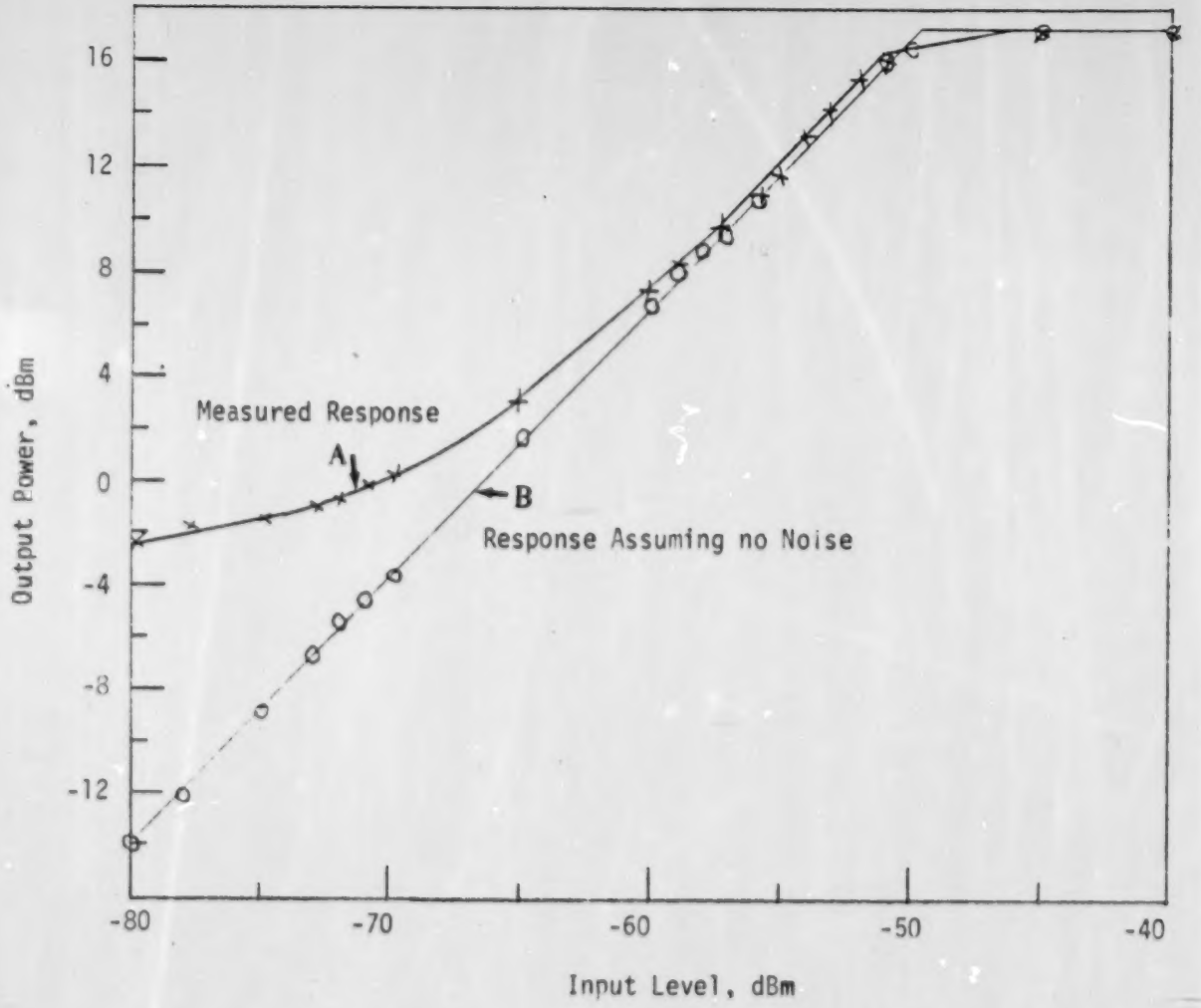

Figure 2.8 IF Amplifier Output Power as a Function of Input Power

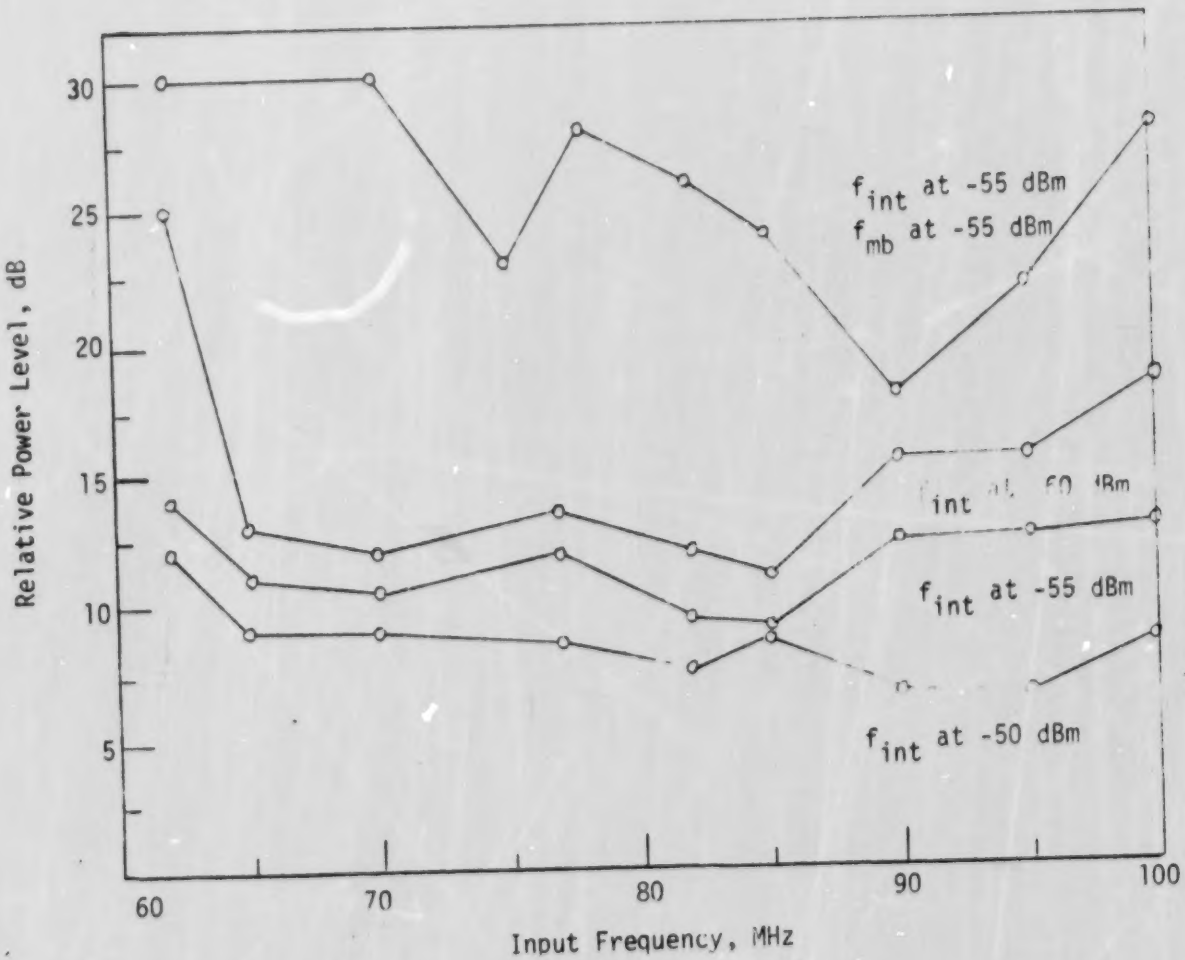

Figure 2.9 Level of Intermodulation Products Relative to Level of f_{mb} as a Function of Frequency for Different Levels of f_{int} where f_{mb} = -50 dBm Except as Noted

BEST COPY AVAILABLE

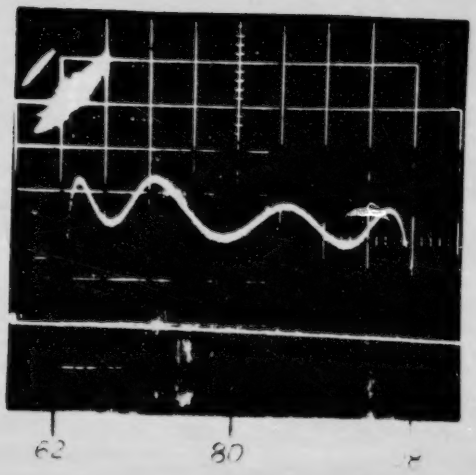

Vertical Scale: 1 dB/cm

Horizontal Scale: MHz as Marked

Figure 2.10 IF Amplifier Frequency Response and Response of Diode Detector

of the amplifier into the nonlinear region produces considerable intermodulation product levels.

The overall frequency response from the input to the mixer to the output of the IF amplifier as measured on a network analyzer is shown in Figure 2.10. This response was obtained for an input level of -55 dBm. The trace below the response curve represents the network analyzer diode detector's characteristic. As can be seen, there is a 1 .5 dB bandwidth of 36 MHz which meets the specifications for the IF amplifier.

3. DEMODULATOR AND OUTPUT AMPLIFIER

3.1 INTRODUCTION

This section presents an analysis of and set of design criteria for an FM demodulator having a 40 MHz bandwidth operating over a range of 60 MHz to 100 MHz with center frequency of 80 MHz. Also presented is the design of a 5 MHz baseband output amplifier. The demodulator consists of three basic components; a wideband limiter, a low pass filter and a wideband discriminator.

We shall first discuss the design of the wideband limiter which is to have an operating bandwidth of at least 40 MHz and a 10 dB dynamic range. Next, a low pass filter which provides suppression of the unwanted harmonic frequencies generated by the limiter is considered. Then an FM discriminator which has a virtually linear DC output characteristic over the operating frequency range is discussed. The last component considered is the baseband amplifier which is used to provide $1V_{pp}$ into 75Ω from the discriminator's output. The performance of the entire demodulator is also described.

3.2 WIDEBAND LIMITER

3.2.1 Design and Analysis

For the receiver, a two stage limiter was chosen. Each stage has a configuration shown in Figure 3.1. For quiescent D-C conditions one can write:

$$0 = V_B - V_{D1} - I_3 R_3 - I_1 R_1 \qquad (3.1)$$

$$0 = V_B - V_{D2} - I_3 R_3 - I_2 R_2 \qquad (3.2)$$

BEST COPY AVAILABLE

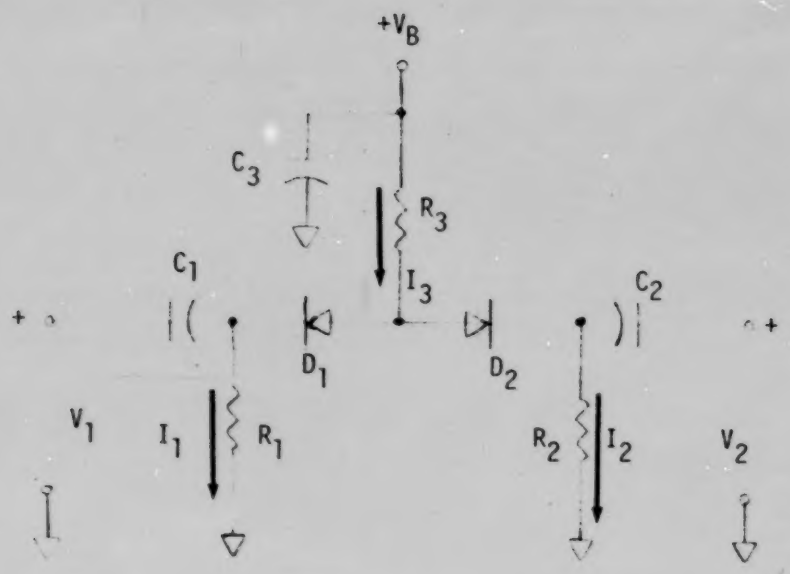

Figure 3.1 Basic Limiter Configuration

where V_{D1} and V_{D2} are the diode voltage drops. The quiescent voltage appearing across R_1 (and R_2) is:

$$V_1 = V_2 = \frac{V_B - V_{D1}}{\frac{(R_1 + R_2)\, R_3}{R_1\, R_2} + 1} \tag{3.3}$$

Since V_1 and V_2 represent the voltage at which the limiter clips the incoming signal, this voltage is called the limiting voltage and is denoted by V_c. It should be noted that Equation (3.3) does not take into account the effects of an actual load on the output. To compensate for this effect, R_2 must be replaced by R_2' in Equation (3.3) such that:

$$R_2' = \frac{R_2\, R_L}{R_L + R_2} \tag{3.4}$$

Where R_L is the load resistance.

An AC signal is now applied to the input. The reactance of C_1 and C_2 is neglected. The amplitude A of the input signal is always taken to be much greater than V_c. In its positive half cycle, the input signal is clipped by the diode D_1. Similarly, the negative half cycle is clipped by the diode D_2. Hence, the output of the limiter will be a modified trapezoidal wave as shown in Figure 3.2.

Since the diodes act as switches, the input and output impedances vary with time. Assuming a sinusoidal signal, of amplitude A, it is seen that when it is between $-V_c$ and V_c both diodes are on and the input and output impedances are the parallel combination of R_1, R_2 and R_3. The time during which the input signal exceeds V_c, D_1 is off and D_2 is on. Here the input

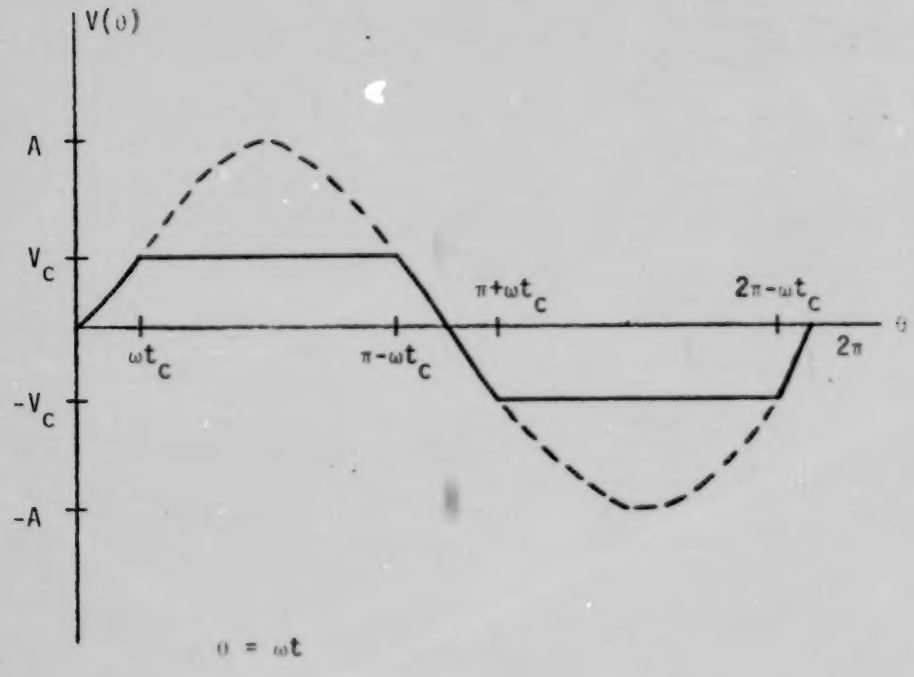

Figure 3.2 Limiter Input (Dotted Line) and Output (Solid Line) as a Function of θ For One Period

impedance is R_1 and the output impedance is R_2 in parallel with R_3. When the input signal is below $-V_c$ diode D_1 is off, but D_2 is on. Now, the input impedance is R_1 in parallel with R_3 and the output impedance is R_2.

This rather complicated result is simplifed as follows. If $A>>V_c$, as is intended, and if $R_3>>R_1$ and $R_3>>R_2$, then the input and output impedances are effectively R_1 and R_2, respectively.

3.2.2 Single Stage Prototype

To test the design concepts, a prototype single stage limiter for operation at 50Ω was built and tested. The results indicated that such a configuration would make an effective limiter. A single stage limiter was then constructed to operate at an impedance of 300Ω, the intended impedance level for a limiter suitable for use in the receiver. Applying the basic design equations, a single stage prototype is obtained with $R_1 = R_2 = 330\Omega$, $C_1 = C_2 = .001\ \mu f$, $R_3 = 1.2K\Omega$ and $C_3 = .01\ \mu f$. The limiting voltage was chosen to be .5 volt and the required value of V_B was 8.65 volts.

To evaluate the quality of operation of this limiter, measurements were made on the change in output power for a given reduction of input power at the channel center frequency (80 MHz). The results of this measurement are shown in Figure 3.3. The 0 dB level of the input corresponds to 13.6 Vp-p while 0 dB on the output is equivalent to .84 Vpp.

As can be seen from Figure 3.3, there is about a .2 dB change in the output for a 1 dB change in the input in the limiting region.

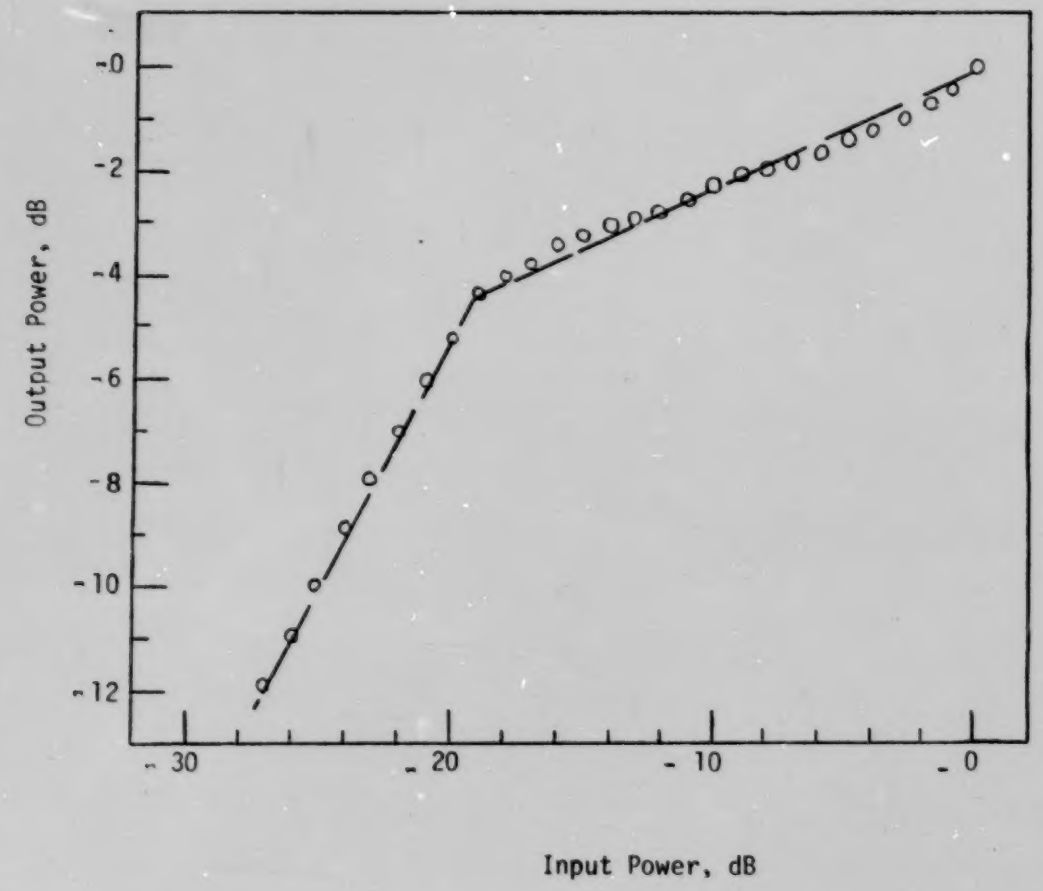

Figure 3.3 Change in Output Power as Function of the Change in Input Power for Single Stage Limiter

Based on the performance of existing systems, this is not sufficient limiting. For a system similar to this one it was decided that for an input variation of 1 dB the output should not change by more than .083 dB over an input range of 12 dB (6). Since this specification could not be met with only one stage of limiting, the use of a two stage limiter was indicated.

3.2.3 Construction of a Two Stage Limiter

The two stage limiter used in the receiver is actually two single stage limiters tied together by a single transistor amplifier.

The second limiter stage is essentially the same as the 300Ω prototype just discussed; the circuit element values are identical. However, V_c is now specified to be .8 V and $V_B \cong$ 22 VDC.

A stage of amplification between the first and second stages is provided to produce hard limiting in the second stage. If the amplifier is driven hard enough it should also provide some additional limiting. A schematic of the amplifer is shown in Figure 3.4. Due to the wide variation of β for the 2N918 transistor, it is impossible to accurately predict the gain of this stage. Therefore the choice of bias voltage and resistors is determined experimentally. The following values were used:

$R_1 = 1.8K\Omega$ $\quad$ $V_1 = 22$ VDC

$R_2 = 1.2K\Omega$ $\quad$ $V_2 = 22$ VDC

$R_3 = 2.2K\Omega$

$R_4 = 2.2K\Omega$

The purpose of R_1 and R_3 is to limit the DC current while the gain is controlled by R_2. Resistor R_4 is necessary to drain off charge on the

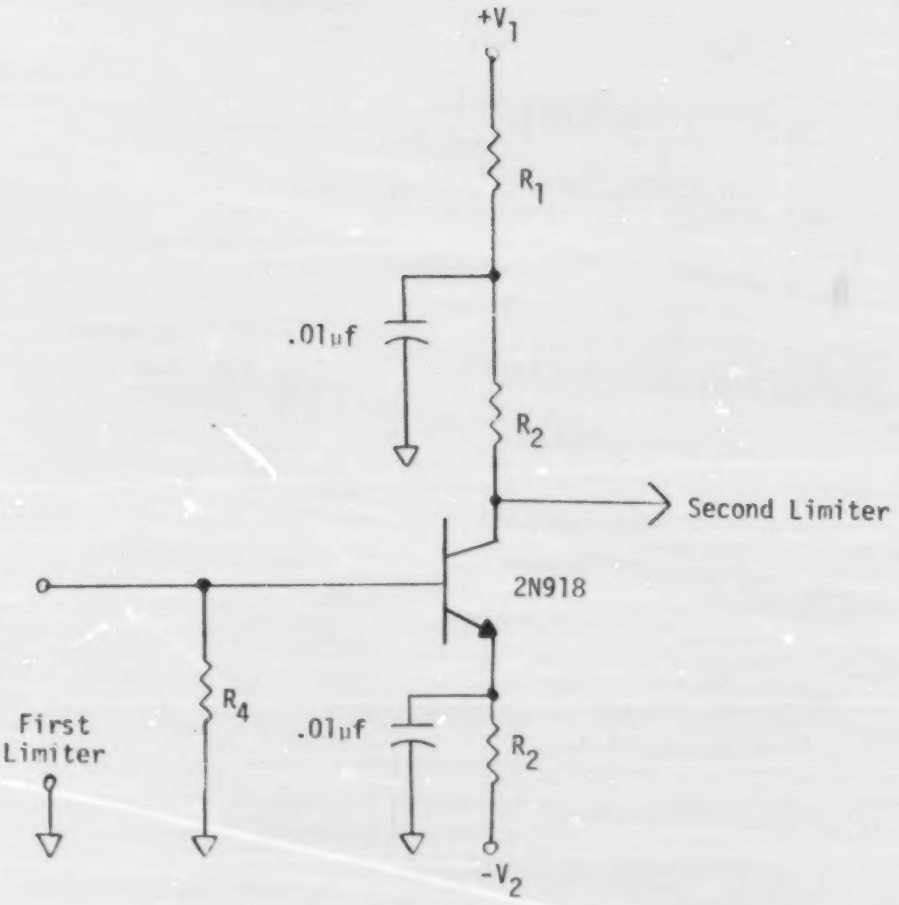

Figure 3.4 Limiter Amplifier Schematic

capacitor at the output of the first limiter to permit normal transistor operation. Using the above values of bias voltage and resistance, the overall gain was found to be nominally 6 dB over the frequency range of interest. The amplifier was tested by driving it from the output of the first limiter and terminating it with the second limiter.

In order to obtain a low source impedance to drive the amplifier, R_2 is chosen as 100Ω in the first limiter. At this level, the output impedance is not so low that too much current will be drawn from the limiter. For a 300Ω limiter input impedance level, R_1 = 330Ω. Since the amplifier has an input inpedance of about 400Ω, it is safe to assume that it does not load the output of the first limiter too badly. Hence, with R_3 = 1.2KΩ and V_B = 2 2V we have V_c = .75V.

3.2.4 Performance

The complete two stage limiter's performance was tested as before. In Figure 3.5 the results of this measurement are shown. As can be seen, the linearity is within our requirements. The output changes by about .83 dB for a 10 dB change of the input. Figure 3.6 shows a photograph of the limiter's output at 80 MHz. Since the output specifications that we are most interested in are those obtained at the output of the low pass filter which follows the second limiter, we will defer further comment on limiter performance until the filter design is discussed.

3.3 LOW-PASS FILTER

3.3.1 Specifications

Due to the adverse effects of the higher order harmonics on the performance of the discriminator, a low pass filter is needed at the output of the limiter. The out-of-band attenuation characteristics

of the filter will be specified by the harmonic content of the limiter output. Theoretically, if $V_c << A$, the output wave will be trapezoidal. In a Fourier analysis of such a wave, the coefficients B_n represent the amplitudes of the fundamental, second harmonic, third harmonic, etc. In appendix 7.4, a Fourier analysis is performed on a trapezoidal wave. The coefficients are;

$$B_1 = \frac{A}{\pi} \left[2\omega t_c - 1/2 \sin 2\omega t_c\right] \tag{3.5}$$

$$B_n = 0 \ (n \text{ even}) \tag{3.6}$$

$$B_n = \frac{4V_c}{n\pi} \cos n\omega t_c \quad (n \text{ odd}) \tag{3.7}$$

$$\omega t_c = \sin^{-1}\left(V_{c/A}\right) \tag{3.8}$$

Using the experimental techniques outlined in Appendix 7.5 the acutal harmonic content of the limiter output was determined. The results are given in Table 3.1. Also given in this table are the theoretically predicted values as obtained from equations 3.5-3.8 with $V_c = .75V$ and A = 6 Vpp. The presense of second, third and fourth harmonic is not surprising considering the actual shape of the output waveform (see Figure 3.6). The presence of the even harmonics is probably due to the more pronounced effect of the junction capacitance of the diodes at this impedance level. The third harmonic is at a lower than predicted level largely due to parasitic reactions.

From the results of the harmonic content, it is now possible to specify the amplitude taper of the harmonic suppression filter. From the data in Table 3.1 and the photograph of the limiter output, it was decided that 30 dB suppression of the second harmonic would be required.

3.2.2 Design and Analysis

Using the information presented in the section on harmonic analysis of the limiter (see Appendix 7.4) it is possible to specify

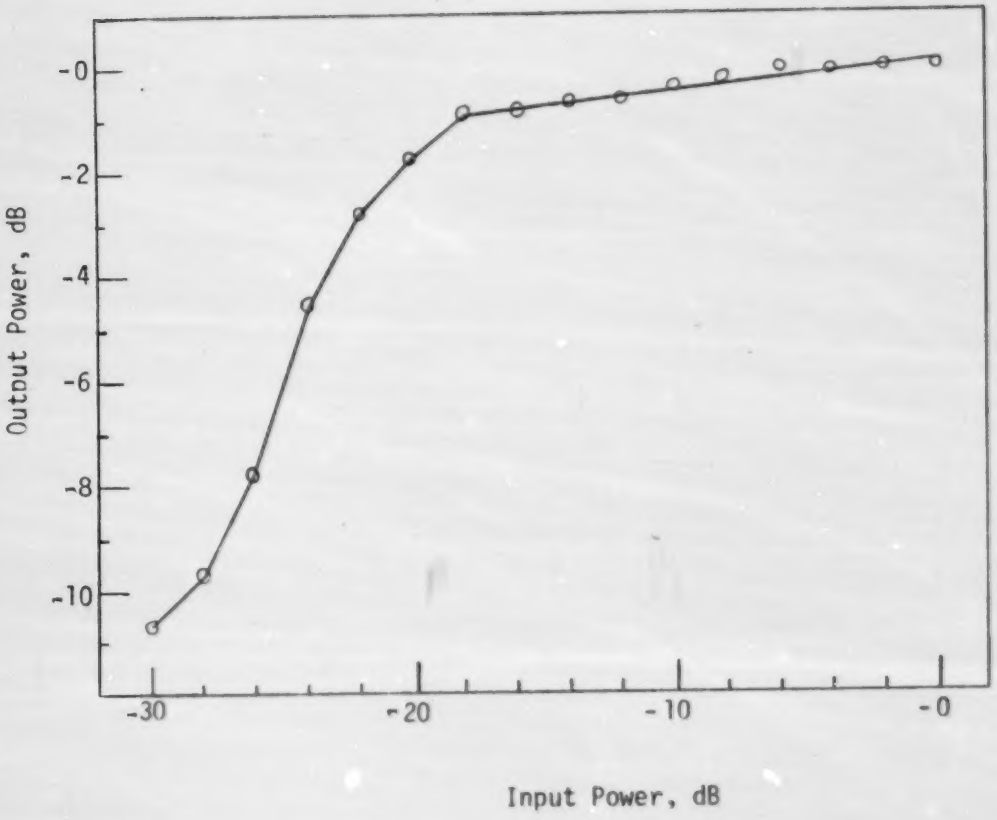

Figure 3.5 Change in Output Power as a Function of the Change in Input Power for a Two-Stage Limiter

Table 3.1 Power Levels of Harmonics in Limiter Output

	Freq. MHz	Predicted Power Level(dB)	Actual Power Level(dB)
Fundamental	60	0	0
2nd Har.	120	$-\infty$	-20
3rd Har.	180	-1	-15
4th Har.	240	$-\infty$	-28

BEST COPY AVAILABLE

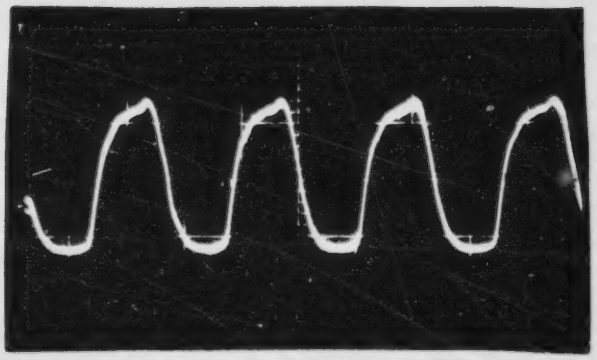

Vertical Scale: .5 V/cm

Horizontal Scale: 5 nSec/cm

Figure 3.6 Photograph of Limiter Output at 80 MHz

the cut-off frequency and the amplitude taper of the low pass filter. Since the lowest frequency of interest is 60 MHz, the lowest second harmonic is at 120 MHz. From data given in Table 3.1, the second harmonic of 60 MHz is already down 20 dB from the fundamental. This means that the filter must provide an additional 10 dB of attenuation at 120 MHz. Also, we would like to have as small an amplitude ripple as possible so as not to defeat the purpose of the limiter. Therefore, a ripple of .01 dB was selected. Finally, the cut-off frequency should be somewhat greater than 100 MHz to insure that the amplitude stays flat out to 100 MHz and to eliminate the effects of phase distortion at the band edge. A value of 105 MHz is adequate for this purpose.

Applying the methods outlined in Appendix 7.1.1 we find that in order to have a ripple of .01 dB, an impedance level of 300Ω, a cut-off frequency of 105 MHz, and an attenuation of 10 dB at 120 MHz we need a total of 9 elements having the following theoretical values:

$L_1 = L_9 = .3705$ μh

$C_2 = C_6 = 7.2136$ pf

$L_B = L_7 = .8209$ μh

$C_4 = C_8 = 8.658$ pf

$L_5 = .8671$ μh

The configuration of this filter is of the form shown in Figure 7.1.2 in Appendix 7.1.1

3.3.3 Performance

The filter was built and tested using standard values of 7 pf for the 7.2136 pf value and 9 pf for the 8.658 pf value. The inductors were hand wound with number 30 wire using 22 MΩ 1/2 watt resistors

as forms. The number of turns required were computed from tables provided by Grover (15). The response of this structure is shown in Figure 3.7 where the insertion loss is plotted as a function of input frequency. For purposes of comparison, theoretical plots of the same structure allowing .01 dB and .5 dB ripple are shown also. Further comment on this comparision is contained in Section 7.1.3.

Several things must be recalled when looking at this data. First, the termination is a purely resistive value of 300Ω, the correct termination for this filter. Secondly, where we have indicated 0 dB, there is in fact some insertion loss which is difficult to measure resulting from the use of a pad to transform from 300Ω to the 50Ω measuring system. Finally, these characteristics will change somewhat when the filter is driven by the limiter and terminated by the discriminator. These effects will be studied more closely when the overall performance is considered.

To evaluate limiter performance including the filter, two types of measurements were made. First, a set of measurements were made on the dynamic range at 60 MHz, 80 MHz, and 100 MHz. In Figure 3.8 we have plotted the output power as a function of the input power for each of the three frequencies of interest. The other measurement was on the output linearity as a function of input frequency. The results of this measurement are shown in Figure 3.9. As can be seen, the output is virtually a straight line from 74 MHz on. However, at the low end the output starts to peak up. This effect is probably due to parasitic reactances and impedance mismatches at the input and output to the filter. It will be shown later how this nonlinearity can be tuned out.

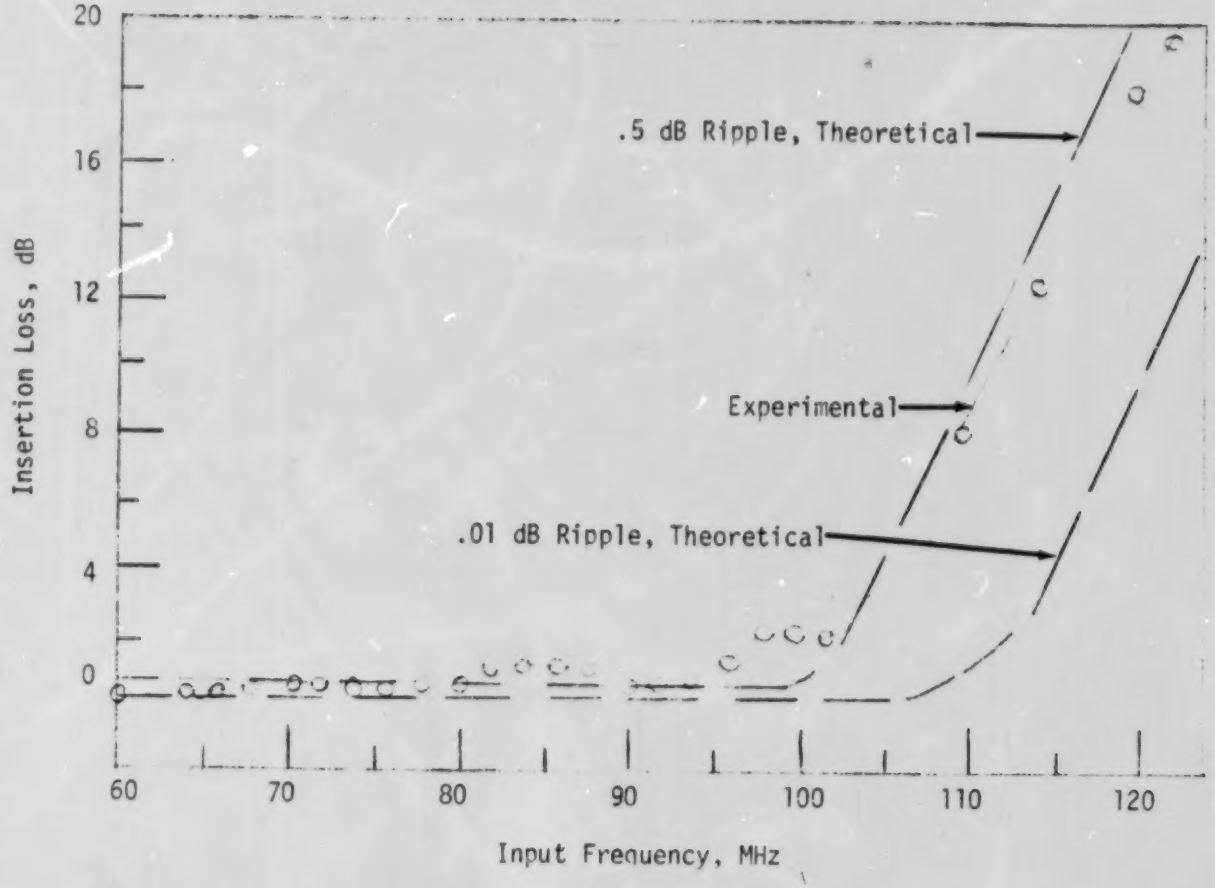

Figure 3.7 Experimental and Theoretical Responses for Limiter Low-Pass Filter

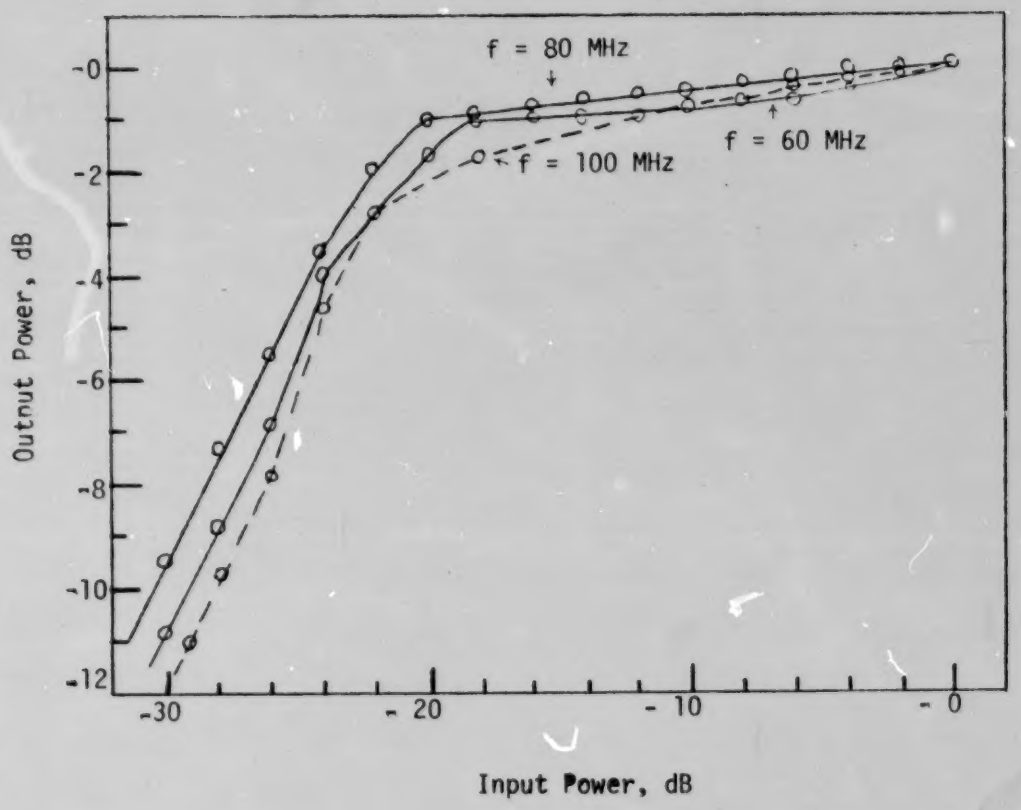

Figure 3.8 Output Power as a Function of Input Power for Three Different Input Frequencies

BEST COPY AVAILABLE

Figure 3.9 Frequency Response of Limiter

3.4 WIDE BAND DISCRIMINATOR

3.4.1 Design and Analysis

Having considered the limiter and filter in great detail, attention will now be given to the design and analysis of wideband discriminator based on a device described by Lee and Seo (16) (17), which consists of a bridge composed of two $\lambda/8$ lengths of transmission line one open circuited, the other short circuited. The circuit diagram is shown in Figure 3.10. Assuming lossless lines, the input impedance of the open and short circuited lines are:

$$Z_{sh} = j\, Z_o \tan \theta \tag{3.9}$$

$$Z_{oc} = -j\, Z_o \cot \theta \tag{3.10}$$

where:

Z_o = characteristic impedance of the line.

$\theta = \omega\sqrt{LC} = 2\pi(\ell/\lambda)$.

λ = wavelength of the input

ℓ = length of the line.

L = inductance per unit length.

C = capacitance per unit length.

ω = angular frequency of the input.

The output voltage of the discriminator can be expressed as

$$V_o = \eta_1(|V_1| - |V_2|) \tag{3.11}$$

$$V_o = \eta_1 V_{in}[(1 + \gamma^2 \cot^2 \theta)^{-1/2} - (1 + \gamma^2 \tan^2\theta)^{-1/2}] \tag{3.12}$$

where:

η_1 = constant related to the diode characteristic

V_{in} = amplitude of input signal

$|V_1|$ = voltage at the output of the short circuited line.

$|V_2|$ = voltage at the output of the open circuited line.

γ = R/Z_o = input resistor constant

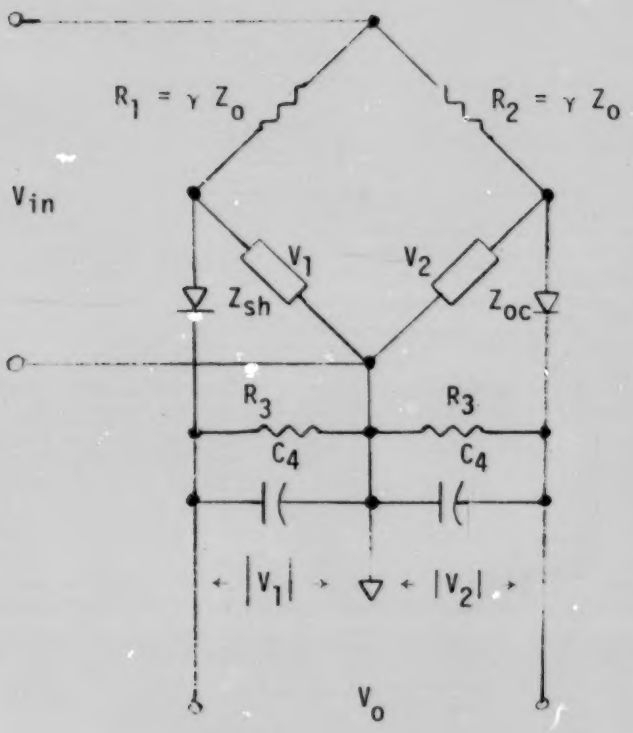

Figure 3.10 Basic Discriminator Configuration

R = input resistor

The sensitivity of the discriminator is expressed as $\partial V_o/\partial\theta$. We desire the value of γ that gives the most sensitivity and greatest output linearity. From Lee and Seo (17), the greatest linearity is obtained with $\gamma = .833$ and the greatest sensitivity for $\gamma = 2$. Let us consider a choice of $\gamma = 1$. Now equation 3.12 reduces to:

$$V_o = V_{in} (|\sin\theta| - |\cos\theta|) \eta_1 \tag{3.13}$$

Notice that the cross-over point ($V_o = 0$) occurs when $\theta = 45°$ or $\ell = \lambda/8$.

This transmission line discriminator is easily implemented at 80 MHz by replacing the shorted and open circuited lines with their lumped element circuit equivalent. Assuming lossless lines, these lumped element equivalents are as shown in Figure 3.11. For the purposes of analysis, let us neglect the diodes. Then we can write the input impedance to the discriminator as:

$$Z_{in} = \frac{(R + Z_1)(R + Z_2)}{2R + Z_1 + Z_2} \tag{3.14}$$

where Z_2 is the input impedance to the open circuit equivalent and Z_1 the input impedance of the short circuit equivalent. Also:

$$Z_2 = -j \frac{(\omega L_2 - 1/\omega C_3)}{[(\omega L_2 - (1/\omega C_2 + 1/\omega C_3)]\ \omega C_2} \tag{3.15}$$

$$Z_i = -j \frac{\omega L_1}{\omega^2 L_1 C_1 - 1} \tag{3.16}$$

The theoretical discriminator characteristic appears as shown in Figure 3.12 where ω_o is the center frequency and ω_c is the cut-off frequency of the short circuit equivalent which is simply a low pass filter. Therefore, we can express ω_c as:

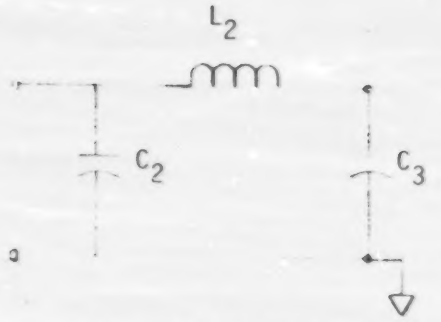

Open Circuit Line Equivalent

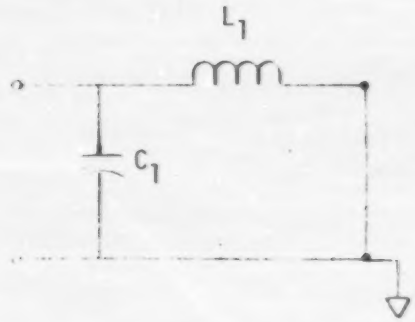

Short Circuit Line Equivalent

Figure 3.11 Open Circuit and Short Circuit Transmission Line Equivalent Circuits

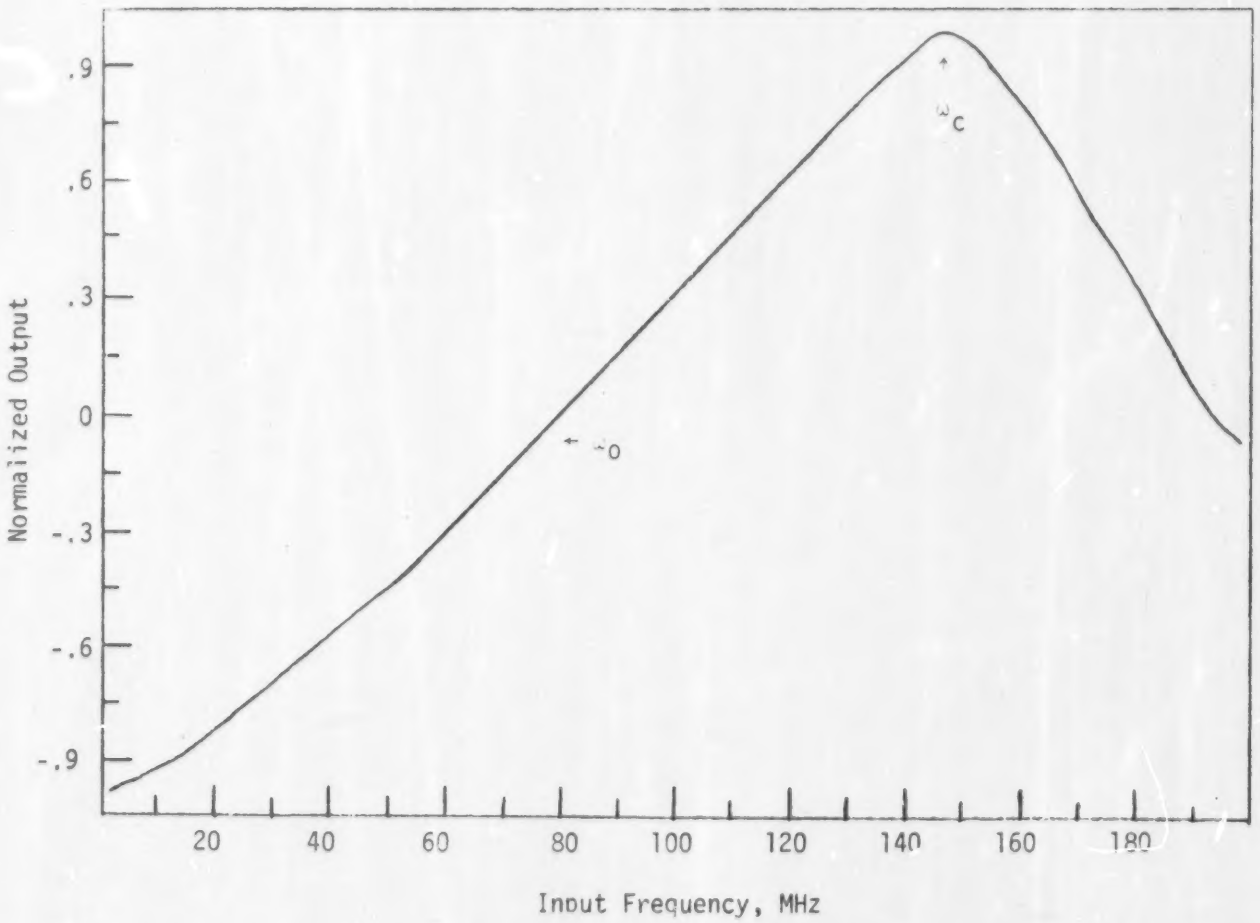

Figure 3.12 Normalized Discriminator Output as a Function of Input Frequency

$$\omega_c = \frac{1}{\sqrt{L_1 C_1}} \tag{3.17}$$

Furthermore at ω_o, $V_o = 0$ and $|Z_1| = |Z_2|$. Since Z_1 and Z_2 are pure imaginary we can write

$$Z_1^2 = Z_2^2 \tag{3.18}$$

For $C = C_1 = C_2 = C_3$ and $L = L_1 = L_2$ we have;

$$\left(\frac{1}{\omega_o C}\right)^2 \left(\frac{\omega_o^2 L C - 1}{\omega_o^2 LC - 2}\right)^2 = \frac{(\omega_o L)^2}{(\omega_o^2 LC - 1)^2} \tag{3.19}$$

Multiplying through, this reduces to:

$$2\omega_o^4 L^2 C^2 - 4\omega_o^2 LC + 1 = 0 \tag{3.20}$$

Solving for ω_o;

$$\omega_o = \frac{\sqrt{1 - \sqrt{2}/2}}{\sqrt{LC}} = \frac{.541}{\sqrt{LC}} \tag{3.21}$$

Finally, the characteristic impedance is given by,

$$Z_o = \sqrt{L/C} \tag{3.22}$$

Using equation (3.21) and (3.22) it is possible to determine what the equivalent lumped values of L and C should be by specifying the center frequency and the impedance level Z_o:

$$L = (.541)\ \frac{Z_o}{\omega_o} \tag{3.23}$$

$$C = (.541)\ \frac{1}{\omega_o Z_o} \tag{3.24}$$

The correct values of R_3 and C_4 necessary on the output will be determined by the desired basebandwidth. For a television baseband channel at least 4.5 MHz is needed. If f_d is the frequency at which the signal is down 3 dB than R_3 C_4 is determined by:

$$R_3 C_4 = 1/2\pi f_d \qquad (3.25)$$

3.4.2 Performance

A prototype discriminator with a center frequency of 80 MHz and a characteristic impedance of 50Ω was built. The design values are L = .054 μh and C = 21.5 pf with $R_1 = R_2 = 47\Omega$. A theoretical plot of output voltage normalized to the input level was made with respect to input frequency for these values of L and C. The results indicated a virtually linear response from 60 to 100 MHz as shown in Figure 3.12.

The prototype was breadboarded using 22 pf for C. The indicators were hand wound according to methods outlined in Grover (16). For the output low pass filter, R_3 = 220 kΩ and C_4 = 300 pf. Performance of this prototype indicated that such a configuration would make a suitable discriminator.

3.4.3 Performance of 300Ω Discriminator

A 300Ω discriminator suitable for use in the receiver was then implemented. Using the design equations, the appropriate values of L and C for a discriminator with Z_o = 300Ω and f_o = 80 MHz are L = .324 μh and C = 3.58 pf. To compensate for component tolerance, etc. it was decided to let C_3 be adjustable. In the actual circuit, values of L = .330 μh and C = 3 pf were used. Also, $R_1 = R_2$ = 300Ω at the input. To obtain the 5 MHz base bandwidth, R_3 = 2.2KΩ and C_4 = 12 pf are used in the output circuit.

Upon attempting to test this circuit, it was found that due to the parasitic capacitance of the circuit and the diode junction capacitance adequate performance could be obtained by removing the two fixed capacitors in the open and short circuit resonators and leaving only C_3 for the purpose of adjusting the center frequency to 80 MHz.

A constant amplitude signal of 1 Vpp was fed into the input and data was collected in the DC output as a function of input frequency giving us the characteristic which is shown in Figure 3.13. Data related to the performance of the open and shorted resonators is presented in Figure 3.14. If such curves are linear then the output characteristic must be linear also. Examination of each curve separately will tell the performance of each resonator and determine its effect on the overall performance. As is expected, both curves are fairly linear and the differences between them at each point compare closely with the results in Figure 3.13. In Figure 3.14, $|V_{sc}|$ is the magnitude of the voltage at the output of the short circuit resonator and $|V_{oc}|$ the output of the open circuit resonator.

3.5 OVERALL PERFORMANCE

Previous testing has indicated that we have a usable limiter and discriminator. The problem is to now make them function effectively together. Point by point measurements indicated a fairly linear output response from 60 to 82 MHz. Beyond 82 MHz, the slope of the discriminator output began to fall off. This indicated that the limiter output was more frequency dependent when driving the discriminator then when driving a purely resistive termination.

With the demodulator connected to the IF amplifier and mixer, swept measurements were made of the linearity of the output of the discriminator. These too revealed that the output fell off slightly above 82 MHz. Observing the separate outputs of the short circuit resonator and open resonators yielded some interesting results. First, there was some ripple on the separate curves which tended to cancel when they were added together. Also, the output of the short

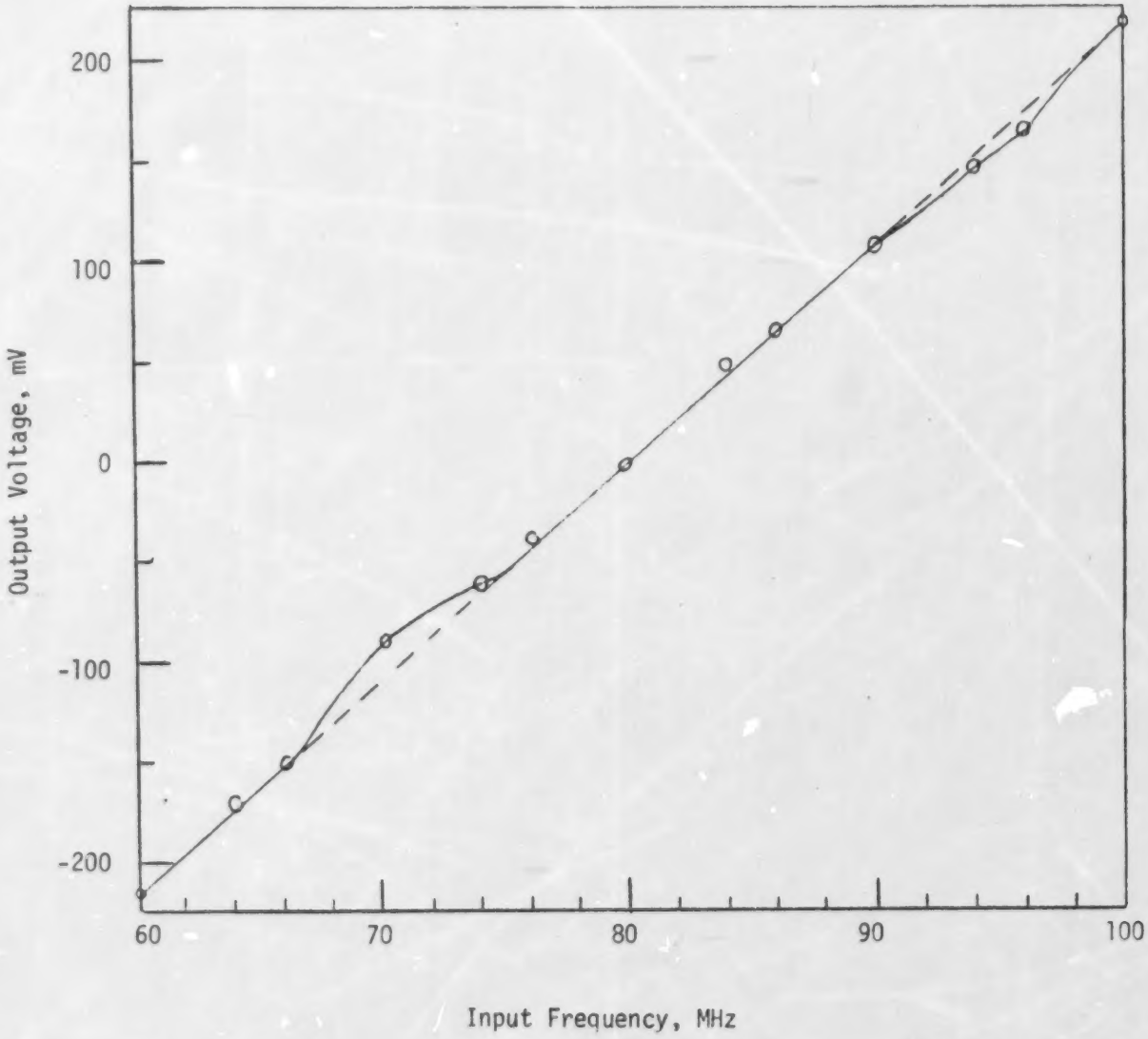

Figure 3.13 Prototype Discriminator Output as a Function of Input Frequency

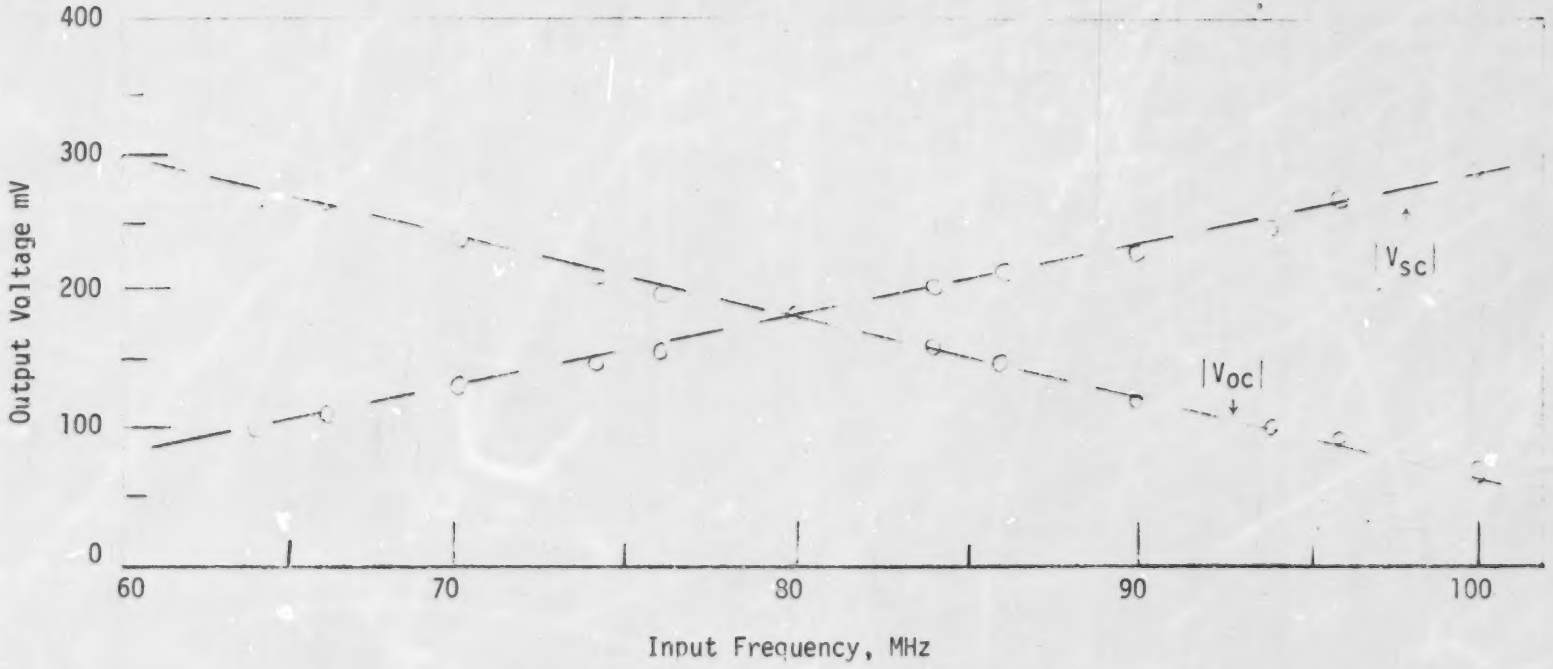

Figure 3.14 Voltage Output as a Function of Input Frequency for the Open and Short Circuit Line Equivalents

circuit resonator was about 1/2 that of the open circuit resonator and considerably more non-linear. Further investigation revealed that the low pass filter at the output of the limiter had a nominal insertion loss of 2 dB.

By replacing the inductor in the short circuit line equivalent and the L-C resonator in the open circuit line equivalent with 300Ω resistors and observing the separate outputs we have an indication of the overall response of the entire system. Figure 3.15 shows the response of our system when the resonating elements are replaced by 300Ω resistors. The base line indicates the zero voltage reference. As can be seen, there is considerable ripple, and the output falls off above 85 MHz.

By adjusting the values of fixed capacitance in the low-pass filter the response could be adjusted as shown in Figure 3.16, to reduce the insertion loss of the filter to a few tenths of a dB over the pass band.

Having considerably improved the overall system response, the reactive elements were reconnected. As expected, the trimming of capacitors values in the filter greatly improved the output characteristic. By trimming the bias voltages on the limiter the output of the discriminator was linearized. The resulting output is shown by Figure 3.17 which is a plot of the discriminator output voltage as a function of input frequency.

In order to study the effect of input level on the output characteristic, a set of measurements were made at various input levels

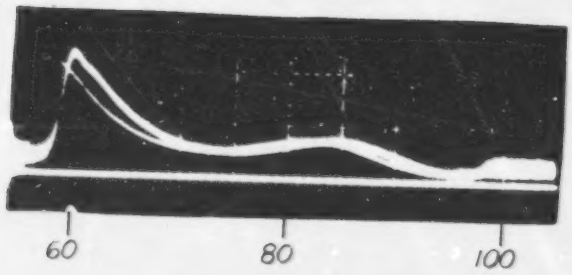

Vertical Scale: 50 mV/cm

Horizontal Scale: MHz as Marked

Figure 3.15 System Response at the Output of the Limiter-Filter

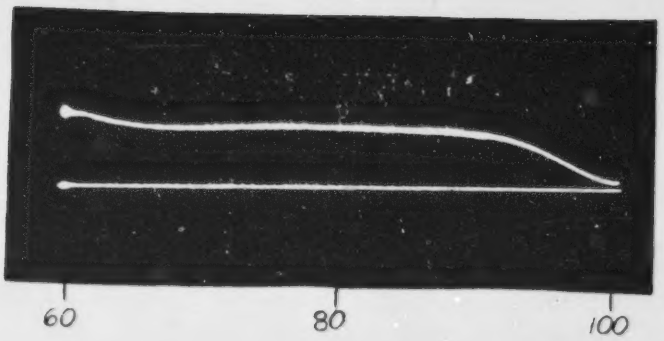

Vertical Scale: 50 mV/cm

Horizontal Scale: MHz as Marked

Figure 3.16 System Response After Tuning Limiter-Filter

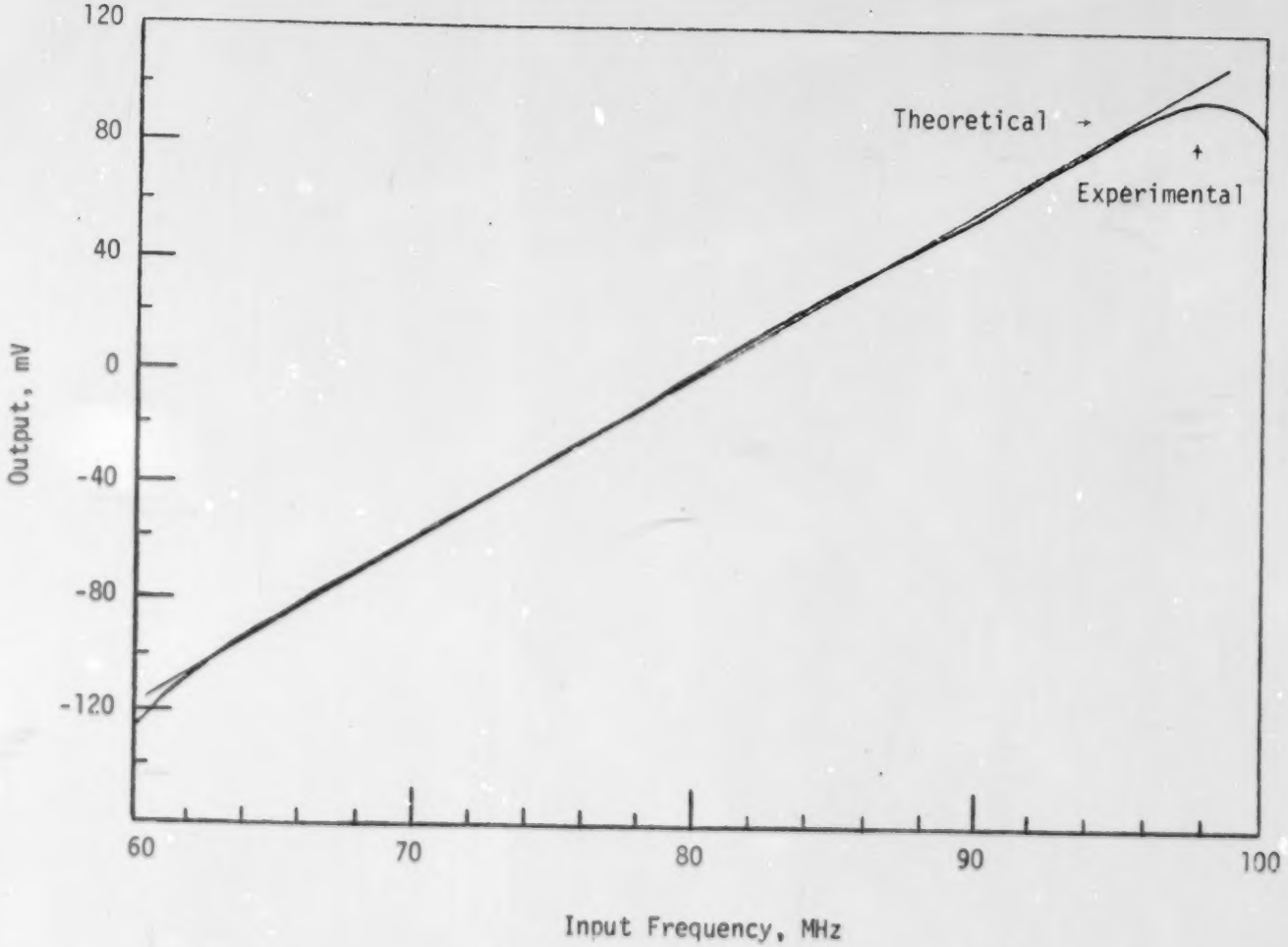

Figure 3.17 Discriminator Output as a Function of Frequency When Connected to Limiter Output

as shown in Figure 3.18. As can be seen the output linearity starts to deteriorate below input levels of -55 dBm. This is well within design specifications, since the expected levels from the output of the branching networks are nominally -50 dBm. These results indicate that the entire system is working properly. We must now consider the design of an adequate baseband output amplifier.

3.6 BASE BAND OUTPUT AMPLIFIER

3.6.1 Design and Analysis

Connected to the output of the discriminator is a differential amplifier which takes the double ended output of the discriminator and converts it to a single ended output at a level of 1Vpp into 75Ω. The circuit diagram of the amplifier is shown in Figure 3.19. In order to prevent video bounce, we must have a response that extends down to DC. Therefore, the amplifier must be directly coupled to the discriminator. This arrangement presented some problems for proper operation of the discriminator.

Originally, R_3 and R_{10} were not part of the circuit. At this point the output was found to be badly distorted. Examination of the individual discriminator outputs at the input to the amplifier revealed that they no longer crossed at the 80 MHz center frequency. The reason for this was due to the biasing on the bases of Q_1 and Q_2. It became apparent that some adjustment to the biasing of Q_1 and Q_2 was needed to return the outputs of the discriminator to the 80 MHz crossover point. This was accomplished by the addition of the bias resistors R_3 and R_{10}, their values being determined experimentally. Adjustment of R_3 along with the bias voltages allowed us to center the output about 0 volts.

Figure 3.18 Discriminator Output for Various Input Levels

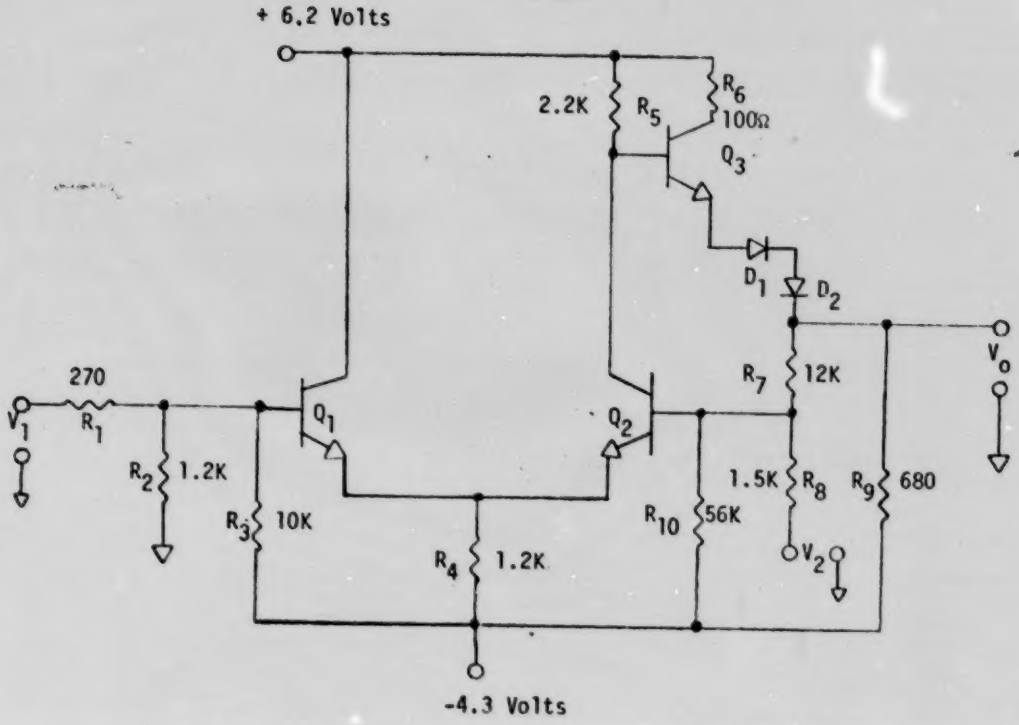

Figure 3.19 Output Amplifier Schematic

The input impedance is controlled by R_1, R_2 and R_3. The overall gain of the circuit is approximately the ratio of R_8 to R_7. To eliminate loading the discriminator outputs as much as possible we would like to have a fairly high impedance but not so high as to limit the basebandwidth to a value below 5 MHz. As can be seen from Figure 3.19, the input impedance is 1.5KΩ and the gain should be about 10.

From quiescent analysis, it can be shown that, in general, for a configuration of this type $R_5 = 2\ R_4$. The actual values of these resistors are not critical. Values of 1.2KΩ and 2.2KΩ for R_4 and R_5, respectively, were chosen.

The value for R_9 is determined from the maximum negative level needed, -.5V in this case. At this level, the load draws about 6.67 mA. A DC analysis shows that a value of about 680Ω is a good choice to allow this point to go to at least -.5V.

The purpose of R_6 is to prevent the immediate destruction of Q_3 in the event of a short circuit on the output. The diodes D1 and D2 insure that Q_3 will not be cut-off anywhere over the range of output voltage from -.5V to +.5V.

The transistors used are 2N918 and the diodes are 1N914.

An overall schematic diagram of the output amplifier and demodulator is given in Figure 3.20. As can be seen, Zener diodes are used to develop the different bias voltages from one + 32 V supply.

3.6.2 Performance

In order to test the performance of this circuit we operated it as a pulse amplifier. All measurements were made with input V_2 grounded and input V_1 connected to a fast rise time pulse generator. Subsequent

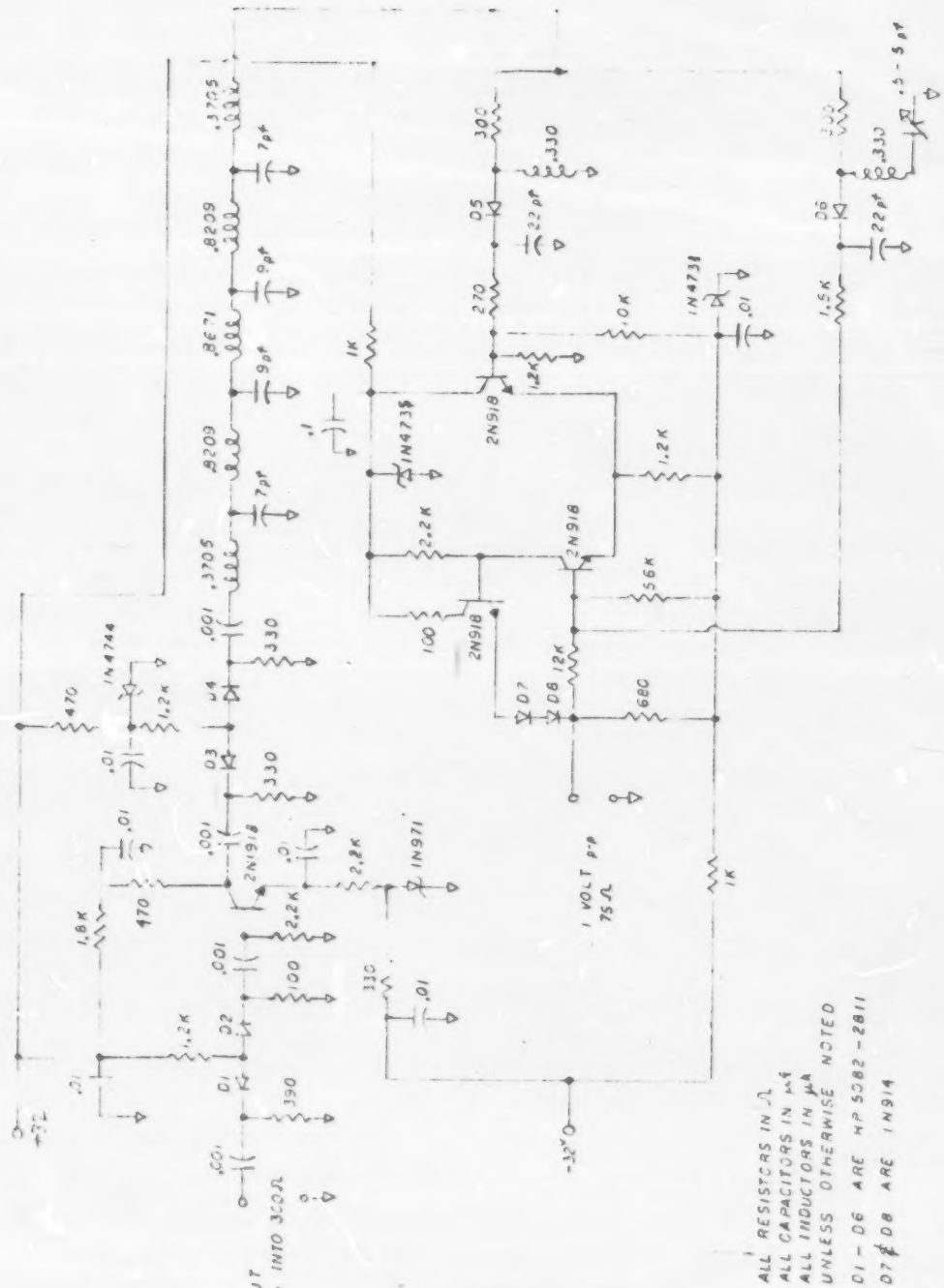

Figure 3.20 Overall schematic of Demodulator and Output Amplifier

testing revealed that the output had a 10 to 90% rise time of about 45 nsec. Delay between input and output is about 5 nsec and the single ended gain is approximately 7. Swept measurements of the output of this amplifier when driven by the discriminator showed that we could get about 1.2 Vpp into 75Ω with no loss of linearity as is shown in Figure 3.21. In Figure 3.22 a family of output curves is presented for differing power levels at the input to the mixer.

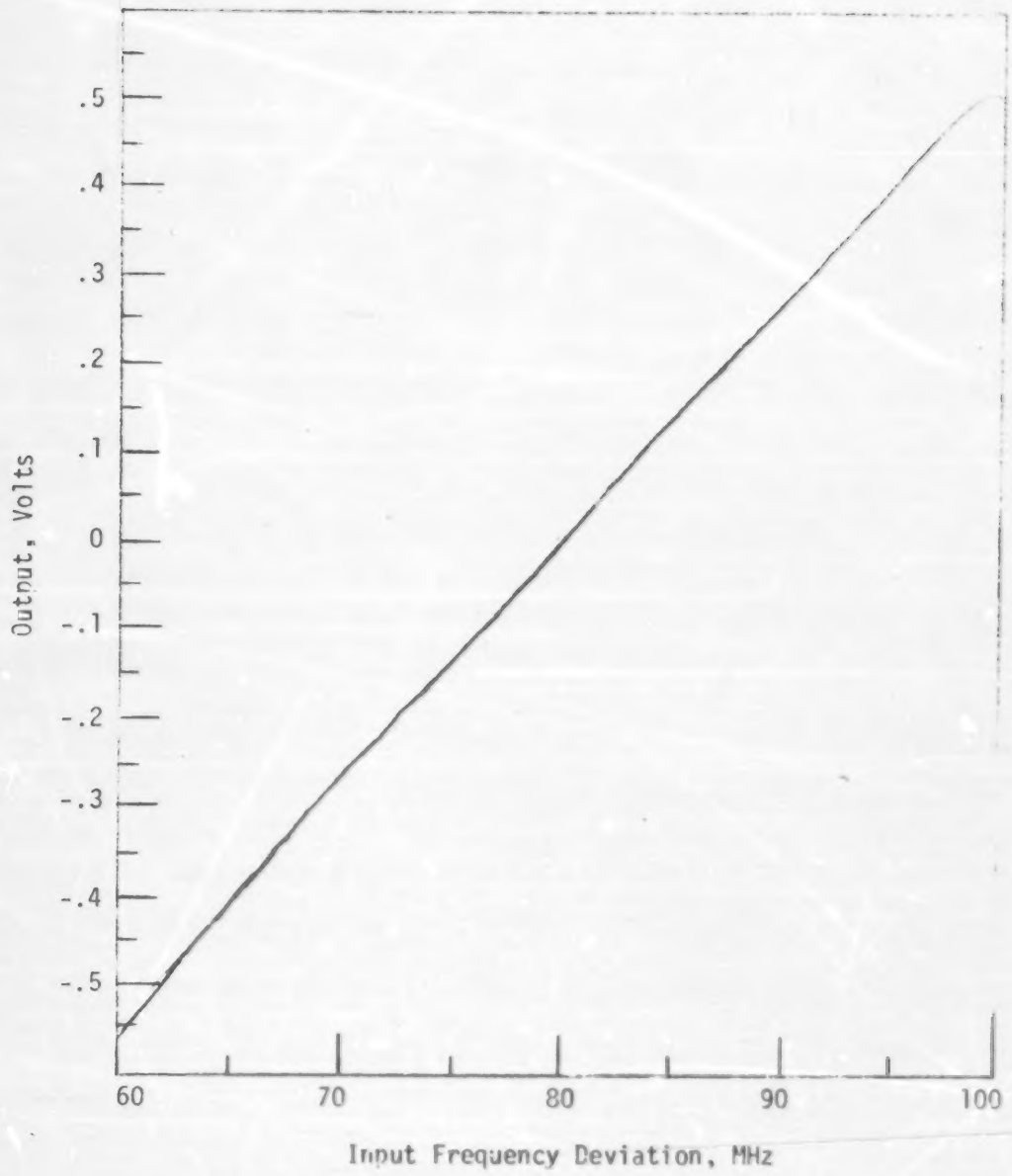

Figure 3.21 Output of Final Amplifier as a Function of Input Frequency Deviation

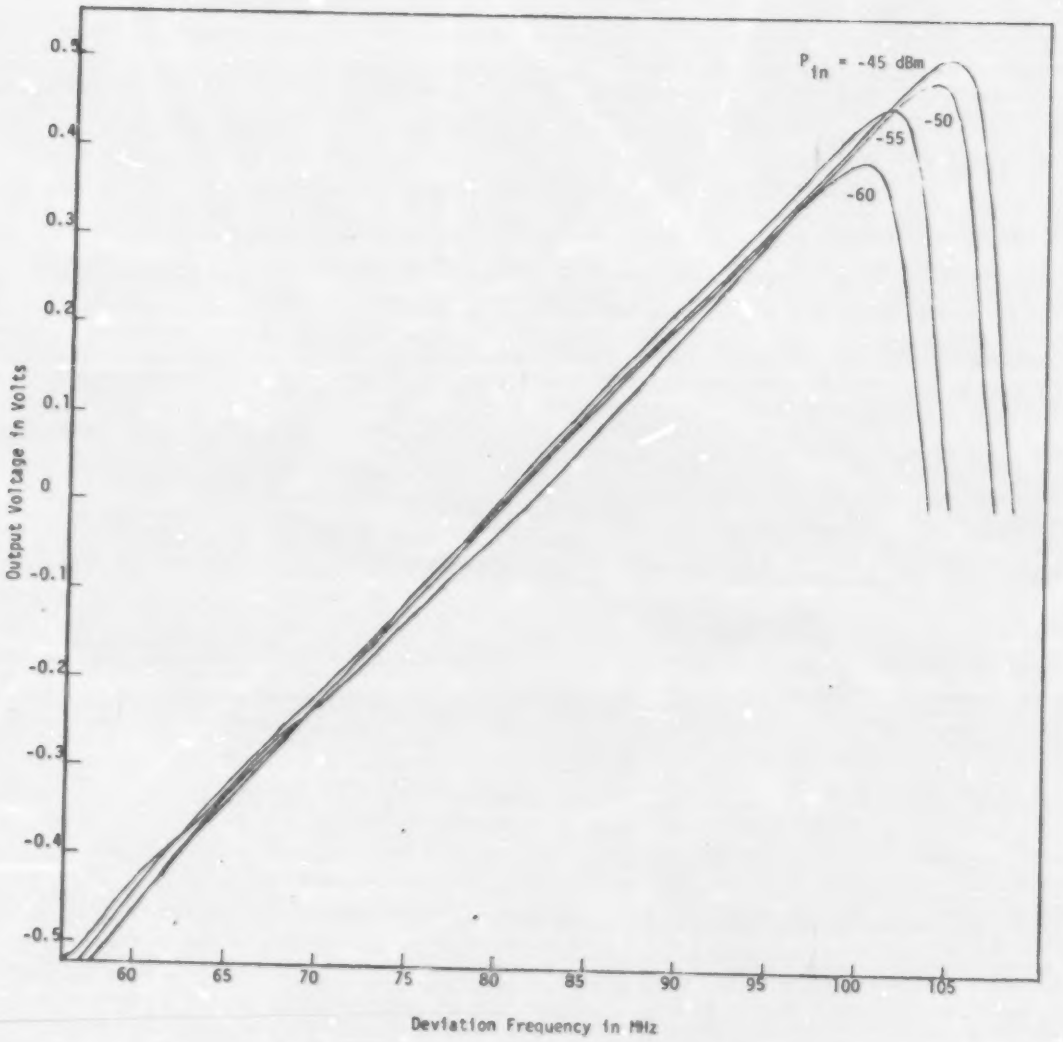

Figure 3.22 Final Amplifier Output Voltage as a Function of Input Frequency Deviation for Differing Input Power Levels

4. BRANCHING NETWORK

4.1 INTRODUCTION

This chapter is devoted to the design and theoretical prototype performance of the branching network. This network must be able to accept the twelve 40 MHz wide contiguous channels which are available at the output of the front end converter and distribute them to the appropriate baseband receivers. Consideration is first given to the desired characteristics of the individual channels, including a discussion of the required selectivity, allowable passband ripple and the amount of reverse isolation needed. This is followed by a discussion of the appropriate design of the channel dropping filters themselves. A suitable method for manifolding the filters is determined which will keep filter interactions to a minimum and provide an input which is compatible to the front end converter output.

The band pass specifications, selectivity, and reverse isolation of each channel are now considered. In order to gain some perspective about the type of selectivity and passband specifications needed for our system, let us first consider the specifications for two systems with requirements similar to ours. As reported by Comsat (18), Intelsat IV has a twelve channel input branching network, each channel having a 3 dB bandwidth of 40 MHz and a .5 dB bandwidth of 36 MHz with $< .1$ dB variation over a 32 MHz range. Leakage from adjacent channel centers $\pm$ 40 MHz away must be 50 dB below the level of the desired signal at the channel center frequency. RCA (7) describes a 24 channel system with quite similar requirements.

As described in Section 1.3 we have 12 channels each requiring a minimum usable bandwidth of 36 MHz and a 3 dB bandwidth of 40 MHz with adjacent band centers 40 MHz apart. Since there is additional filtering after the second mixer, there is no need to place as strenuous a requirement as RCA or Comsat on our out-of-band taper. Hence, we have opted for 30 dB attenuation of adjacent bandcenters. As was shown in Section 2.4, this taper, coupled with the tapers of the two IF band-pass filters, was able to provide 30 dB of suppression at the adjacent channel band edges. It is desirable to minimize the pass band ripple but still have as few elements per filter as possible. We found the value of .1 dB to be the best compromise for passband response.

Unfortunately the LO frequency for the mixer of each channel corresponds to the RF center frequency of the next-to-adjacent channel. In order to prevent interference between the LO leakage from the next-to-adjacent channel and the FM signal of interest for the given channel, the LO leakage level should be no more than the minimum detectable signal of the amplifier which is -86 dBm (see Section 2.7). Assuming that the LO level is +10 dBm, the leakage signal is at a level of -20 dBm (see Figure 2.5). This means a minimum of 66 dB reverse isolation is required at the channel's LO frequency for each filter as shown in Figure 4.1. The means of implementing this isolation are discussed in Section 4.2.

4.2 CHANNEL DROPPING FILTER DESIGN AND THEORETICAL PERFORMANCE

Initial consideration had been given to using stagger tuned amplifiers to implement the channel dropping filters. This arrangement has several important advantages. First, instead of a net

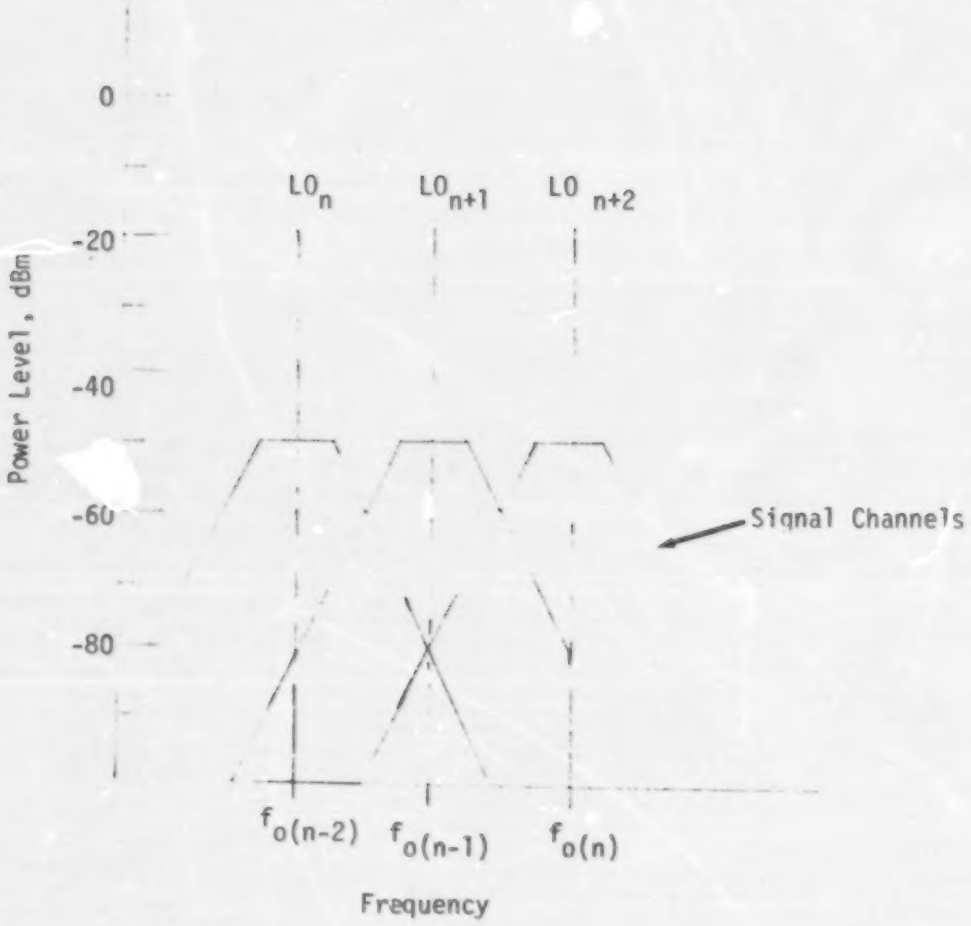

Figure 4.1 Power Levels and Frequencies of LO Relative to the Signal Channels, Dotted Lines are LO Power Level Before Isolation, Solid Lines Indicate Level After Isolation

insertion loss as would be the case if passive elements were used, a net insertion gain could be realized. Also, each transistor stage could provide a broadband reverse isolation of 20 dB. However, preliminary calculations showed that a minimum of 5 stages would be needed to obtain the desired response. In view of the cost of implementing such a structure, it was felt that a more conventional approach be tried.

Subsequent investigations revealed that use of side coupled half-wavelength ($\lambda/2$) resonators implemented in stripline presented the best solution based on overall economy and ease of implementation. An example of such a structure is shown in Figure 4.2. Matthaei et. al. (19) give step by step methods for determining the dimensions of the resonators and their spacing. For our purposes it was found that the nomograms supplied by Matthaei did not have sufficient accuracy for determining the dimensions. For this purpose, T. Monsees has implemented a FOCAL program using a Fibonacci search and polynomial representation of the elliptic integrals in Matthaei's equations 5.05-1 and 5.05-4 to accurately determine the dimensions. Use of this program is explained in Appendix 7.6 of this report.

By applying the methods outlined in section 7.1.3, the number of resonators is first determined. For a passband ripple of .1 dB, bandwidth of 36 MHz and attenuation of 30 dB, 40 MHz from the band center, at least 5 resonators are needed for each filter.

In order to get some idea as to the difficulties encountered when attempting to physically realize these filters, a prototype design for use at f_o = 1240 MHz, the bandcenter, is considered. This filter

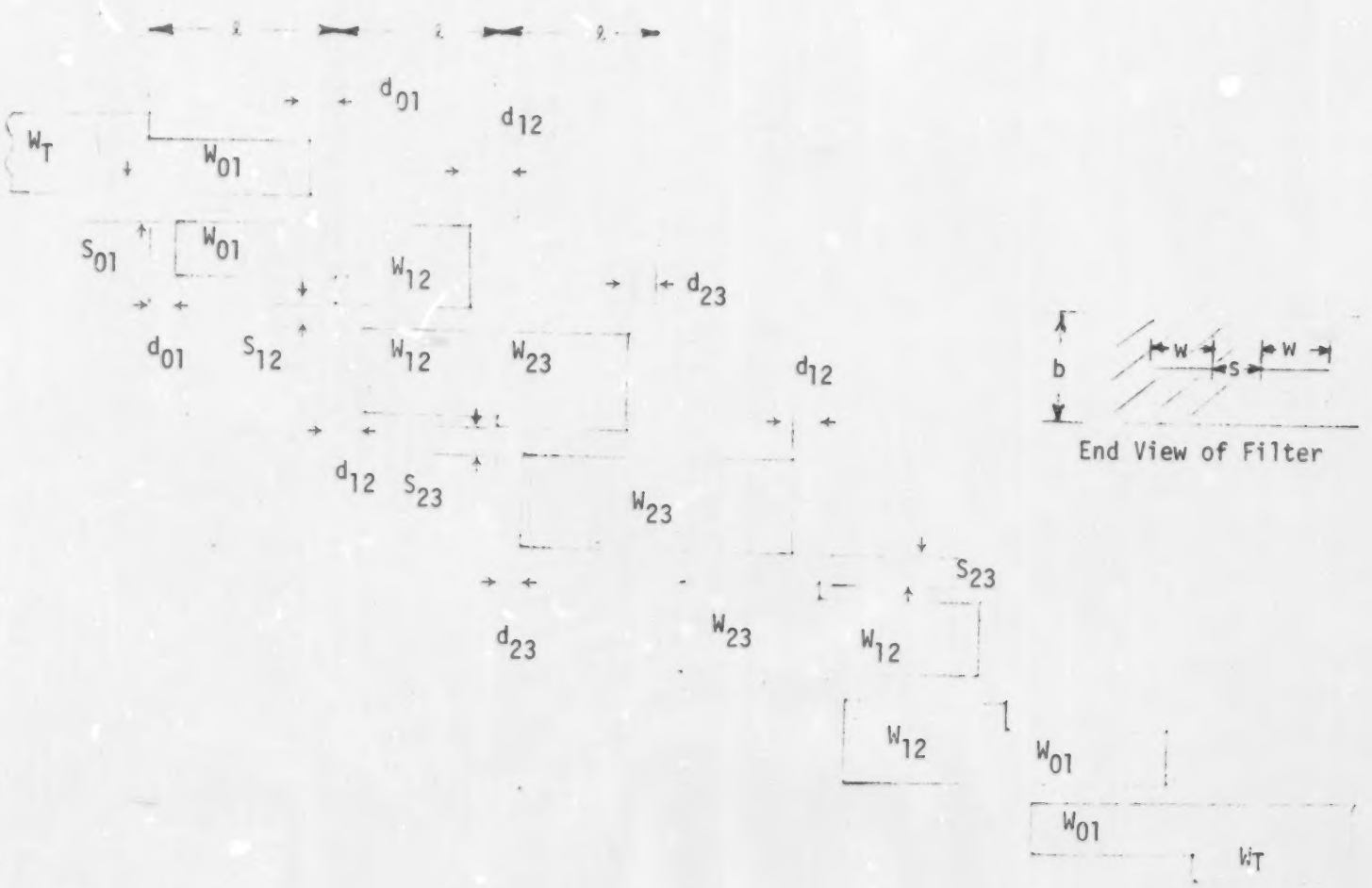

Figure 4.2 Five Resonator Parallel Coupled Resonator Filter

is to be fabricated on 3M* type GX-060-55 1/16" thick "Cu-Clad" board which has $\varepsilon_r = 2.56$. Applying the methods of Section 8.09 of Matthaei et. al. (19) the values of even and odd mode impedance for each of the resonators are first computed. Then applying the methods of Section 5.05 of Matthaei and Appendix 7.6 of this report, the filter dimensions are obtained as shown in Table 4.1.

All of these filters are symmetric devices. Hence, based on the forward characteristics of 40 dB attenuation 40 MHz away from band-centers, they should be able to provide at least 60 dB of isolation to the LO leakage from the baseband channel mixer. An additional 10 dB of isolation can be obtained with a single transistor amplifier which has a nominal reverse isolation of 20 dB and a forward gain of 10 dB. A standard amplifier for this is given in Figure 4.3. The operating characteristics for this amplifier are given in Figure 4.4 - 4.6. It should be noted that the amplifier has a nominal gain of 10 dB and reverse isolation is greater than 17 dB. Input and output return loss are > 10 dB and > 5 dB respectively. Forward isolation is nominally 8 dB.

Using MICTPT (20) it is possible to simulate, on a computer, the filter itself to obtain its theoretical frequency response as shown in Figure 4.7. As can be seen this filter should provide .1 dB passband ripple with 35 dB of attenuation 40 MHz from bandcenter and an attenuation of 68 dB 80 MHz from bandcenter. It seems quite possible that the filter alone will be able to provide the necessary

---

*Trade name Minnesota Mining and Manufacturing Company, Minneapolis, Minnesota.

Table 4.1 Dimensions of Parallel Strips
Normalized to b = 1/8 inch

j	$w_{j,j+1}$	$s_{j,j+1}$	$d_{j,j+1}$
0	.6500 ± .0003	.1739 ± .0001	.165
1	.7143 ± .0001	.6463 ± .0003	.165
2	.7155 ± .0001	.7318 ± .0003	.165

The length ℓ is a quarter wavelength at the center frequency f_o.

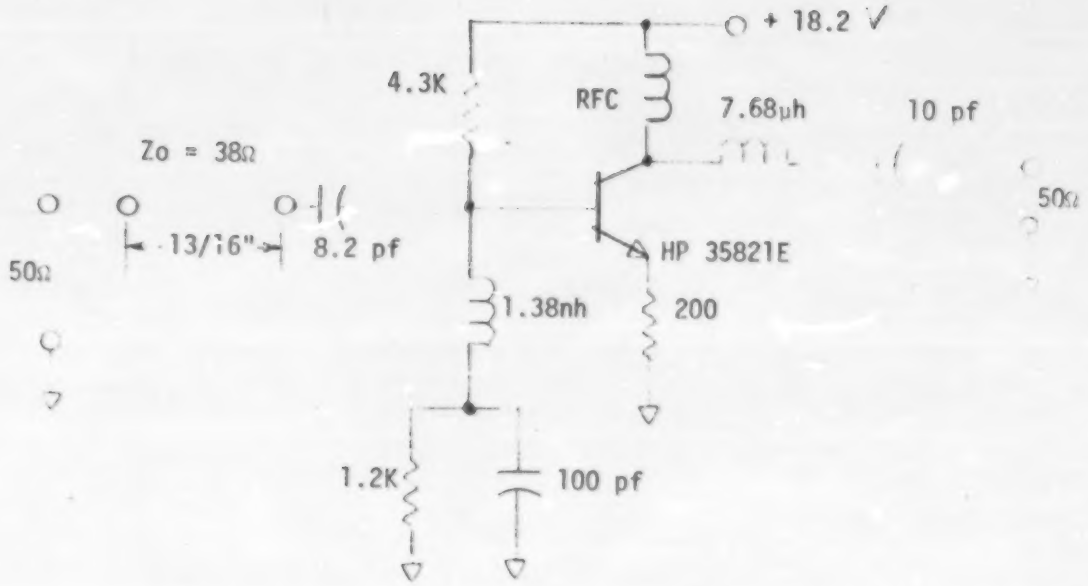

Figure 4.3 Filter Amplifier Schematic

BEST COPY AVAILABLE

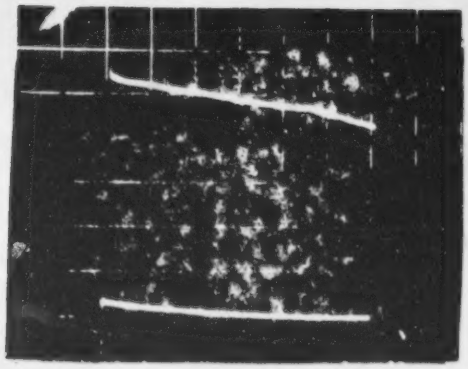

Amplifier Gain (V: 2 dB/cm)
(Lower Trace is 0 dB Reference)

Reverse Isolation (V: 5 dB/cm)
(Upper Trace 0 dB Reference)

Figure 4.4 Filter Amplifier Gain and Reverse Isolation Over the Range of 1.0 to 1.4 GHz

BEST COPY AVAILABLE

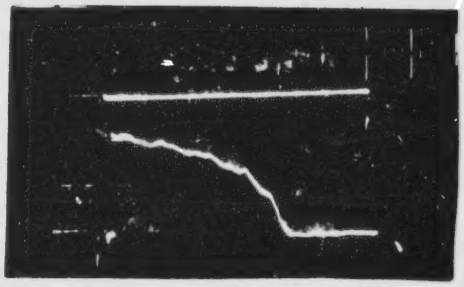

Input Return Loss (V: 10 dB/cm)

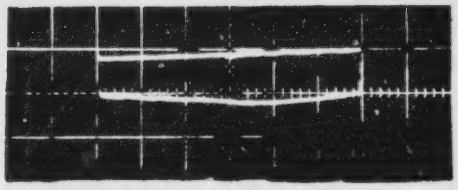

Output Return Loss (V: 5 dB/cm)

Figure 4.5 Input and Output Return Loss Swept Over the Range of 1.0-1.4 GHz with Upper Trace Showing 0 dB Reference

BEST COPY AVAILABLE

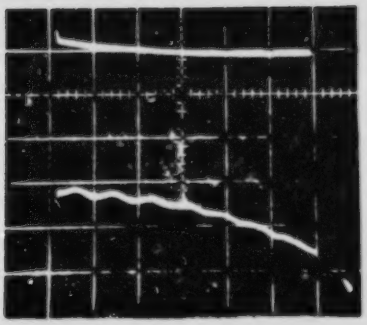

Figure 4.6 Forward Isolation:Frequency Swept from 1.0 to 1.4 GHz
with Top Trace or 0 dB Reference and
Vertical Scale of 2 dB/cm

BEST COPY AVAILABLE

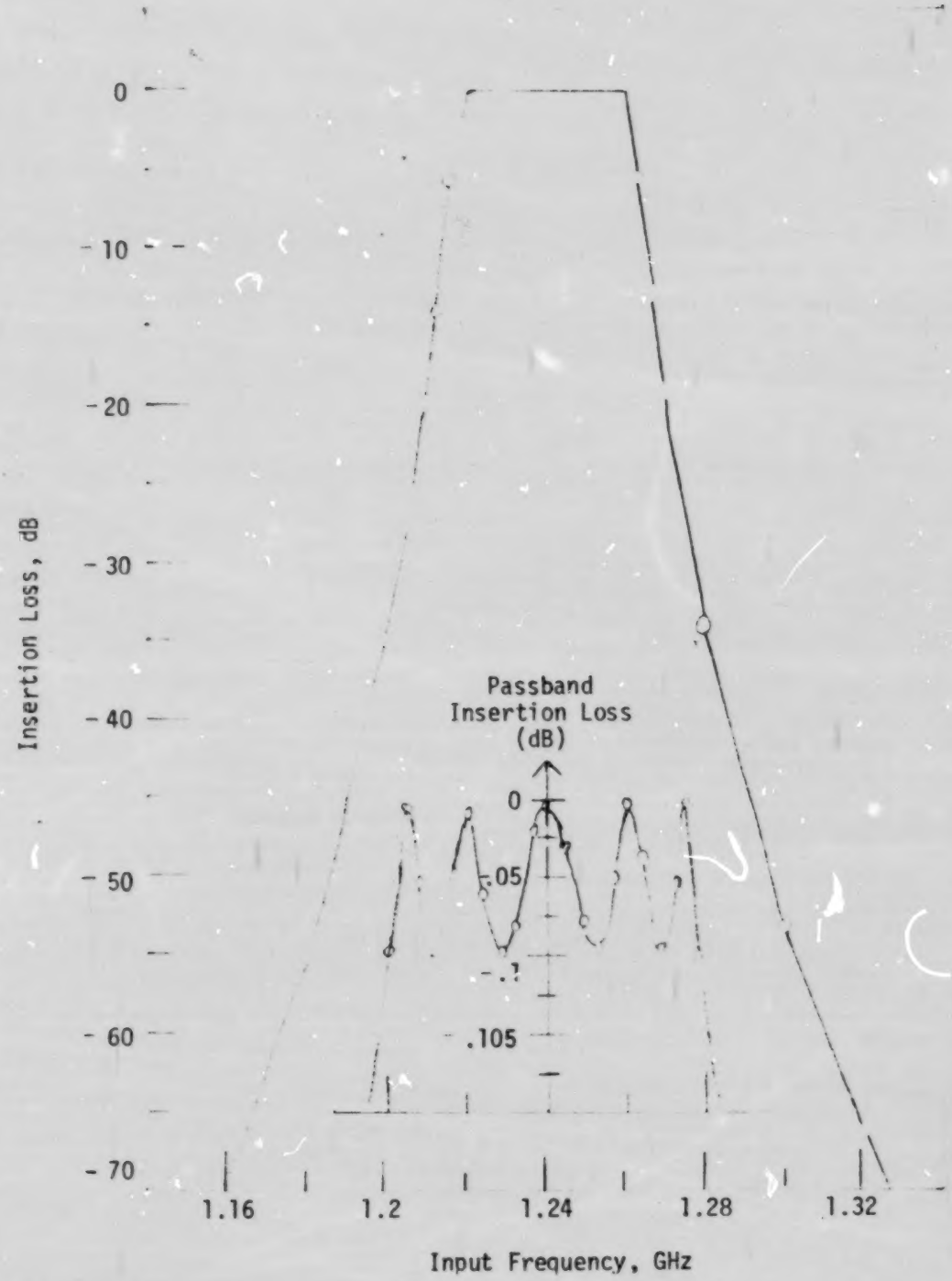

Figure 4.7 Theoretical Prototype Channel Dropping Filter Performance

reverse isolation. However, these characteristics are based on ideal loss free considerations. Ultimately, the need for an amplifier stage will be determined by the experimentally measured characteristics of an actual filter. Even if the reverse isolation requirements are met, distributed losses in the filters and manifold may require the need for the extra gain afforded by the amplifier.

4.3 PROTOTYPE FILTER PERFORMANCE

When the prototype 5 resonator filter outlined in Section 4.2 was built and tested subsequent measurements indicated a response of the form shown by the experimental curve given in Figure 4.8. As can be seen, there is no visible ripple; the response is somewhat rounded. The 4 dB bandwidth is 40 MHz and the midband insertion loss is approximately 4.2 dB. As will be seen, these results are the best that can be expected based on our present choice of materials.

Applying methods outlined by Matthaei (19) the expected value of midband insertion loss is first calculated. The increase in midband insertion loss due to the finite Q's of the resonators is given by

$$(\Delta L_A)_0 = 20 \log \left(\frac{C_n}{Q} + 1\right) \approx 8.686 \frac{C_n}{Q} \tag{4.1}$$

where C_n is obtained from Figure 4.13-2 of Matthaei (19) and

$$Q = wQ_u \tag{4.2}$$

where w is the fractional bandwidth and Q_u is the unloaded Q of a single resonator. The Q's of each of the resonators are assumed the same. In general

$$Q_u = \frac{Q_c}{1 + Q_c \tan\delta} \tag{4.3}$$

where tanδ is the dissipation factor and Q_c is the Q due to copper losses. Q_c is obtained from Fig. 5.04-4 of Matthaei (19). Applying Equ. 4.1 - 4.3 to our particular filter, we find that $Q_u \cong 251$ and $(\Delta L_A)_0 \cong 4$ dB. Allowing .2 dB for connector losses, the measured value of 4.2 dB is not an unreasonable value of midband insertion loss.

Since the resonator Q's are now known, it is possible to use MICTPT (20) to model the actual lossy structure on a computer. In this manner, the theoretical response shown in Figure 4.8 is obtained. Also, for comparison purposes, a point-by-point plot of the experimental response is shown. As can be seen, the shapes of both the experimental and theoretical lossy response are similar. However, the experimental response is shifted down 10 MHz. This corresponds to an error of about .8%. This error is not unreasonable when one considers the work of Cohn (21) who was able to achieve a minimum error of .6% after 3 attempts in building a similar structure. This error is largely due to the inability to accurately determine the dimensions $d_{j,j+1}$ as shown in Figure 4.2. It will be desirable in future designs to flatten out the response somewhat and insure that the 3 dB bandwidth is at least 40 MHz. However, the response shape is to a great degree limited by the resonator Q's.

4.4 MANIFOLD DESIGN AND PROTOTYPE PERFORMANCE

A suitable manifolding scheme must be realized to distribute the signals and keep filter interactions to a minimum while providing a low VSWR to the front end converter output. A straightforward approach to this problem would be to split the output of the front end using a 3 dB hybrid with all even and odd channels on separate

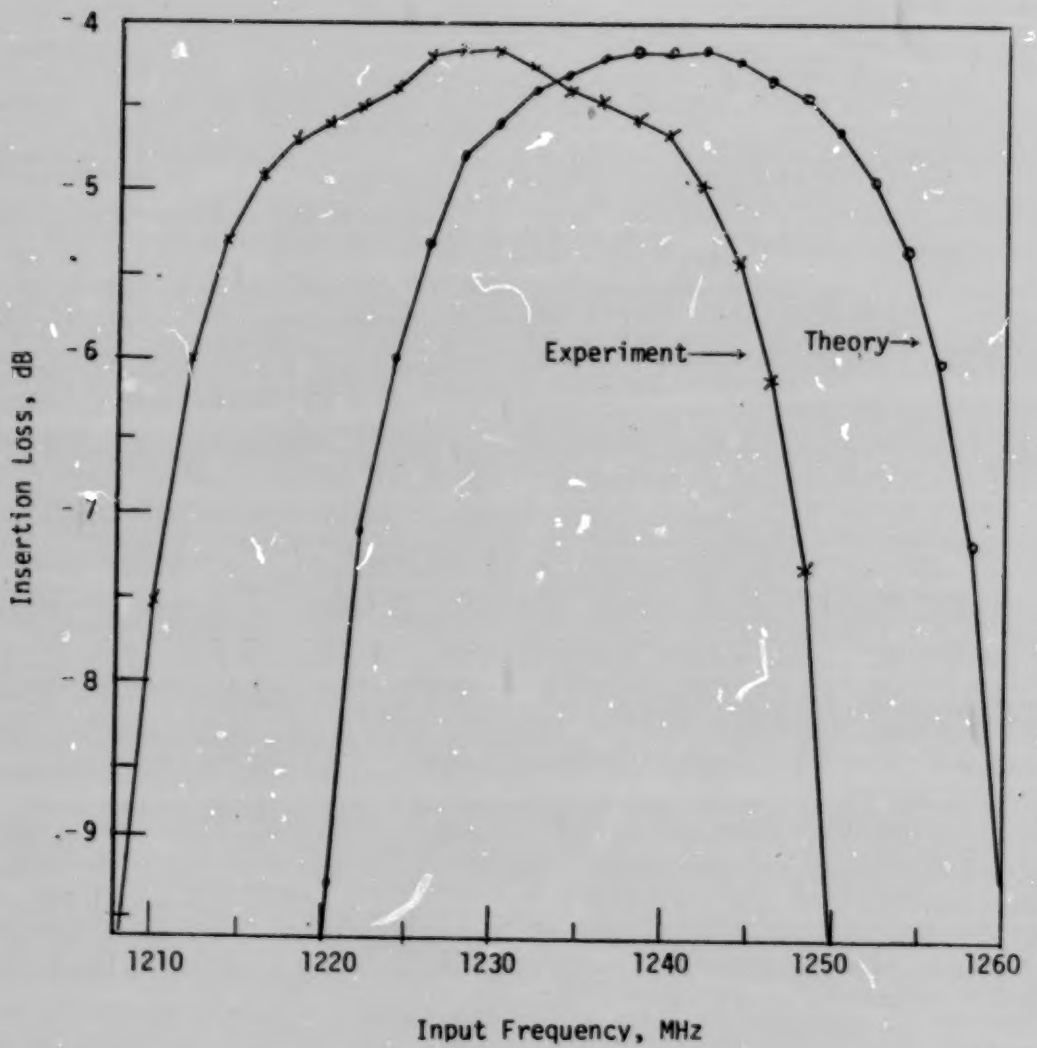

Figure 4.8. Experimental and Theoretical Responses for Prototype Channel Dropping Filter

lines. Circulators would be used at the inputs to each filter. In this way, the filters would be electrically isolated from each other and their interaction minimized. Also, a low VSWR is presented to the front end output. This approach, however, is undersirable since the use of circulators adds to the size, weight, and insertion loss of the structure and increases its cost.

Edson and Wakabayaski (22) suggest the use of singly terminated filters appropriately spaced along one "feeder" transmission line. To provide a low input VSWR, adjacent channel band edges are to be down 3 dB. The physical arrangement of the filter is such that the impedance of the center filter is pure real with all filters to the left of center providing a capacitive reactance and those to the right being inductive at the center frequency of the input. These susceptances modify the original transmission line into two separate regions having opposite impedance tapers. Although this method avoids the use of circulators, it does produce other problems. The spacing of the filters along the feeder line must be determined experimentally. The method is optimum for channels near the center and breaks down for channels at both ends.

A more systematic approach to the design of multiplexers is described by Atia (23). Doubly terminated filters are appropriately spaced along a feeder transmission line. The correct spacing is determined by computer optimization to reduce loading effects of near-by filters, and there is no required cross-over points for adjacent bandedges. Optimum performance for all channels can be obtained with little filter interaction. Although this method was reported for a waveguide multiplexer design, the same approach can be applied to realize similar structures in stripline.

The arrangement of the branching network intended for use in our receiver is shown in Figure 4.9. The channel dropping filters are as described in Section 4.2. A 3 dB hybrid is used to separate the even and odd channels into two separate 50 Ω distribution lines in order to reduce the amount of adjacent channel interference. Two isolators are necessary to provide a low input VSWR for the front-end converter output and to provide isolation for the even (or odd) channels rejected by the filter manifold. It may be possible to use only one isolator at the input if the hybrid provides sufficient isolation between the two distribution lines. Since dielectric and copper losses are greater at the higher frequencies, it is desirable to locate the higher frequency filters nearer the source.

Appropriate line lengths ($\ell_{j,j+2}$) between the filters can be determined by computer techniques. Since the even and odd numbered filters are to be well isolated, the operation of the entire branching network is satisfactorily determined by considering either set of filters. Hence, for analysis purposes, only the odd numbered filters are considered. The spacings are adjusted such that at its center frequency each filter sees and open circuit looking away from the source. This process is initiated by first using MICTPT (20) to find the input impedance to BPF_1, at the center frequency for BPF_3 (f_3). A Smith Chart is then used to determine the length of line ($\ell_{1,3}$) required for BPF_3 to see an open circuit at f_3 when looking toward BPF_1. Then the input impedance for the parallel combination of BPF_3 and BPF_1 in series with $\ell_{1,3}$ is computed at f_5. Again, using a Smith Chart, the appropriate length of line ($\ell_{3,5}$) is determined as before. In this manner, the required line lengths are

BEST COPY AVAILABLE

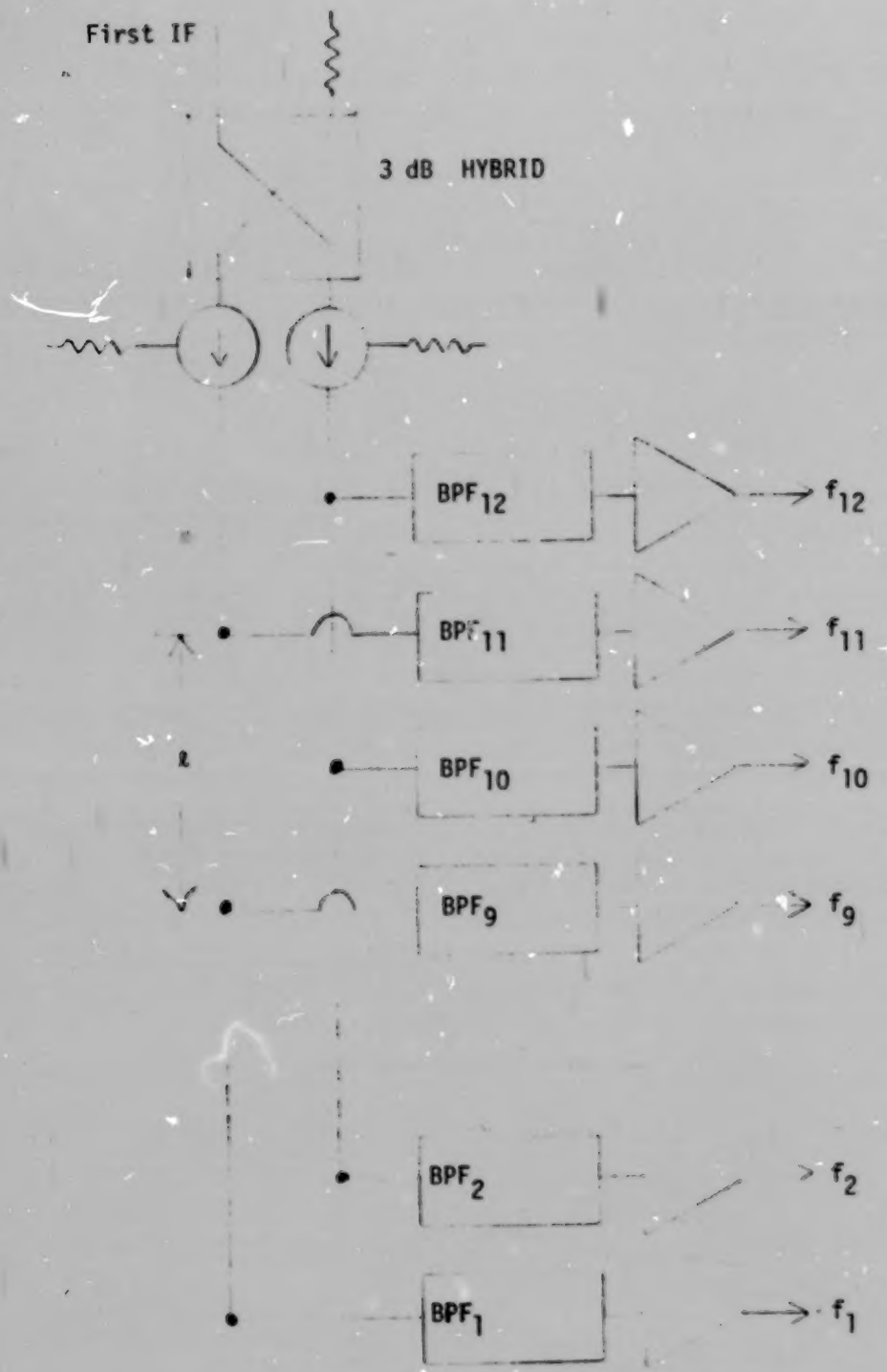

Figure 4.9. Branching Network

determined. Initial calculations yielded line lengths which were too short to be physically realizable. By adding a half wavelenth ($\lambda_5/2$) line to the originally calculated length for $\ell_{3,5}$ and repeating the procedure, physically realizable line lengths are obtained as shown in Table 4.2, where the guided wavelength λ_j in inches corresponding to the center frequency of the jth filter (f_j) is given by:

$$\lambda_j = \frac{3 \times 10^{10}}{f_j\sqrt{\varepsilon_r}\,(2.54)} \text{ in.} \tag{4.4}$$

when ε_r, the relative permitivity of the substrate, is taken to be 2.56 (see Section 4.2). The structure is to be realized as a 50 Ω stripline with taps on the line for connection to the appropriate filters.

In order to test how well this branching network scheme should perform, MICTPT (20) is again used to examine the insertion loss of each filter and the return loss at the input to the manifold as a function of frequency. The results of this calculation are shown in Figure 4.10. The out-of-band attenuation characteristics closely resemble those for a typical filter operating without interaction with other filters (see Figure 4.7). The in-band return loss is reasonable with typical values > 15 dB. The worst case is for BPF_1, which is at the end of the line. Figure 4.11 shows a typical passband response of the filters used in this scheme. Although the response is not equi-ripple as shown in Figure 4.7, the maximum ripple variation is still only ~.1 dB. Hence, although there is some impedance interaction with the rest of the network, it does not appear to seriously degrade filter performance.

Table 4.2 Line Lengths for Manifold

j	$(\ell_{j,\,j+2})\ (\lambda_{j+2})$	$\ell_{j,\,j+2}$ [inches]
1	$.0335\lambda_3$	.2208
3	$(.0145)\lambda_5 + \lambda_5/2$	3.1673
5	$(.4710)\ \lambda_7$	2.716
7	$(.4292)\ \lambda_9$	2.330
9	$(.3961)\ \lambda_{11}$	2.030

The results of these calculations indicate that doubly terminated 50 Ω filters connected at appropriate points along a 50 Ω distribution line should provide an adequate means of implementing the branching network. It must be pointed out that the analysis of the performance does not take into account the discontinuities of the distribution line where the filters are tapped in. Also, the distribution line and the filters are considered to be loss free. However, in spite of these simplifications, the analysis does provide enough information for the synthesis of a first-cut prototype design. Furthermore, a more realistic model for the manifold could be implemented in a subsequent design effort.

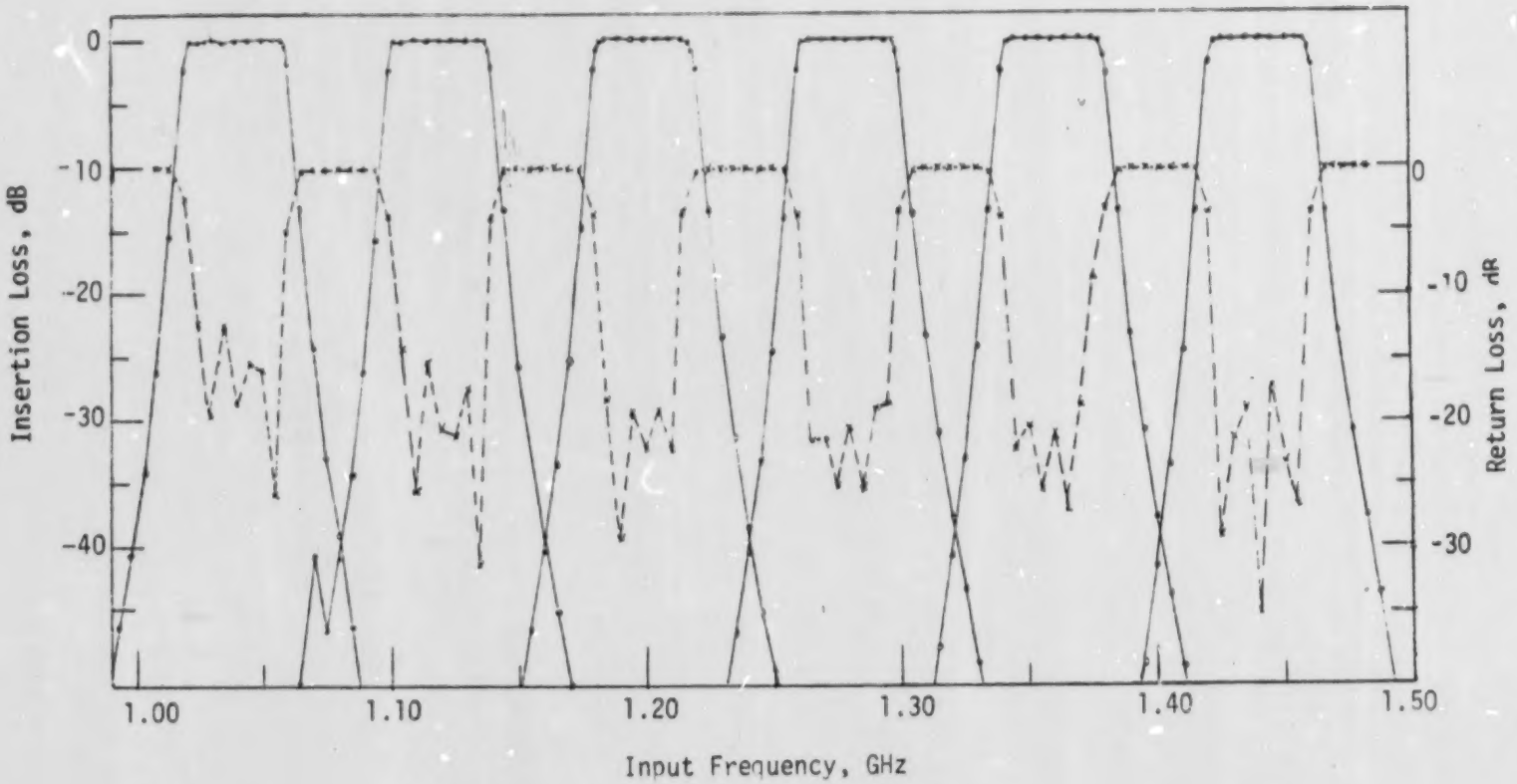

Figure 4.10. Branching Network Insertion Loss (Solid Line) and Return Loss (Dotted Line) as a Function of Input Frequency

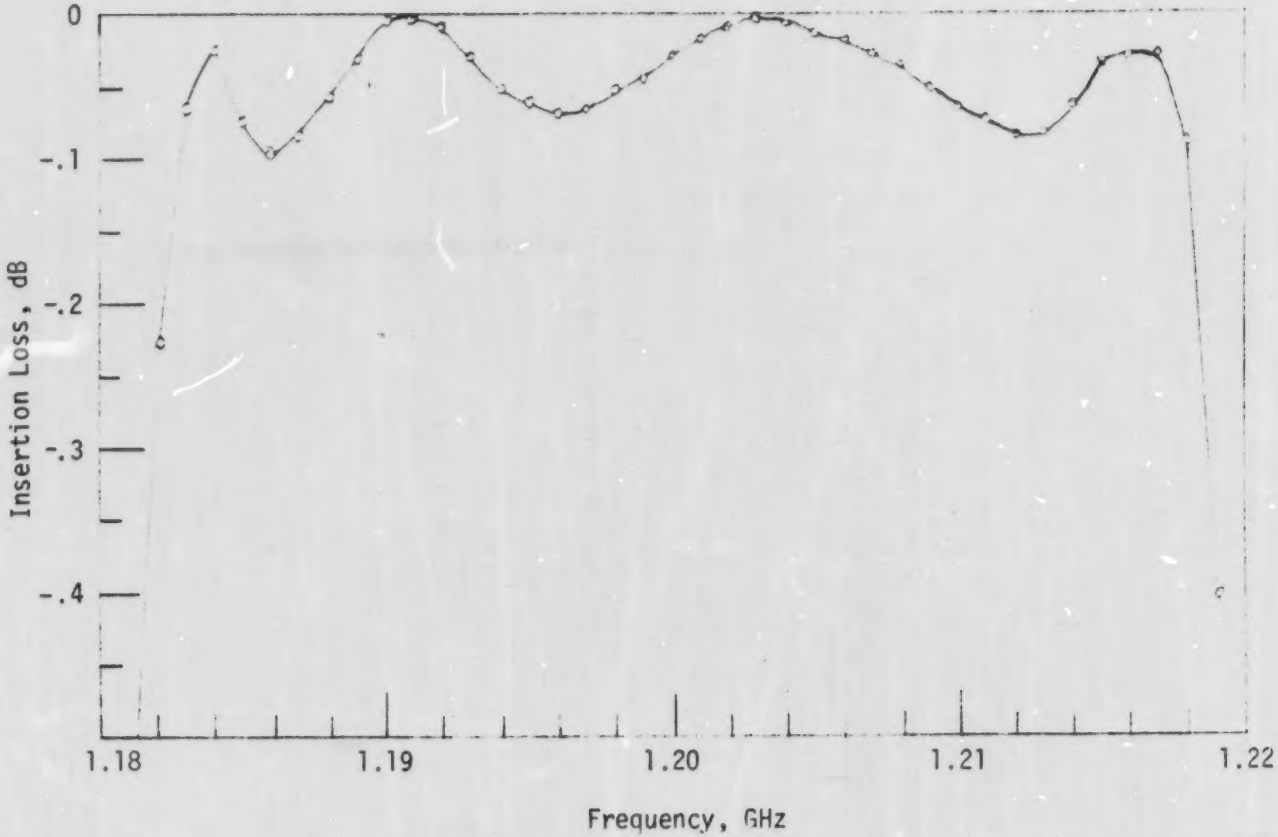

Figure 4.11. Passband Response of a Typical Filter

5. CONCLUSIONS

5.1 PRINCIPAL RESULTS

As part of the low cost objective of the receiver, several innovative design approaches were used to implement various subsystems. Instead of using the conventional approach of cascading several transistor stages containing discrete components, the IF amplifier used in the present effort uses a cascade of 3 linear high frequency integrated circuits driving a single feedback pair of transistors. Such an arrangement is very economical since it is easy to design, uses few components and can be assembled in a short time.

The 4-pole and 7-pole filters used in conjunction with the IF amplifier for shaping the channel passband used standard fixed capacitors and required a total of 4 tuning capacitors for alignment. The inductors had to be hand wound. However, if used in large quantities they could be custom manufactured quite economically. The measured passband ripple of these structures was greater than the theoretically predicted value due to the use of lossy elements having a 5% tolerance. The passband response could have been smoothed had we opted for more adjustable elements. However, since the increased filter ripple did not seem to adversely affect the overall system performance, such measures were deemed unnecessary. In this manner we have attempted to keep the time for filter assembly and alignment to a minimum.

For the limiter, we have used two identical back-to-back diode arrangements separated by a single transistor amplifier. A brief theoretical analyses of this circuit is given in Section 3.2 and a

set of design equations are formulated. Experimental results were found to correlate well with the theory. The measured dynamic range and frequency response of this structure indicated that it would perform quite well in the overall system.

Since the discriminator will detect the higher order frequency components contained in the limiter's output, it was necessary to insert a 9-pole low-pass filter between the limiter and discriminator. This filter was constructed entirely with fixed elements and gave satisfactory performance.

The approach used in the discriminator's design is particularly unique. A modified transmission line discriminator which uses a lumped element equivalent for the transmission line networks has been implemented. This structure has an extremely linear output response. A complete analysis of the conversion from distributed to lumped parameter systems is given in Section 3.4. The results of this analysis were used to determine a set of design equations and predict the theoretical performance. The discriminator used in this receiver uses only two standard input resistors, two standard inductors and one variable capacitor for adjusting the center frequency.

The baseband output amplifier is a relatively standard design. To convert from L-band to the 80 MHz IF a low-cost commercially made mixer has been used.

The proper branching network design has been determined by computer simulation. The channel dropping filters utilize a side coupled resonator design implemented in stripline. To eliminate adjacent channel filter interaction two manifolds separated by a 3 dB

hybrid are employed with odd and even numbered channels on separate manifolds. The optimum spacing of the filters along the manifolds is determined by computer simulation.

All of the baseband channel subsystems have been housed in a 1 x 3 x 12 3/16 inch box supplied courtesy of Martin-Marietta, Aerospace, Communications and Electronics division. The complete package is shown in Figure 5.1. Its total weight is 1 2/3 lbs. To prevent oscillation, shielding was required between the first and second preamplifier stages and also between the IF amplifier output and limiter input. To prevent interference from spurious signals the box is made RF tight overall. Two DC feed through connectors are required for connection to a ± 32 volt power supply. The RF and LO inputs use OSM connectors. The video output uses a BNC connector. Complete performance results for the subsystems considered in this report are given in Table 5.1. The estimated cost of components, assembly, alignment, etc. are given in Table 5.2.

Table 5.3 shows the estimated cost of the branching network. It is anticipated that the LO chain could be built for about $3000 and the antenna cost should be no more than $2000. The estimated delivered cost of the entire receiver is given in Table 5.4.

Based on the performance results of existing prototypes and the cost analysis it can be seen that a low cost multi-channel receiver can be realized.

5.2 FUTURE WORK

The work previously described in by no means complete. A number of important areas of interest have yet to be explored.

(1) The overall link performance characteristics of the baseband channel must be investigated. This would include determining the amount of AM to PM conversion, FM linearity of the overall system, and a measure of the overall group delay. The group delay measurements are of course required for determining the design of group delay equalizers, if they are in fact needed.. Ultimately this system will have to be tested by using an actual color TV FM signal applied to the input.

(2) Now that a set of basic design criteria for the branching network has been developed a prototype model should be constructed and tested.

(3) Consideration should be given to implementing circuitry for obtaining the 12 required LO frequencies.

BEST COPY AVAILABLE

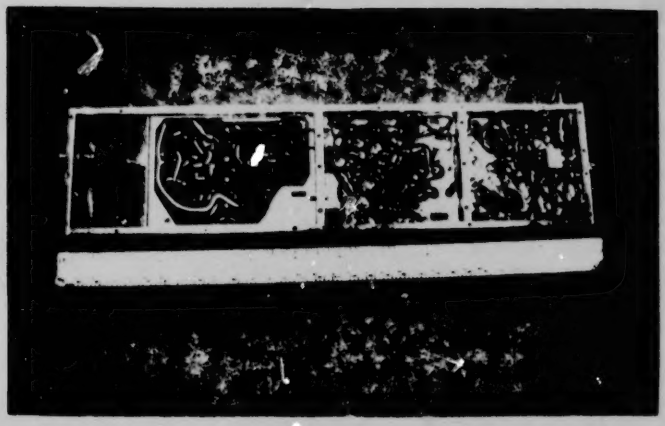

Figure 5.1 Baseband Channel Package

Table 5.1 Performance Specifications For Baseband Channel

Input Level	-40 dBm Max into 50Ω
Minimum Detectable Signal	-86 dBm
Input Return Loss	>15 dB
Output	1 Vpp into 75Ω
IF	80 MHz
Overall Bandwidth	1.0 - 1.5 GHz
Bandwidth per Channel	36 MHz ± .5 dB
Channel Selectivity	30 dB Suppression of adjacent Channel Bandedges
DC Power Supply	± 32 volts 10 watts
Dimensions	1 x 3 x 12 3/16 inches
Weight	1 2/3 lbs.
Mixer -	
LO Input Level	+ 10 dBm
LO Input Return Loss	>10 dB
IF Amplifier -	
Output Level	+ 16 dBm Max into 300Ω
Output Noise Level	- 2.67 dBm
Dynamic Range	15 dB
Limiter -	
Nominal Input Level	+ 10 dBm
Dynamic Range	10 dB
Input Impedance	300Ω
Discriminator	
Input Impedance	300Ω
Output Linearity	<1% Deviation from Linearity

Table 5.2 Cost Estimate for One Baseband Channel

Price per Unit in Quantities of 1000

Bill of Materials:	
Miscellaneous Resistors and Capacitors	$ 4.30
Miscellaneous Semiconductors	22.00
Mixer	20.00
OSM Connectors (2)	2.25
Aluminium for Housing	2.00
Miscellaneous Hardware	2.00
	$52.55
Labor (Estimated)	
Machining of Housing	$35.00
PC Board Processing	2.00
RF Assembly and Test	75.00
	$112.00
Total	$164.55

Table 5.3

Estimated Cost of the Branching Network

Quan.	Item	Cost
1	3 dB Hybrid	50.00
2	Circulators	300.00
3	Loads for Hybrid and Circulators	30.00
12	Channel Dropping Filters	600.00
2	Manifolds	200.00
	Miscellaneous Hardware (connectors, etc.)	50.00
	Assembly and Test	350.00
	TOTAL	$1580.00

Table 5.4

Estimated Delivered Cost of the
Entire Ground Station

Antenna	$2000.00
Westinghouse Front-End	250.00
Branching Network	1580.00
12 Baseband Channels	3600.00
LO Chain	3000.00
DC Power Supply	200.00
Alarm Circuits	500.00
Total Delivered Price	$11,130.00

6. ACKNOWLEDGEMENT

This work was supported by the Center for Development Technology of Washington University through NASA Grant NGR-26-008-054.

7. APPENDICES

7.1 FILTER DESIGN

7.1.1 Introduction

The following sections will be concerned mainly with the techniques used to design the filters which were used in the IF amplifier and limiter (see Chapters 2.4, 2.5, and 3.3). We will concentrate mainly on the design of the low pass, high pass, and band-pass filters, doubly terminated and having a Tchebycheff response. We first describe a fundamental set of design equations based on the low pass prototype, then show how the band-pass and high pass structures can be realized from this basic prototype. We will then proceed to show how the design equations can be implemented with computer programs suitable for use on a small on-line computer to quickly and accurately design actual structures.

7.1.2 Prototype Equations and Low-Pass Filter Design

It can be shown from the work of Matthaei et. al. (19) that one can use the Tchebycheff polynomials to obtain an expression that relates the out of band insertion loss at a given frequency to the ripple, cut-off frequency, and the number of reactive elements in a low-pass filter;

$$L_F(\omega_a) = 10 \log_{10} \left\{1 + \varepsilon \cosh^2 \left[n \cosh^{-1} \frac{\omega_a}{\omega_1}\right]\right\} \qquad (7.1.1)$$

where: L_F = insertion loss in dB

n = number of elements

ω_1 = cut-off frequency in rad/sec

ω_a = frequency in rad/sec beyond the cut-off frequency where we desire to have a loss of L_F.

and: $$\varepsilon = \left[\log_{10}^{-1} \left(\frac{L_R}{10}\right)\right] - 1 \qquad (7.1.2)$$

where L_R is the ripple in dB, (see Figure 7.1.3).

This equation was then written in a FOCAL program as shown in Figure 7.1.1, to solve for the number of elements required for a given ripple, L_R, cut-off frequency, W_c, out-of-band attenuation, LF, and W, the frequency at which this out-of-band attenuation is specified.

It will be shown later how equation 7.1.1 can be used to determine the number of elements for high-pass and band-pass filters through appropriate mappings.

Structurely, the low-pass filter can exist in four different forms, each having the same response as illustrated in Figure 7.1.2 The values g_1 through g_n represent normalized values of series inductance and parallel capacitance. In Figure 7.1.2 a and b, g_o is the normalized generator resistance, R'_o. In Figure 7.1.2 c and d, g_o is the normalized generator conductance G'_o, where $G'_o = 1/R'_o$. In Figure 7.1.2 b and c, g_{n+1} is the normalized load resistance R'_{n+1}. For Figure 7.1.2 a and d, g_{n+1} is the normalized value of the load conductance G'_{n+1}, where $G'_{n+1} = 1/R'_{n+1}$.

For all doubly terminated Tchebycheff filters with L_R pass-band ripple, the g_k values which are the values of series inductance and shunt capacitance normalized to the scale $g_o=1$ and $\omega'_1 = 1$ may be computed in the following manner. We first find:

$$\beta = \ln \coth\left(\frac{L_R}{17.37}\right) \tag{7.1.3}$$

$$\gamma = \sinh\left(\frac{\beta}{2n}\right) \tag{7.1.4}$$

```
C FOCAL-12

01.11 A !!,"LF",LF,!,"LR",LR,!,"W",W,!,"WC",WC,!!
01.12 S A=FEXP(.23025*LF); S B=A-1
01.14 S C=FEXP(.23145*LR); S D=C-1
01.16 S E=FSQT(B/D)
01.17 S G=FLOOR(E*FSQT(E^2-1))
01.18 S A=W/WC; S H=FLOOR(A*FSQT(A^2-1))
01.20 S N=G/H
01.25 T N
```

Figure 7.1.1 FOCAL Program for Determing the Number of Elements in a Low-Pass Filter

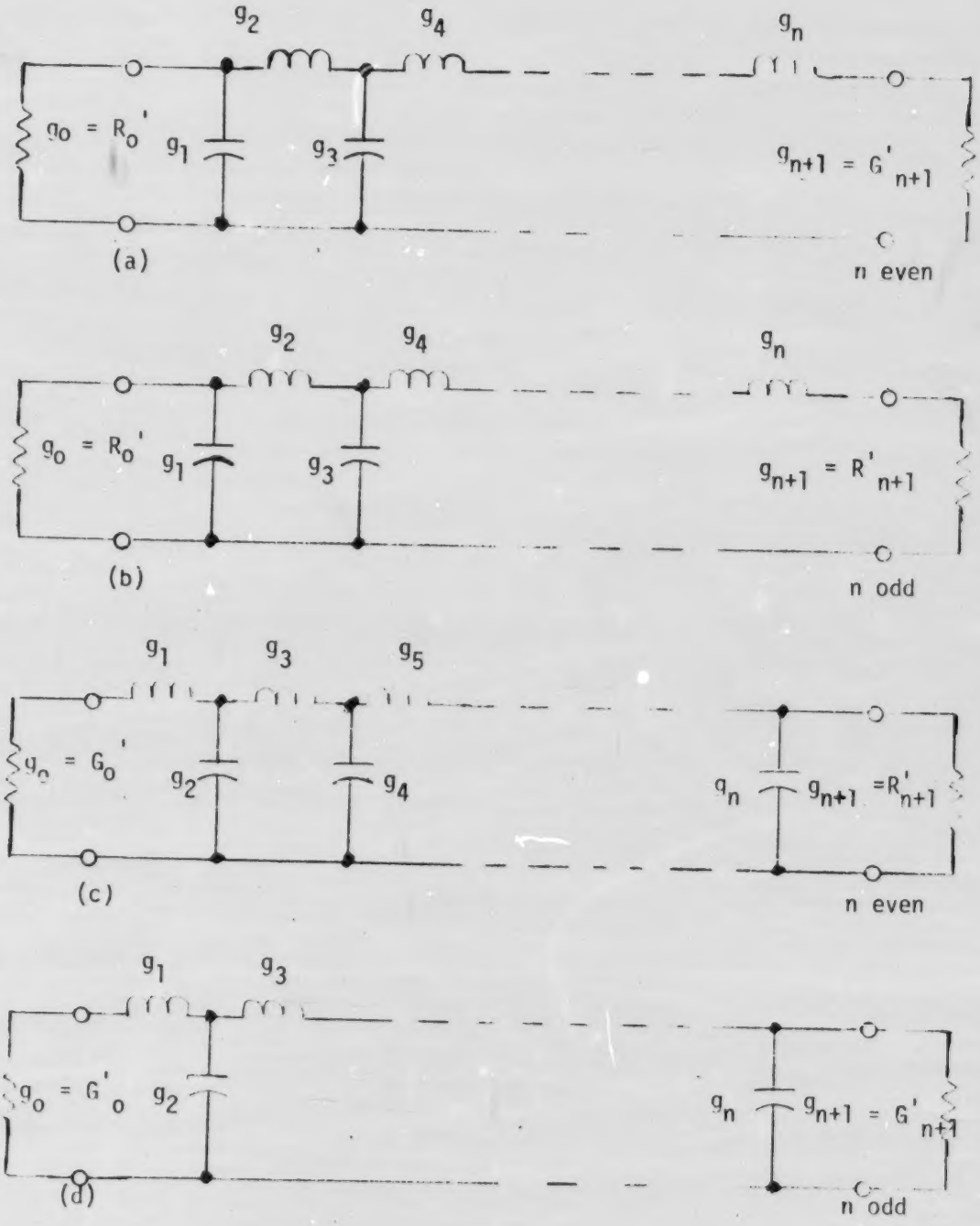

Figure 7.1.2 Low-Pass Filter Configurations

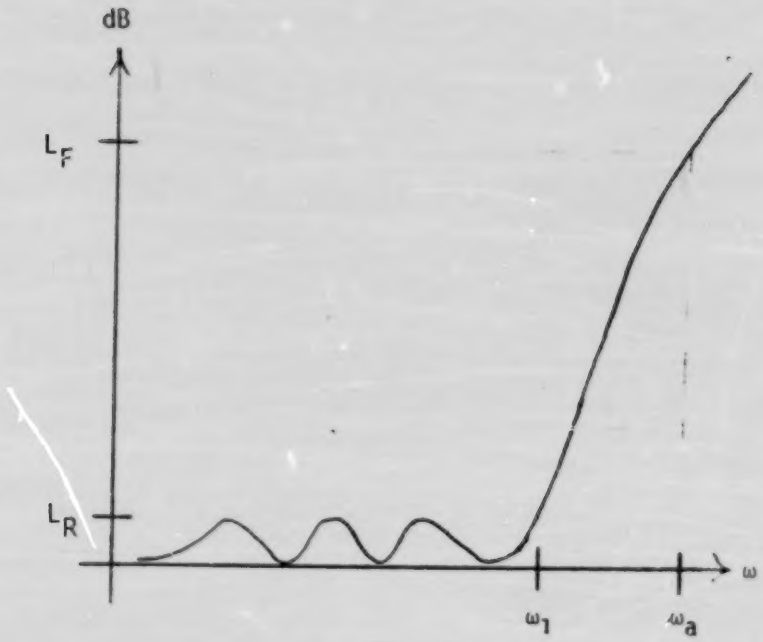

Figure 7.1.3 Low-Pass Filter Frequency Response

$$a_k = \sin\left[\frac{(2k-1)\,\pi}{2n}\right] \qquad k = 1,2,3, \cdots n \tag{7.1.5}$$

$$b_k = \gamma^2 + \sin^2\left(\frac{k\pi}{n}\right) \tag{7.1.6}$$

From the a_k and b_k parameters we can then generate the g_k parameter:

$$g_1 = \frac{2a_1}{\gamma} \tag{7.1.7}$$

$$g_k = \frac{4\, a_{k-1}\, a_k}{b_{k-1}\, g_{k-1}} \qquad k = 2,3, \cdots n \tag{7.1.8}$$

and

$$\begin{aligned} g_{n+1} &= 1 \quad \text{for n odd} \\ g_{n+1} &= \coth^2(\beta/4) \quad \text{n even} . \end{aligned} \tag{7.1.9}$$

For any low-pass structure shown in Figure 7.1.2, one can then determine the actual values of series inductance and parallel capacitance by using the following equations;

$$L_k = \left(\frac{R_o}{R_o'}\right)\left(\frac{\omega_1'}{\omega_1}\right) g_k = \left(\frac{G_o'}{G_o}\right)\left(\frac{\omega_1'}{\omega_1}\right) g_k \tag{7.1.10}$$

$$C_k = \left(\frac{R_o'}{R_o}\right)\left(\frac{\omega_1'}{\omega_1}\right) g_k = \left(\frac{G_o}{G_o'}\right)\left(\frac{\omega_1'}{\omega_1}\right) g_k \tag{7.1.11}$$

$$R_{n+1} = g_{n+1}\; R_o \tag{7.1.12}$$

where; ω_1 = cut-off frequency in rad/sec

R_o = impedance level in Ω

R_{n+1} = terminating resistance in Ω .

All primed quanties are normalized quanties. In general we set $\omega_1' = 1$, and $G_o' = R'_o = 1$

In order to solve for the required g values and the actual L and C values it is possible to write a FOCAL program to solve equation 7.1.3 through 7.1.12 as shown in Figure 7.1.4.

Here the ripple in dB, LR, number of elements, N, impedance level in ohms, RO, and the cut-off frequency in MHz, WC are to be specified. Upon execution, a print out of the normalized g values, G(K) and the corresponding values of series inductance, L(K), in μh, parallel capacitance, C(K), in pf, and the required value of terminating resistance, RT are obtained. These values are the possible values for all of the configurations shown in Figure 7.1.2. However, it is easy to see that for Figure 7.1.2 a and b, one must select the odd k subscripted values of C and the even k values for the inductors. For Figure 7.1.2 c and d, we find that this situation is reversed.

In order to show how these filter programs can be used to realize actual structures consider the design of the low pass filter and between the output of the limiter and input to the discriminator (see Chapter 3.3) the filter must have the following specifications; $\omega_c/2\pi$ = 105 MHz, L_R = .01 dB, R_o = 50Ω, L_F = 10 dB at 120 MHz. Setting LF = 10, LR = .01, W = 120, Wc = 105 in the program of Figure 7.1.1, the required number of elements is found to be 9.13823. Of course the actual number of elements used is 9. With a knowledge of the number elements, the program in Figure 7.1.4 is used to determine the g values and the actual element values. Setting LR = .01, N = 9, RO = 300, and Wc = 105, the results shown in Figure 7.1.5 are obtained.

BEST COPY AVAILABLE

```
* FOCAL-12

01.11 A "L=",L,"N",N,"  D(OHMS)",D,"  C(MHZ)",F
01.21 T !!,"  K       (K)      L(K)(UH)    C(K)(PF)",!!

02.11 S PI=3.14159265; D=L*17.47; W1=2*PI*F*1E6
02.21 S I=FEXP(1); S E=FEXP(-1); W=FLOG((I+E)/(I-E))
02.31 S BB=W/2*N; S A=(FEXP(BB)-FEXP(-BB))/2
02.41 S K=1; D 4.2; S N=2*N/(A*B) 3.4
02.51 F K=2,N; D 4.2
02.61 T (N/2-FITR(N/2))*2)4.1,4.3,4.3

03.11 S A=AN; S B=BN; S C=CN
03.21 S AN=FSIN(2*K-1)*PI/2/N; S BN=CA*CA+CB*BN((2*PI/N)**2
03.31 S CN=A*A+B*BN/BU*CU
03.41 S L=(N*D/W1; S C=CN/R/W1*1E9 4.5

04.11 S E=FEXP(BW/4); S V=FEXP(-BW/4)
04.21 S CF=L(E+V)/(E-V)**2*1E6 4.4
04.31 S CF=1
04.41 T 2.3,K,"    ",%6.5,CF,!!,"RF = ",%6.3,CF*D,!!!!
04.51 T 2.3,K,"    ",%6.5,CN,"    ",L*1E6,"    ",%4.4,C*1E12,!
```

Figure 7.1.4 FOCAL Program for Generating the g Values and Determing the Values of the Elements in a Low-Pass Filter

BEST COPY AVAILABLE

K	C(K)	L(K)[MH]	C(K)[PF]
1	.691444	1.37116	4.11512
2	1.42734	1.64692	7.21426
3	1.83434	1.82449	9.11664
4	1.71254	1.77574	8.55259
5	1.91579	1.86662	9.62911
6	1.71254	1.77574	8.55259
7	1.83434	1.82449	9.11664
8	1.42734	1.64692	7.21426
9	1.61444	1.37116	4.11512
10	1.00000		

Figure 7.1.5 Print Out of Low-Pass Filter Design Program

One of the basic configurations shown in Figure 7.1.2 must now be chosen. Since the filter has an odd number of elements and should provide a high input impedance at frequencies beyond ω_c, the prototype shown in Figure 7.1.2 d is selected. Thus the odd k subscripted values of L(k) and the even k subscripted of C(k) are used. Hence, the circuit appears as shown in Figure 7.1.6. Also, the terminating resistance RT = 300Ω. This circuit was built up and tested using hand wound inductors and fixed values of capacitance having a 5% tolerance. In Figure 3.7 one can compare the measured frequency response of the actual structure to the theoretically predicted response.

The experimental response as indicated in Figure 3.7 has about .5 dB pass band ripple and falls off much quicker than the theoretically predicted response for a .01 dB ripple filter. As expected from the theory, allowing a theoretical pass band ripple of .5 dB for the same structure results in a theoretical taper which is closer to the experimental results. It is then reasonable to assume that we could, if desired, trim the element values to smooth the passband ripple and provide less of a taper.

7.1.3 Band-Pass Filter Design

By making use of a suitable low-pass to band-pass mapping, one can use the basic low pass design equations to obtain the design parameters for a band-pass filter. The band-pass response is obtained by first folding the low-pass response to produce a symmetic curve about the frequency origin and then translating this response to the desired center frequency, ω_0, to produce the band pass response as shown in Figure 7.1.7. The low-pass to band-pass mapping is;

BEST COPY AVAILABLE

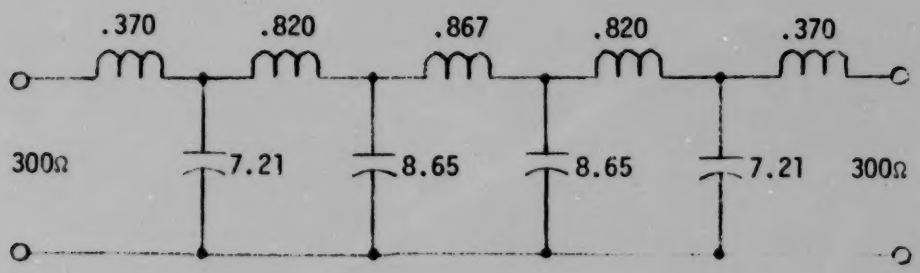

All Inductors in μh

All Capacitors in pf

Figure 7.1.6 Low-Pass Limiter Filter

BEST COPY AVAILABLE

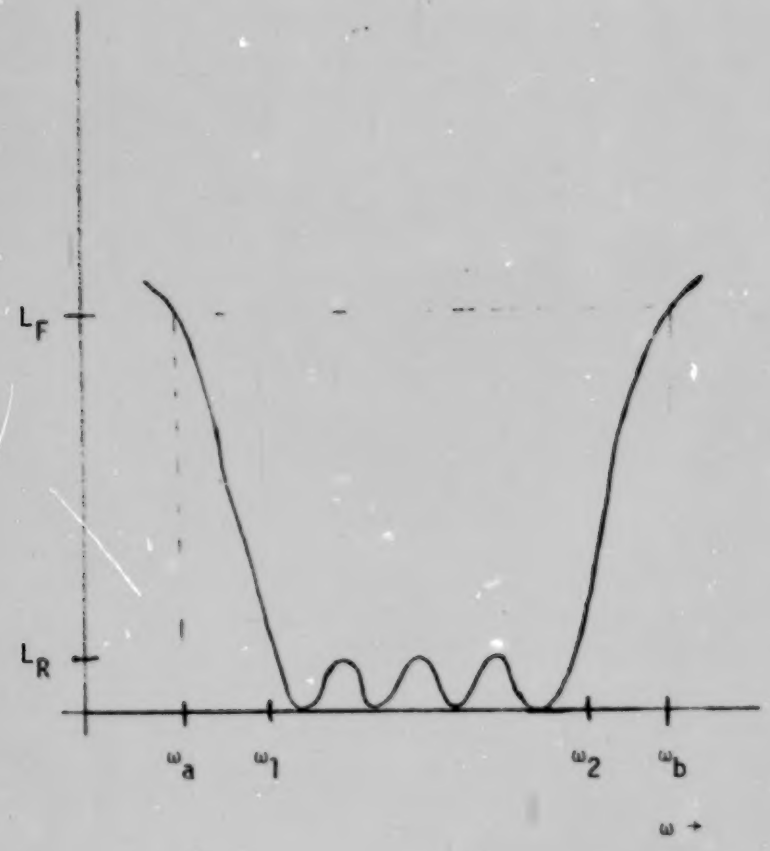

Figure 7.1.7 Frequency Response of a Band-Pass Filter

BEST COPY AVAILABLE

```
FOCAL-12

1.01 A !!,"LP",LP,!,"L ",L ,!,"W",W,!,"W",W,"1",!,!!
1.03 S A(1)=PS;F(I=2*S;I)  S J=(I-1)/PS  S Z=(I+I-1)/(I*I)
1.04 S X=PX;F(.23125;#LP)  S X=X-1
1.05 S C=PA;F(.23125;#LA)  S C=C-1
1.06 S P=P;F(B/D)
1.07 S B=FL;F(P+P;T(S+2-1))
1.08 S A=FL;F(A+PS;F(A+2-1))
1.09 S N=G/A
1.10 T !A.2,N
```

Figure 7.1.8 FOCAL Program to Determine the Number of Elements for a Band-Pass Filter

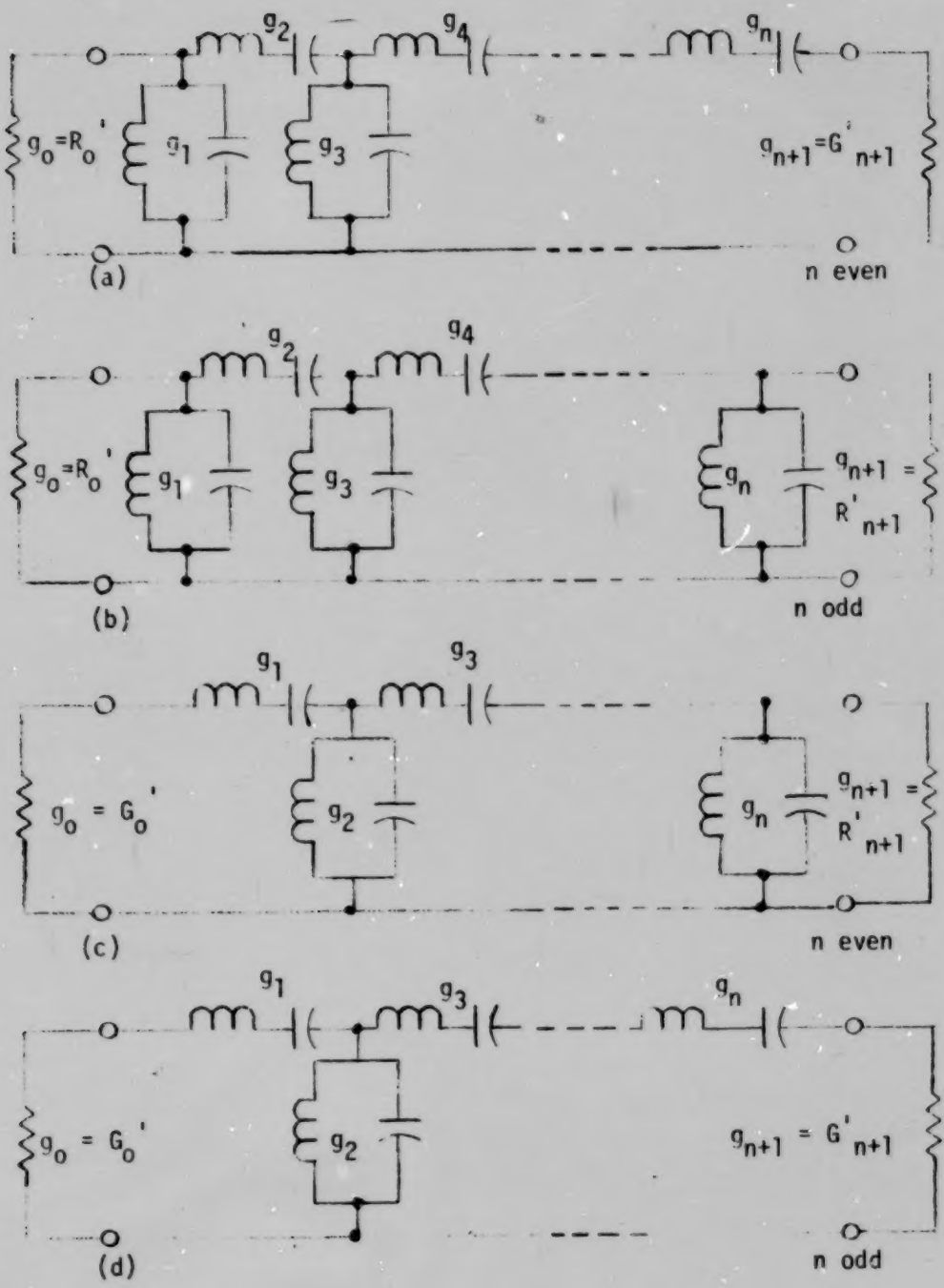

Figure 7.1.9 Possible Band-Pass Filter Configurations

$$\frac{\omega_a'}{\omega_1'} = \frac{1}{w}\left(\frac{\omega}{\omega_o} - \frac{\omega_o}{\omega}\right) \qquad (7.1.13)$$

where w, the fractional bandwidth is

$$w = \frac{\omega_2 - \omega_1}{\omega_o} \qquad (7.1.14)$$

$$\omega_o = \sqrt{\omega_1 \omega_2} \qquad (7.1.15)$$

and ω_a' and ω_1' refer to the low pass response as indicated in Figure 7.1.3 while ω, ω_o, ω_1, refer to the band pass response as shown in Figure 7.1.7. Hence, equation 7.1.1 can be modified as;

$$L_A(\omega) = 10 \log_{10} \left\{1 + \varepsilon \cosh^2 \left(n \cosh^{-1}\left(\frac{1}{w}\left[\frac{\omega}{\omega_o} - \frac{\omega_o}{\omega}\right]\right)\right)\right\} \qquad (7.1.16)$$

where $$\varepsilon = \log_{10}^{-1}\left(\frac{L_R}{10}\right) - 1 \qquad (7.1.2)$$

This can be solved to give the required number of L - C resonators, n. As was done for the low pass case, the equation can be implemented in a FOCAL program that solves for n if the ripple, LR, the upper and lower cut-off frequencies, W1 and W2, the out-of-band attenuation LF, and W, the frequency at which LF dB of attenuation is desired are specified. This program is shown in Figure 7.1.8.

Like the low-pass filter, the band-pass filter can have four different realizations, each one having the same response. These forms are shown in Figure 7.1.9. The parameters g_o and g_{n+1} are defined in exactly the same manner as for the low pass filter. The g_k values represent the normalized impedance of each series resonator and normalized susceptance of the shunt resonators. Again, these are the same g parameters as generated in the low-pass design. If $R_o' = 1$ and $\omega_1' = 1$, the series impedance is;

$$X_s = \omega_o L_s = \frac{1}{\omega_o C_s} = \frac{R_o}{w} g_k \qquad (7.1.17)$$

and the shunt susceptance is:

$$B_p = \omega_o C_p = \frac{1}{\omega_o L_p} = \frac{g_j}{wR_o} \qquad (7.1.18)$$

where $R_{n+1} = g_{n+1} R_o$ (7.1.19)

The k subscript on the g parameters is changed to j in equation 7.1.18 to differentiate between those g values which pertain to the series resonators and those which refer to the shunt resonators as shown in Figure 7.1.9.

Once again it is possible to generate the g values as in the low-pass case. For this case, equations 7.1.17, 7.1.18 and 7.1.19 are used to determine the actual L and C values and the required terminating resistance. To use this program, one must specify LR, the pass-band ripple in dB, N, the number of resonators, RO, the input impedance level, LF, the lower frequency limit of the pass-band, and UF, the upper limit of the passband. This program is shown in Figure 7.1.10.

Upon execution, the values of series inductance in μh, LS(K)[UH] and series capacitance in pf, CS(K)[PF] are obtained, as well as the parallel values of inductance in μh, LP(K)[UH] and capacitance CP(K)[PF] in pf. In addition, the terminating resistance RT is obtained in Ω. The set of values to be used depends on which configuration in Figure 7.1.9 is chosen. In Figure 7.1.9 a and b, for even values of k, one uses the series values of L and C while the odd values of k give the required parallel L and C. The situation is reversed in Figure 7.1.9 c and d.

BEST COPY AVAILABLE

```
FOCAL-12

1.11 A "L=",LA,"N",N,"ED(OHMS)",!,"LF(MHZ)",LF,"HF(MHZ)",
1.21 F !!,"  K    LS(K)[H]    CS(K)[PF]    LP(K)[H]    CP(K)

2.11 S PI=3.14159;S H=LA/17.37;S WL=2*PI*LF*1E6
2.15 S WH=2*PI*HF*1E6;S BW=FSQR((WH-WL)*WL);S Z=(WH-WL)/BW
2.21 S F=FEXP(J);S S=FEXP(-J);S HA=FLOG((1+S)/(1-S))
2.31 S GG=HA/2*N;S GA=(FEXP(GG)-FEXP(-GG))/2
2.41 S K=1;D 3.2;S GN=2*AN/(GA+D);D 3.4;D 3.42
2.51 F K=2,N;D 3
2.61 I (N/2-FITR(N/2)-.25)4.1,4.3,4.3

3.11 S AJ=AN;S BJ=4N;S GJ=GN
3.21 S AN=FSIN((2*K-1)*PI/2/N);S BN=GA*GA+(F,LN(K*PI/N))T2
3.31 S GN=A*AJ*AN/BJ*GJ
3.41 S LS=(GN+BJ)/(A*A);S CS=A/(W*GN*BJ)
3.42 S LP=(A*BJ)/(GN*W);S CP=GN/(BJ*A*BJ);D 4.5

4.11 S W=FEXP(BA/4);S V=FEXP(-BA/4)
4.21 S GF=((W+V)/(W-V))T2;S RT=RJ*GF;G 4.4
4.31 S RT=RJ
4.33  T !!,"RT = ",26.5,RT,!!
4.51 T %2.3,K,"   ",A6.4,LS*1E6,"   ",C5.1E12;D 4.6
4.61 T "   "LP*1E6,"   ",CP*1E12,!
```

Figure 7.1.10 Band-Pass Design Program

As an example of the application of there techniques consider the problem of designing the band pass filter located between the I.F. output of the mixer and the input to the IF amplifier (see Chapter 2.4). According to the specifications described there, the filter requires a 50Ω input impedance, .01 dB pass-band ripple, upper and lower cut-off frequencies of 98 MHz and 62 MHz respectively and an attenuation of at least 30 dB at 40 MHz. First, using the program shown in Figure 7.1.8 to determine the number of resonators, we set LF = 30, LR = .01, W = 40, W2 = 98 and W1 = 62 and find that n = 3.990. Thus, n = 4 is used. Now the second program (Figure 7.1.10) is applied to obtain the actual values of L and C. Setting LR = .01, N = 4, RO = 50, LF = 62 and UF = 98 we obtain the result shown in Figure 7.1.11.

Since there is an even number of resonators, either configuration a or c in Figure 7.1.9, can be used. If one chooses Figure 7.1.9 a, the odd values of k give the parallel L's and C's while the even k values give the series L's and C's. The resulting configuration was shown in Figure 7.1.12. The value of the terminating resistance for this structure is 55.0374 ohms.

7.1.4 High Pass Filter Design

The basic design equations for the low-pass filter can again be used for high-pass design by making the frequency transformation;

$$\omega' = -\frac{\omega_1 \omega_1'}{\omega} \qquad (7.1.20)$$

where ω' and ω_1' are the angular frequency variables related to the low-pass response shown in Figure 7.1.8 while ω_1 and ω are the angular frequency variables related to the corresponding high pass response

BEST COPY AVAILABLE

```
G
L:=.11
N:4
U(OHMS):5
LF(KHZ):60
HF(KHZ):9

 K    LS(K)[UH]    CS(K)[PF]    LP(K)[UH]    CP(K)[PF]

 1     1.1579       96.4564     3.16614      63.2315
 2     1.26584      15.7113     3.03922      106.134
 3     1.22237      14.2738     3.13548      116.307
 4     1.14316      29.1212     1.37283      47.3544

      55.1374
*
```

Figure 7.1.11 Print Out for Band-Pass Design Program

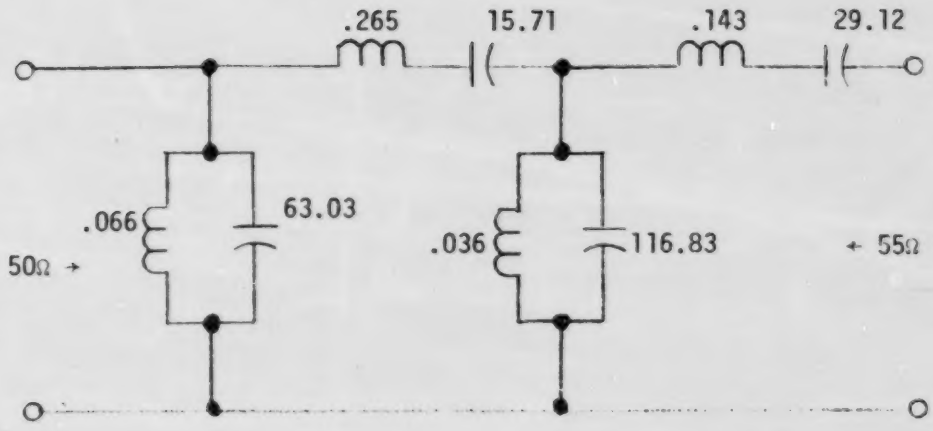

All Inductors in μh

All Capacitors in pf

Figure 7.1.12 Input Band-Pass Filter

shown in Figure 7.1.13. In effect, this transformation interchanges the origin with the point at infinity and the positive frequency axis with the negative axis.

The effect of this transformation is to change the inductive reactance $\omega' L'$ in the low-pass prototype to a capacitive reactance in the high pass filter:

$$-\omega_1 \omega_1' L'/\omega = -1/\omega C \qquad (7.1.21)$$

and any capacitive susceptance $\omega' C'$ in the low pass filter is then transformed to an inductive susceptance:

$$-\omega_1 \omega_1' C/\omega = -1/\omega L \qquad (7.1.22)$$

Hence the same g_k values used for the low-pass prototype can be used to obtain element values for a high-pass design.

If this transformation is applied to the standard low-pass design programs we can obtain programs to design high-pass filters. For example see Figure 7.1.14. To determine n, one specifies LR, the ripple in dB, WC, the cut-off frequency, LF, the out-of-band attenuation, at the frequency W. To determine the required element values we can use the FOCAL low-pass program which solves equations 7.1.3 thru 7.1.12 and apply equations 7.1.2 and 7.1.22 to obtain the high-pass filter design program shown in Figure 7.1.15.

Thus, to determine the element values one must specify LR, N, RO, and WC. Like the low-pass and band-pass filters, the high-pass can also exist in four equivalent forms as illustrated in Figure 7.1.16. As in the case of the low pass filter, the design program gives values which are applicable to all four forms. To determine

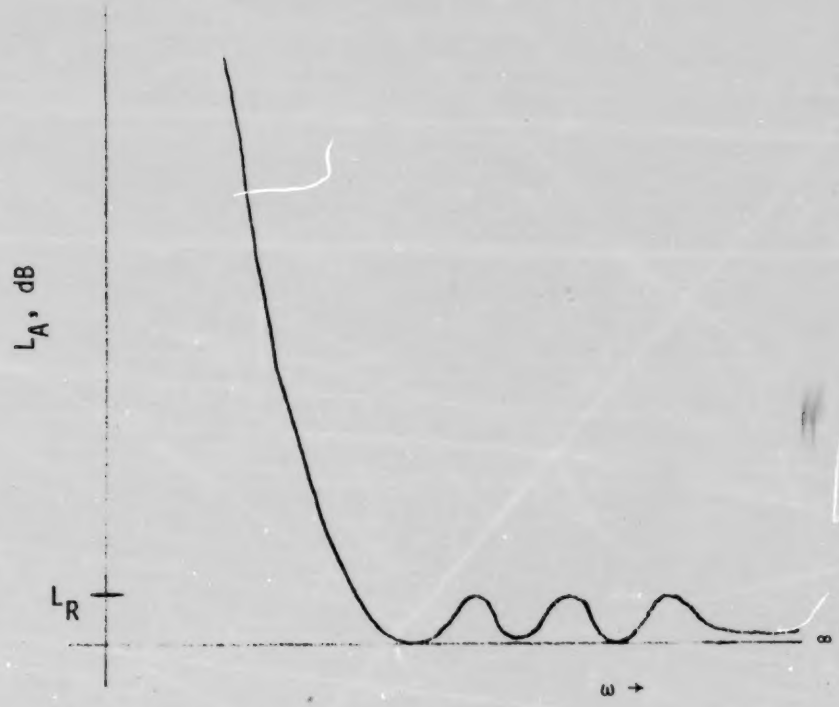

Figure 7.1.13 Frequency Response of a High-Pass Filter

BEST COPY AVAILABLE

```
C FOCAL-12

01.01  A !!,"LF",LF,!,"LR",LR,!,"M1",M1,!,"M2",M2,!!
01.14  S A=FEXP(.23025*LF); S B=A-1
01.16  S C=FEXP(.23025* LR); S D=C-1
01.30  S F=FSQT(M/D)
01.1   S G=FLOG(F+FSQT(F↑2-1))
01.11  S N=2*M2-M1
01.12  S X=N/M2; S H=FLOG(X+FSQT(X↑2-1))
01.14  S W=G/H
01.15  T W
```

Figure 7.1.14 FOCAL Program for Determining the Number of Elements in a High-Pass Filter

BEST COPY AVAILABLE

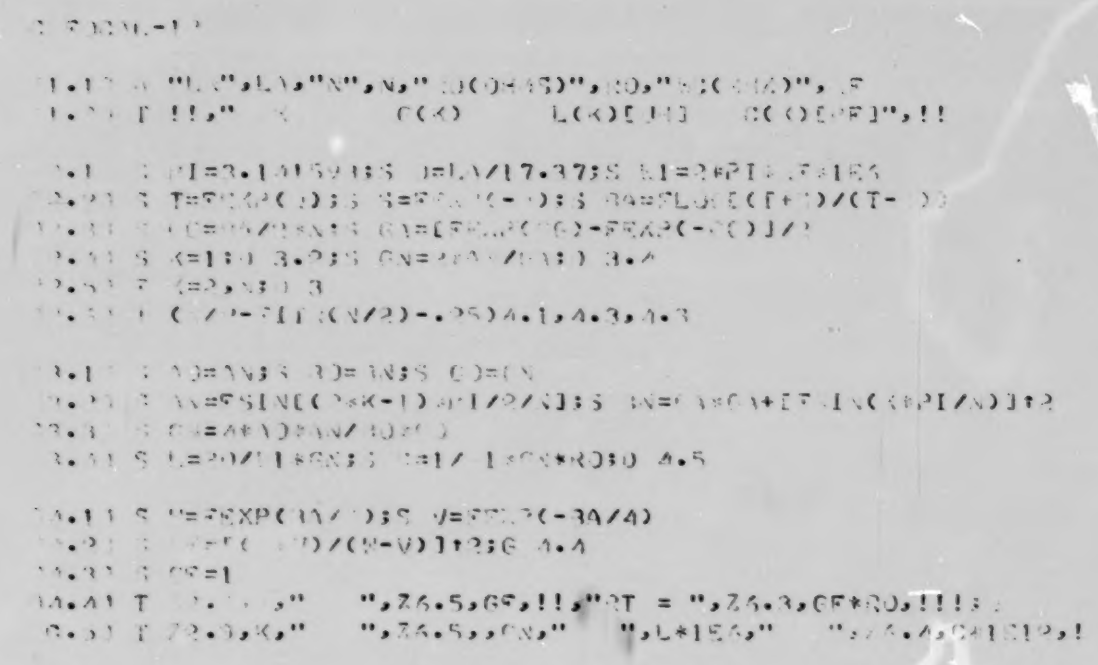

Figure 7.1.15 High-Pass Design Program

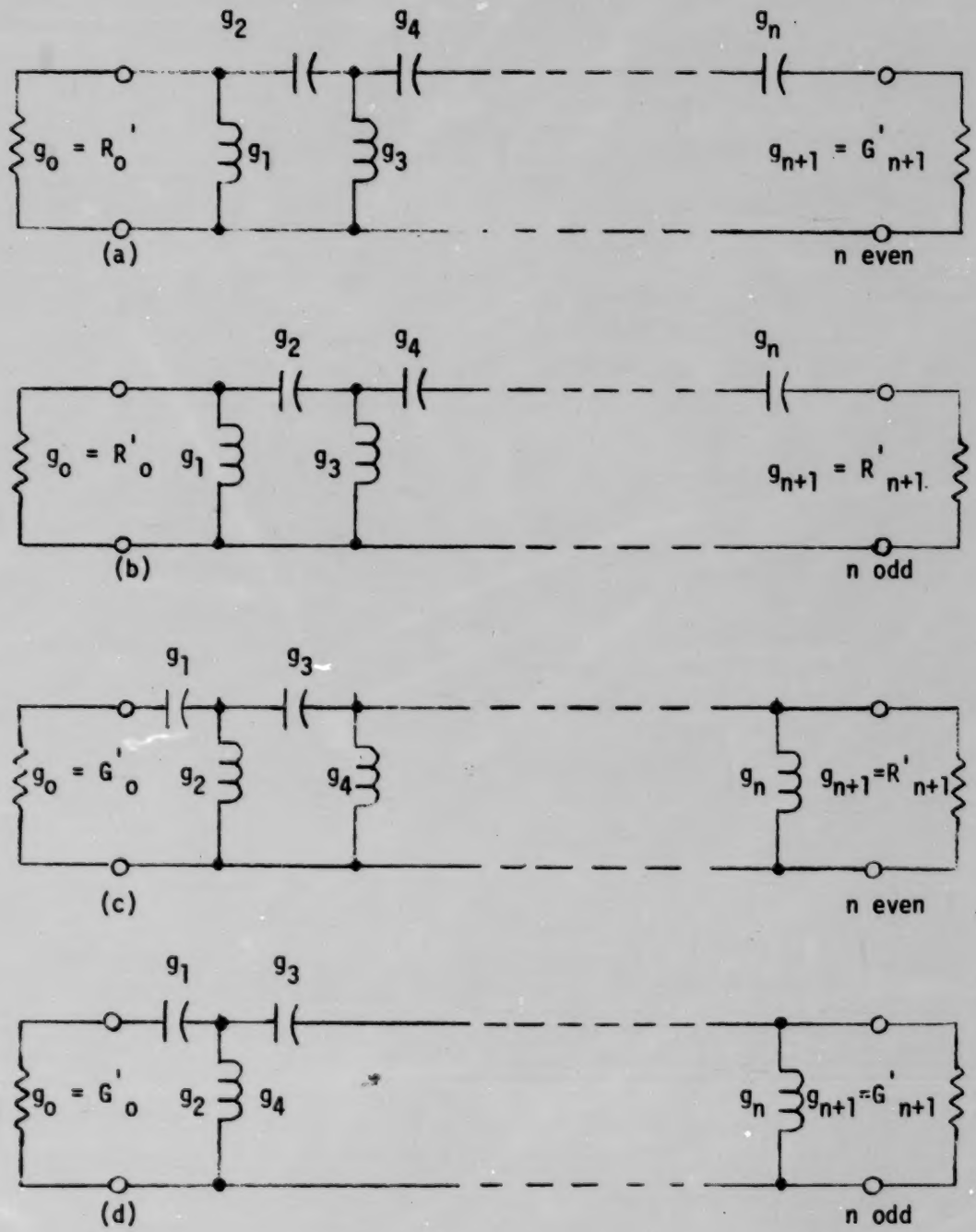

Figure 7.1.16 Possible High Pass Configurations

BEST COPY AVAILABLE

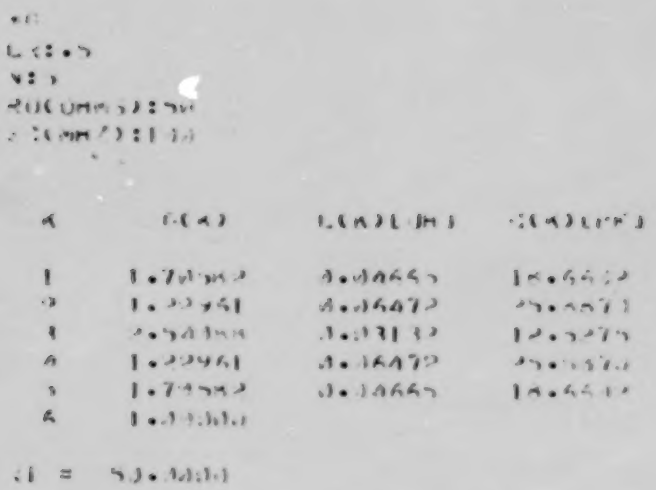

Figure 7.1.17 Print Out of High-Pass Design Program

which values apply to a given configuration, note that for Figure 7.1.16 a and b the odd k subscripted values of inductance and the even k subscripted values of capacitance are to be used. For Figure 7.1.16 c and d, the situation is reversed.

As a design example, consider a high-pass filter with a cut-off frequency of 100 MHz, impedance level of 50Ω, pass-band ripple of .5 dB and an attenuation of 10 dB at 85 MHz. Using first the program for determining the number of elements (Figure 7.1.14) set LR = .5, WC = 100, LF = 10, and W = 85 and find that N = 5.248; choose n = 5. Having a knowledge of the number of elements one can now apply the second program (Figure 7.1.15) to determine the required values of L and C. Setting LR = .5, N = 5, RO = 50, and WC = 100 we obtain the result shown in Figure 7.1.17. Since the filter has an odd number of elements and assuming it is desirable for the input to the filter to present an open circuit impedance above ω_c, configuration d of Figure 7.1.16 is chosen. Hence, the circuit shown in Figure 7.1.18 is obtained. Note that the terminating resistance is 50Ω for the structure.

7.2 VOLTAGE CONTROLLED OSCILLATOR

For the purpose of making swept measurements in the performance of the amplifier of Chapter 2, a voltage controlled oscillator (VCO) was constructed that could be frequency modulated in a linear manner over the range of 60 - 100 MHz and which provided a fairly constant power output over that range.

As is shown in Figure 7.2.1, the circuit is a series tuned Hartley Oscillator with a varactor diode in the resonator circuit.

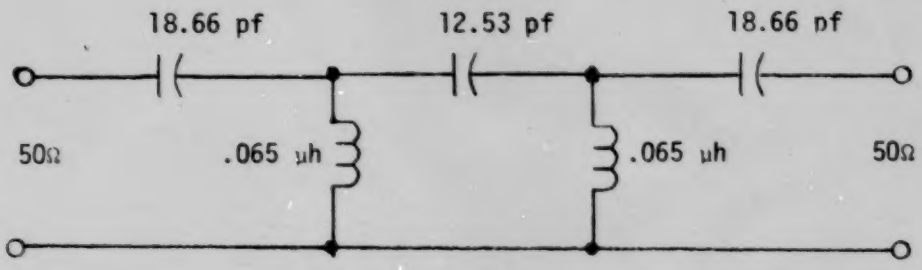

Figure 7.1.18 High-Pass Filter Design Example

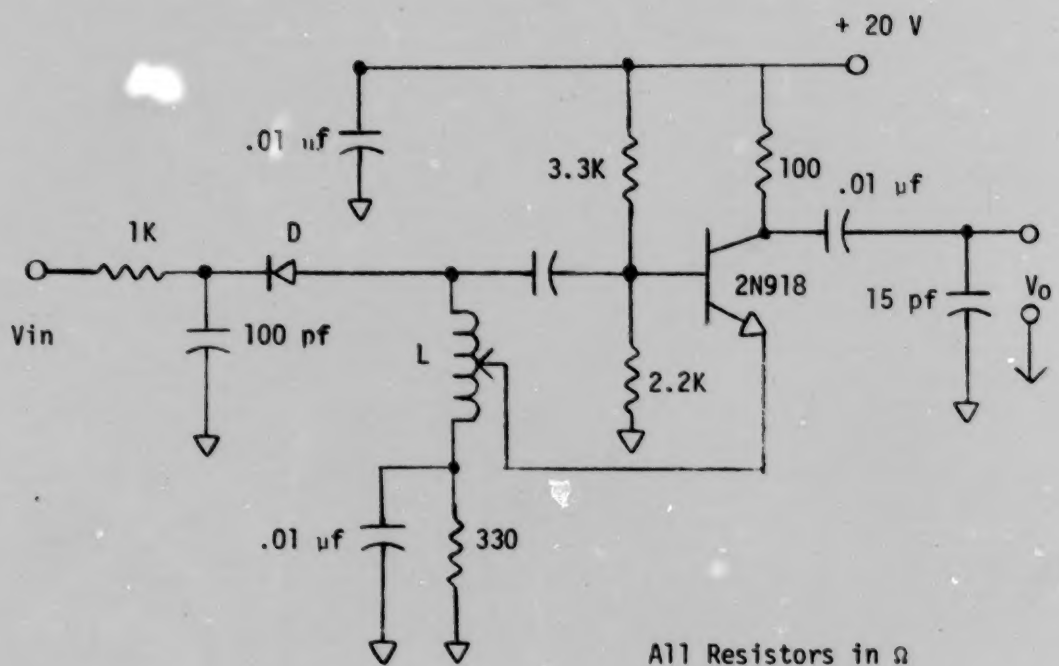

All Resistors in Ω

L: 5 turns of number 22 wire wound on 1/4 inch form

D: 5-10 pf Varactor

Figure 7.2.1 Voltage Controlled Oscillator

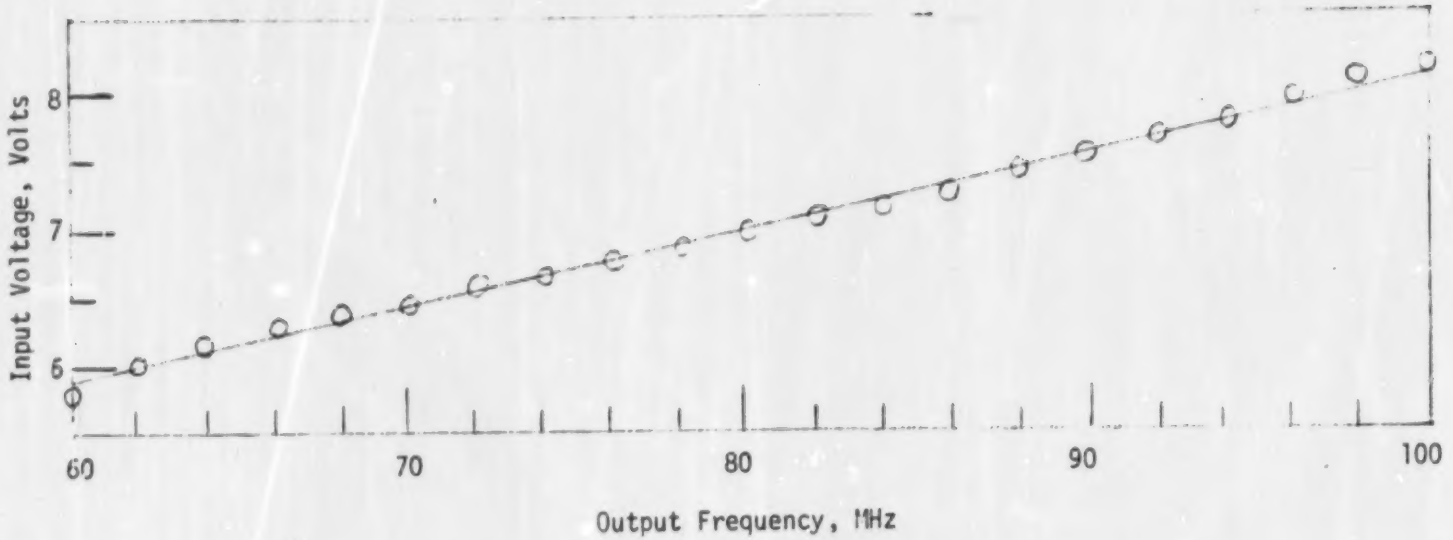

Figure 7.2.2 VCO Output Frequency as a Function of Input Voltage to the Varactor

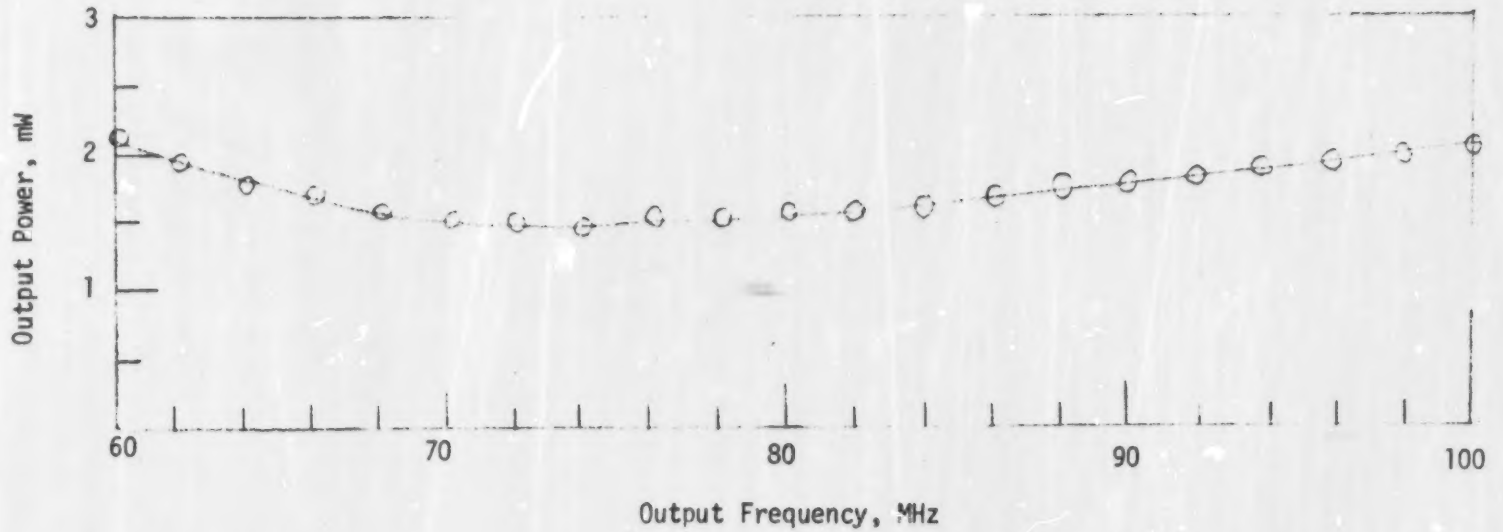

Figure 7.2.3 VCO Output Power as a Function of Output Frequency

Hence, by changing the bias to the varactor, the frequency of oscillation is changed. Figure 7.2.2 shows the tuning curve which is linear to 1%. The power output over the same frequency range is shown in Figure 7.2.3. The output is reasonably constant, exhibiting only 1.3 dB of variation over the tuning range. These measurements were made with the output loaded to 50Ω. In order to have the VCO perform to specifications indicated here, it is recommended that it always be loaded with 50 Ω.

7.3 LUMPED ELEMENT QUARTER WAVELENGTH TRANSFORMER

Quarter wavelength sections of transmission line are routinely used as impedance transformers. At frequencies below 1 GHz, the use of a transmission line for this purpose is impractical due to the length of line required. However, from the methods outlined in Everitt and Anner (24) one can replace the line by a lumped element equivalent circuit as shown in Figure 7.3.1. For this quarter wavelength ($\lambda/4$) transformer, the characteristic impedance required to provide a match between two different load resistances, (Z_o and Z_r) is;

$$Z'_o = \sqrt{Z_o Z_r} \tag{7.3.1}$$

For the lumped element equivalent:

$$Z_o' = |X_1| = |X_2| = |X_3| \tag{7.3.2}$$

where X_1 and X_2 are inductive and X_3 is capacitive. If f_o is the center frequency at which a perfect match is obtained, one finds the following lumped element values for the $\lambda/4$ transformer:

$$L_1 = L_2 = \frac{Z_o'}{2\pi f_o} \tag{7.3.3}$$

$$C_3 = \frac{1}{Z_o'(2\pi f_o)} \tag{7.3.4}$$

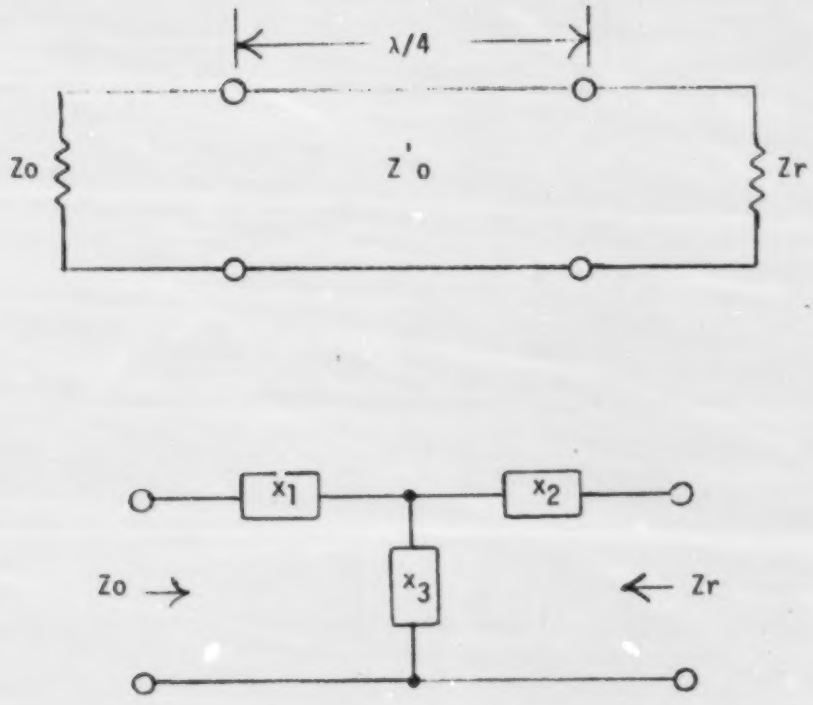

Figure 7.3.1 λ/4 Transmission Line and Equivalent Circuit

As an example, consider the lumped element equivalent λ/4 transformer which matches 300Ω to 50Ω at 80 MHz. From equation 7.3.1, Z_o' = 121.5Ω and from equations 7.3.2 and 7.3.3 one obtains $L_1 = L_2 = .242$ μh and $C_3 = 16.45$ pf. Figure 7.3.2 shows the theoretical magnitude of the reflection coefficient, $|\rho|$ plotted as a function of input frequency for this structure.

It is possible to effectively cascade these λ/4 transformers to obtain a match over a wider frequency range if so desired. Matthaei,(25) provides a detailed analysis and a set of design equations for making such broad-band impedance matching structures.

7.4 FOURIER ANALYSIS OF A TRAPEZOIDAL WAVE

To good approximation, the output of the limiter described in Chapter 3 is represented by the waveform shown in Figure 3.2. Hence,

$$V(\theta) = \begin{cases} A\sin\theta & 0 \le \theta \le \omega t_c \\ V_c & \omega t_c \le \theta \le \pi - \omega t_c \\ A\sin\theta & \pi - \omega t_c \le 0 \le \pi + \omega t_c \\ -V_c & \pi + \omega t_c \le \theta \le 2\pi - \omega t_c \\ A\sin\theta & 2\pi - \omega t_c \le \theta \le 2\pi \end{cases} \qquad (7.4.1)$$

is the limiter's output over one period. It is possible to represent $V(\theta)$ as a Fourier series of the form:

$$V(\theta) = \sum_{n=1}^{\infty} B_n \sin n\theta \qquad (7.4.2)$$

since $V(\theta)$ is an odd function. The Fourier coefficients B_n correspond to the amplitudes of the higher order harmonics contained by $V(\theta)$.

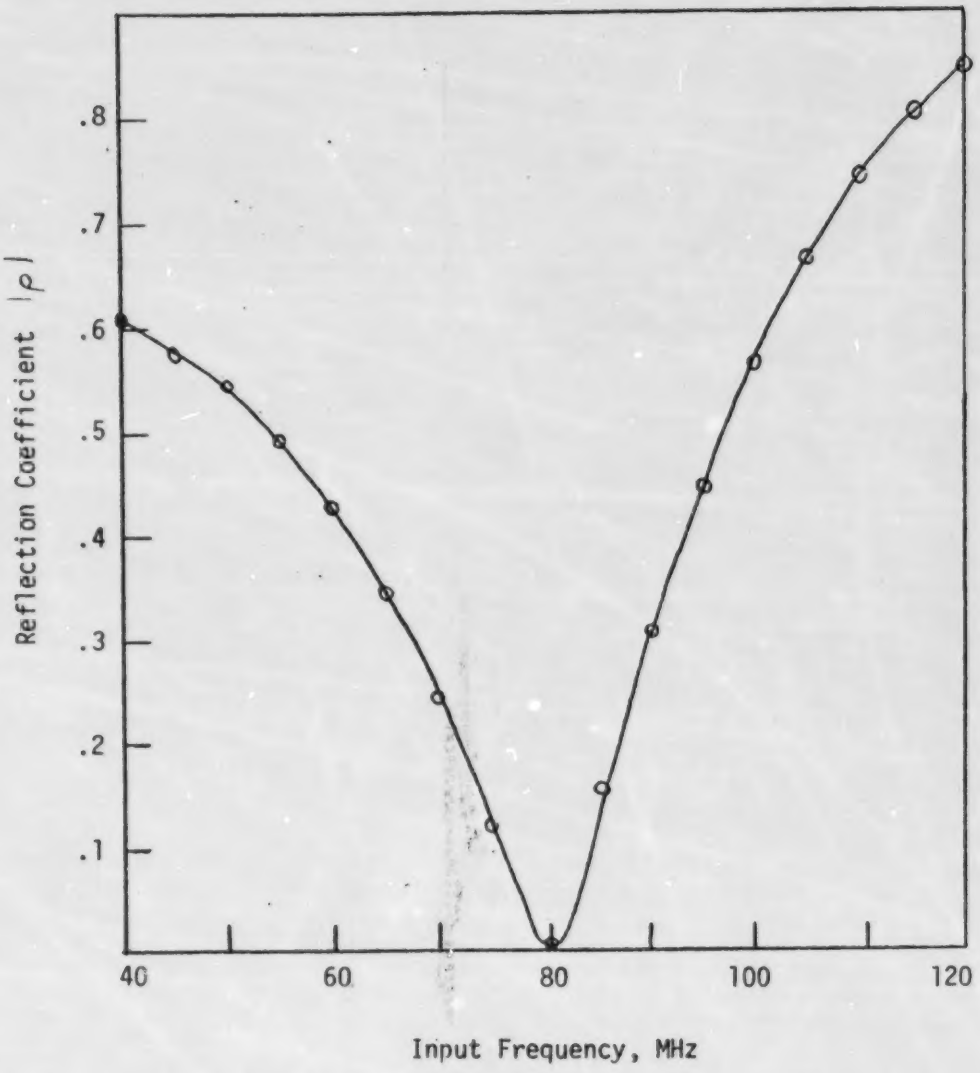

Figure 7.3.2 Magnitude of Reflection Coefficient as a Function of Frequency for λ/4 Transformer

These are given by;

$$B_n = \frac{2}{T} \int_o^T V(\theta) \sin n\theta \, d\theta \qquad (7.4.3.)$$

Therefore, for the limiter output, the amplitudes of the harmonics will be given by:

$$B_n = \frac{2}{T} \left\{ A \int_o^{\omega t_c} \sin\theta \sin n\theta \, d\theta + V_c \int_{\omega t_c}^{\pi-\omega t_c} \sin n\theta \, d\theta \right.$$

$$+A \int_{\pi-\omega t_c}^{\pi+\omega t_c} \sin\theta \sin n\theta \, d\theta - V_c \int_{\pi+\omega t_c}^{2\pi-\omega t_c} \sin n\theta \, d\theta$$

$$\left. +A \int_{2\pi-\omega t_c}^{2\pi} \sin\theta \sin n\theta \, d\theta \right\} \quad n \geq 2 \qquad (7.4.4)$$

Solving these integrals and substituting $\omega t_c = \theta$ we have

$$B_n = \frac{2V_c}{n\pi} (1 - \cos n\pi) \cos n\omega t_c \quad n \geq 2 \qquad (7.4.5)$$

To solve for B_1, the fundamental equation 7.4.4 is used with n=1:

$$B_1 = \frac{A}{\pi} \left[2\omega t_c - \frac{1}{2} \sin 2\omega t_c \right] \qquad (7.4.6)$$

Also it should be noted that

$$\omega t_c = \sin^{-1}\left(V_c/A\right) \qquad (7.4.7)$$

Further, as can be seen from equation 7.4.5, all even coefficients are zero. The theoretical and experimental amplitudes are compared in Table 3.1.

7.5 MEASUREMENT TECHNIQUES

7.5.1 Measurement of Limiter Harmonics

An experimental set-up like the one shown in Figure 7.5.1 was used to measure the harmonic content of the limiter's output. A 100 MHz low pass filter at the output of the generator was used to eliminate its harmonics. The 100 MHz high pass filter is necessary to eliminate the fundamental component of the limiter output so that the limiter harmonics can be measured without overdriving the spectrum analyzer.

The procedure used for measuring the harmonic content is quite simple. First, without the high pass filter in place, a reference level of 0 dB is set on the spectrum analyzer. Next, the high pass filter is reinserted and the spectrum analyzer is set to the second harmonic frequency. Attention is then decreased in the variable attenuators to bring the level of the second harmonic up to that previously set for the fundamental. The attenuation removed is noted and a correction is made for the insertion loss of the high pass filter at this frequency. This yields directly the level by which the harmonic is down from the fundamental. By using a procedure such as this, we are able to obtain the experimental results shown in Table 3.1.

7.5.2 Measurement of Inductance with Hewlett-Packard Automatic Network Analyzer.

In order to accurately determine the inductance of the hand-wound inductors used in the filter designs described in Chapter 2.4, 2.5, 3.3, they were measured using the experimental set-up shown in Figure 7.5.2. The oscillator is set to 100 MHz and the attenuators are adjusted to provide sufficient power to operate the analyzer. To calibrate the

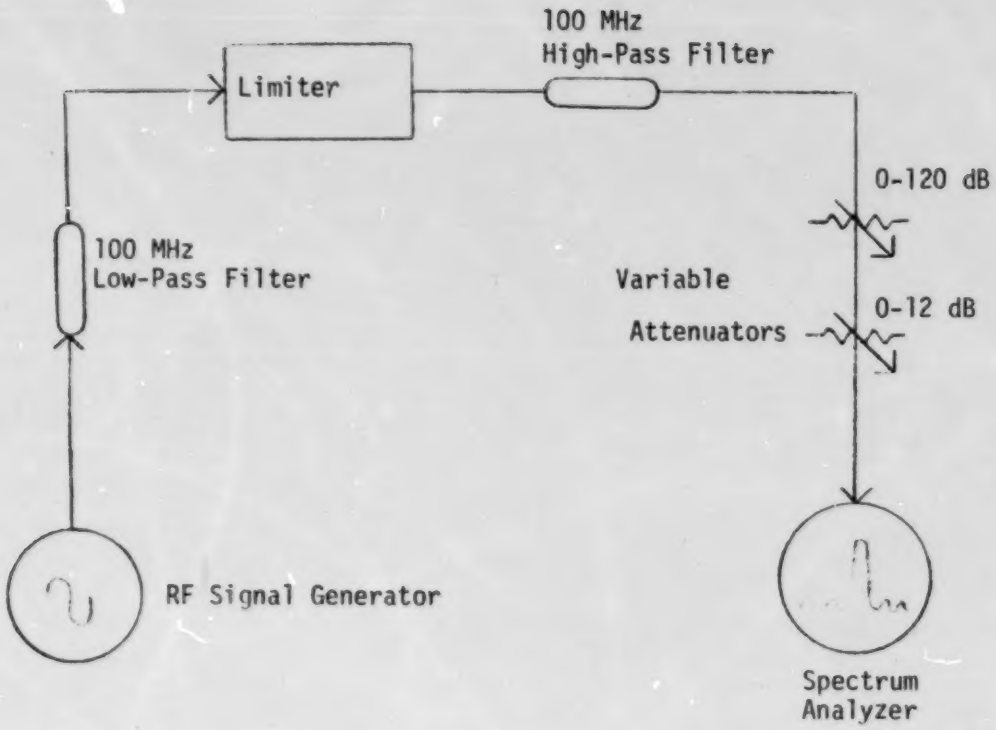

Figure 7.5.1 Experimental Set-Up Used to Measure Harmonic Content of the Limiter

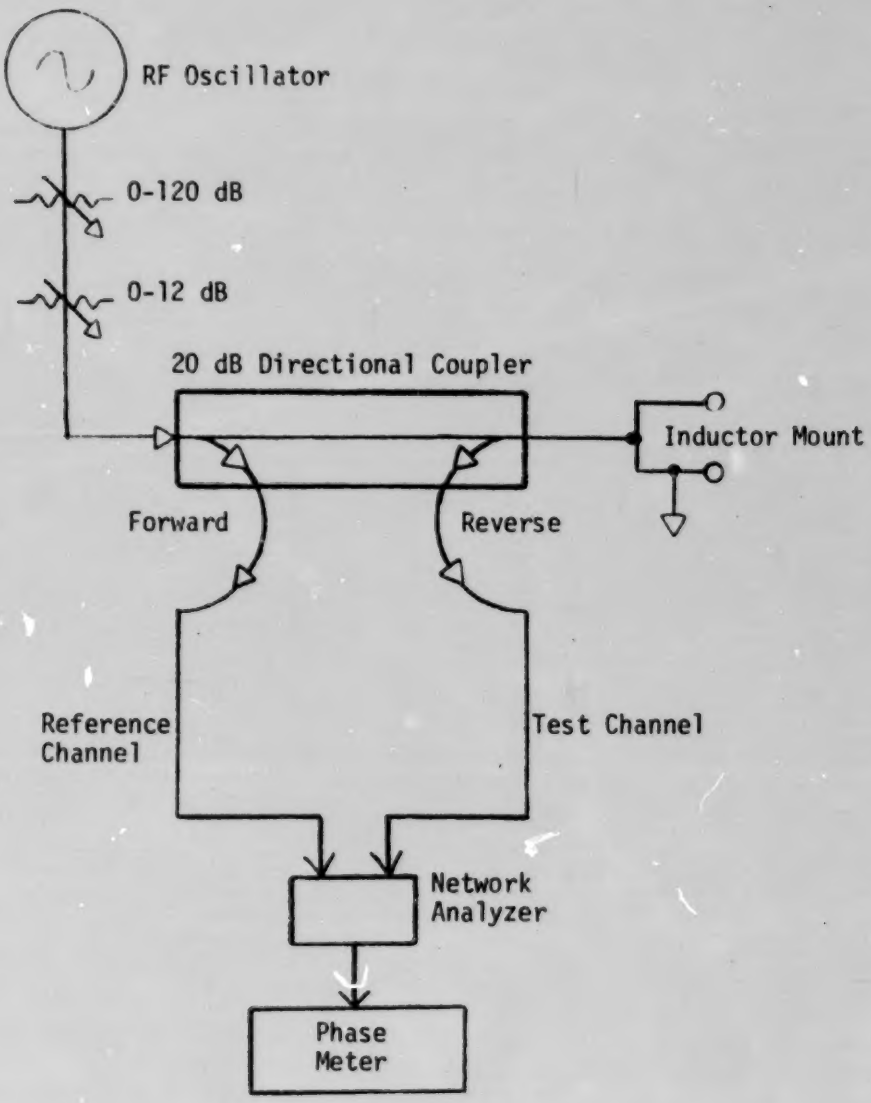

Figure 7.5.2 Set-Up for Inductance Measurement

phase meter the inductor is temporarily shorted out and the cable lengths in the reference and test channels are adjusted to give a 180° indication on the phase meter. The short is then removed and the meter should return to 0°. If the meter doesn't return to exactly 0° it can be trimmed by use of the vennier control on the phase meter. The inductance can now be measured by placing the inductor into the mount and noting the value of the phase angle θ. To compute the inductance, L, substitute θ into the following formula:

$$L = \frac{1}{4\pi} \frac{1 + \sqrt{1 + \tan\theta}}{\tan\theta} \quad \mu h \tag{7.5.1}$$

If one wants to adjust the value of inductance, it is convenient to know the resulting phase for a given inductance. For L in μh and θ in degrees we have:

$$\theta = \cos^{-1} \frac{(4\pi L)^2 - 1}{(4\pi L)^2 + 1} \tag{7.5.2}$$

In making these measurements care should be taken to keep the inductor leads as short as possible. Also, the output frequency of oscillator should be monitored and kept constant. In this manner, it is possible to measure inductance to an accuracy of 5%.

7.6 DETERMINATION OF PARALLEL LINE $\frac{\lambda}{4}$ COUPLED FILTER DIMENSIONS USING A FIBONACCI SEARCH

From the even and odd mode characteristic impedances of each parallel set of coupled resonators in the parallel coupled strip-line resonator filter (see Figure 4.2), Matthaei et. al. (19) supply equations for determining the strip dimensions using elliptic

integrals of the first kind. Based on these equations, Matthaei (19) presents a set of design nomograms. It was found that the accuracy of these nomograms was insufficient for our purposes. By employing a Fibonacci search and polynomial representation of the elliptic integrals, T. Monsees has developed the FOCAL program shown in Figure 7.6.1 and 7.6.2 which solve for the normalized dimensions w/b and s/b, (see Matthaei, p. 175) to whatever desired accuracy.

The use of these programs is rather straight forward. The appropriate values for the even and odd mode characteristic line impedances are calculated in the usual manner (19). The nomograms (19) are then used to first determine the maximum and minimum values of the range over which one would expect to find the correct values of w/b and s/b (see Figure 4.2). Initial values of s/b and w/b are also determined in this manner. The program shown in Figure 7.6.1 is applied first. Setting S/B MIN, S/B MAX, W/B (the initial value), ACC'CY (required accuracy expressed in parts per 10^n), ZO ODD and ZO EVEN to their appropriate values, a print out of two possible values of S/B are found. These are averaged and the result used in the second program, along with the appropriate nomogram values for W/B MAX and W/B MIN. This program gives two possible values of W/B. The first program is run again using the average the two print out values from the second program for W/B. Now the S/B MAX and S/B MIN used are the two values from the first run of this program. One then proceeds to iterate in this manner until the final values of s/b and w/b are within the required accuracy.

```
01.01 A "W/B MIN"XL,"W/B MAX"XU,"ACC'CY"DX,"S/B"C1
01.02 A "Z0,ODD"Z0,"Z0,EVEN"ZE
01.03 S PA=0

02.01 S L=2*FITR((XU-XL)/DX)+1;S S(2)=1;S S(3)=2
02.03 S S(1)=S(2);S S(2)=S(3);S S(3)=S(1)+S(2);I (S(3)-L)2.03
02.05 S LX=XL;S UX=XU
02.07 S X(1)=(S(1)/S(3))*(UX-LX)+LX;S XN=X(1);D 3;S Y(1)=YN;S AB=2
02.09 S X(AB)=(S(AB)/S(3))*(UX-LX)+LX;S XN=X(AB);D 3;S Y(AB)=YN
02.11 I (FABS(Y(2))-FABS(Y(1)))2.13;S UX=X(2);S YU=Y(2);S X(2)=X(1)
02.12 S Y(2)=Y(1);S AB=1;G 2.15
02.13 S LX=X(1);S YL=Y(1);S X(1)=X(2);S Y(1)=Y(2);S AB=2
02.15 S S(3)=S(2);S S(2)=S(1);S S(1)=S(3)-S(2);I (2-S(3))2.09
02.17 S XN=X(AB);I (FABS(XN-XL)-DX)2.25;I (FABS(XN-XU)-DX)2.25
02.19 I (-FABS(FSGN(YU)-FSGN(YL)))2.23;T !,"EX. MIN "XN;J
02.23 T !,XN,!;G 7.1
02.25 T !,"NR",!;J

03.20 S D=C1+XN*1.5708;S M=TH;D 6
03.30 I (PA)2.25,3.32;S M=M/TH;G 3.35
03.32 S M=M*TH
03.35 S M1=1-M;D 4
03.42 D 5
03.50 S YN=ZE-94.2478*K1/1.6*K;R

04.10 S K1=1.3863+.11197*M1+.07253*M1↑2
04.20 S K1=K1+[.5+.12135*M1+.028873*M1↑2]*FLOG(1/M1);R

05.10 S K=K1;S M1=1-FSQT(1-M↑2);D 4
05.20 R

06.10 S TH=[FEXP(D)-FEXP(-D)]/[FEXP(D)+FEXP(-D)];R

07.10 I (PA)2.25,7.2;J
07.20 S PA=1;S ZE=Z0;G 2.01
```

Figure 7.6.1 Part I of Search Program

```
01.01 A "S/B MIN"XL,"S/B MAX"XU,"ACC*CY"DX,"W/B"C1
01.02 A "Z0,ODD"Z0,"Z0,EVEN"ZE
01.03 S C1=C1*1.5708;S PA=1

02.01 S L=2*FITR((XU-XL)/DX)+1;S S(2)=1;S S(3)=2
02.03 S S(1)=S(2);S S(2)=S(3);S S(3)=S(1)+S(2);I (S(3)-L)2.03
02.05 S LX=XL;S UX=XU
02.07 S X(1)=(S(1)/S(3))*(UX-LX)+LX;S XN=X(1);D 3;S Y(1)=YN;S AB=2
02.09 S X(AB)=(S(AB)/S(3))*(UX-LX)+LX;S XN=X(AB);D 3;S Y(AB)=YN
02.11 I (FABS(Y(2))-FABS(Y(1)))2.13;S UX=X(2);S YU=Y(2);S X(2)=X(1)
02.12 S Y(2)=Y(1);S AB=1;G 2.15
02.13 S LX=X(1);S YL=Y(1);S X(1)=X(2);S Y(1)=Y(2);S AB=2
02.15 S S(3)=S(2);S S(2)=S(1);S S(1)=S(3)-S(2);I (2-S(3))2.09
02.17 S XN=X(AB);I (FABS(XN-XL)-DX)2.25;I (FABS(XN-XU)-DX)2.25
02.19 I (-FABS(FSGN(YU)-FSGN(YL)))2.23;T !,"EX. MIN "XN!
02.23 T !,XN,!;G 7.1
02.25 T !,"NR",!;Q

03.20 S D=C1+XN*1.5708;S M=TH;D 6
03.30 I (PA)2.25,3.32;S M=M/TH;G 3.35
03.32 S M=M*TH
03.35 S M1=1-M;D 4
03.42 D 5
03.50 S YN=ZE-94.2478*K1/1.6*K;R

04.10 S K1=1.3863+.11197*M1+.07253*M1↑2
04.20 S K1=K1+(.5+.12135*M1+.028873*M1↑2]*FLOG(1/M1);R

05.10 S K=K1;S M1=1-FSQT(1-M↑2);D 4
05.20 R

06.10 S TH=(FEXP(D)-FEXP(-D)]/(FEXP(D)+FEXP(-D)];R

07.10 I (PA)2.25,7.2;Q
07.20 S PA=1;S ZE=Z0;G 2.01
```

Figure 7.6.2 Part II of Search Program

8. BIBLIOGRAPHY

1. J. P. Singh, R. P. Morgan and F. J. Rosenbaum, "Satellite Networks for Education," Proceedings of the International Telemetering Conference, Vol. 7., pp. 429-439, Los Angeles, Calif. December 1972.

2. B. A. Newman, J. P. Singh, and F. J. Rosenbaum, "Design of a 12 GHz Multicarrier Earth Terminal for Satellite - CATV Interconnection," Memorandum No. 71/7, Center for Development Technology, Washington University, St. Louis, Mo., November 1971.

3. "Ground Signal Processing Systems, Summary Reports on Analysis, Design and Cost Estimating," NASA CR-72709, Contract NAS 3-11520. General Electric, Space Systems Organization, Valley Forge Space Center, Philadelphia, Pa., June 1970.

4. J. P. Hessler, Y. C. Hwang, J. J. Zampini, "Low Cost Ground Receiving Systems for Television Signals from High-Powered Communications Satellites," Vols. I and II, NASA CR -20933, Final Report. General Electric Company, Electronics Laboratory, Syracuse, N. Y.

5. B. B. Lusignan, P. Z. Bulkeley, J. M. Janky, and R. B. Taggert, Jr., "The Design and Development of Low-Cost Microwave Adaptor Suitable for Television Reception from High-Power Communications Satellites," NASA CR-72773, Center for Radar Astronomy, Stanford University, Stanford California, October 31, 1970. See Also: K. Ohkubo, C. C. Han, J. Abernaz, J. M. Janky, and B. B. Lusignan, "Optimization in the Design of a 12 Gigahertz Low Cost Ground Receiving System for Broadcast Satellites," Vol. I and II, NASA CR-121185, October 15, 1972.

6. A. Whalen (Trust Experiment Mgr.) "Breadboard Design and System Analysis for the ATS-F Trust Experiment Small Ground Station," NASA, Goddard Space Flight Center, Greenbelt, Maryland, September, 1971.

7. M. V. O'Donovan, C. M. Kudsia, L. A. Keyes, "Design of a Light-Weight Microwave Repeater for a 24-Channel Domestic Satellite System," RCA Review, Vol. 34, pp. 506-528, September 1973.

8. J. D. Parker, "Report on the Geneva Space Telecommunications Conference-Broadcasting Aspects," IEEE Transactions on Aerospace and Electronic Systems, AES-8, No. 4, pp. 505-509, July 1972.

9. J. B. McCuller and J. P. Singh, "A Computer Program for Small Terminal Fixed/Broadcast Satellite System Parameter Optimization," Report R(T)-74/1, Center for Development Technology, Washington University, St. Louis, Missouri, October 1973.

10. T. W. Stagl, N. H. Morgan, and J. P. Singh, "Computer-Aided Communication Satellite System Analysis and Optimization," Report R(T)-73/2, Center for Development Technology, Washington University, St. Louis, Missouri, October 1973.

11. J. E. Degenford and B. A. Newman, "12 GHz Image and Sum Enhanced Mixer Diode Converter," Westinghouse Defense and Electronic Systems Center, Baltimore, Maryland. October 1973.

12. E. J. Drazy, R. E. Sheckey, and H. C. Wang, "TH-3 Microwave Radio System: Network," The Bell System Technical Journal, Vol. 50, No. 7, pp. 2137-2153, September 1971.

13. Motorola Inc., Linear Integrated Circuits Data Book, November 1973.

14. J. Millman, H. Taub, Pulse, Digital, and Switching Waveforms, McGraw-Hill, New York, 1965, pp. 147-150.

15. F. W. Grover, Inductance Calculations: Working Formulas and Tables, Dover Publications Inc., New York, 1962.

16. C. W. Lee and W. Y. Seo, "Super Wide-band FM Line Discriminator," Proceedings of the IEEE (Letters), Vol. 51, pp. 1675-1676, November 1963.

17. C. W. Lee, "An Analysis of a Super Wideband FM Line Discriminator," Proceedings of the IEEE, Vol. 52, pp. 1034-1038, September 1964.

18. E. T. Jilig, "The Intelsat IV Spacecraft," COMSAT Technical Review, Vol. 2, No. 2, Fall 1972.

19. G. L. Matthaei, L. Young, and E. M. T. Jones, Microwave Filters Impedance Matching Networks and Coupling Structures, McGraw-Hill, New York, 1964.

20. D. H. Olsen and F. J. Rosenbaum, "MICTPT-A Minicomputer General Purpose Microwave Two-Port Analysis Program," IEEE Transactions on Microwave Theory and Techniques (Letters), MTT-22, No. 3, pp. 340-341, March 1974.

21. S. B. Cohn, "Parallel-Coupled Transmission Line Resonator Filters," IRE Transactions on Microwave Theory and Techniques, Vol. MTT-6, pp. 223-227, April 1958.

22. W. A. Edson and J. Wakabayaski, "Input Manifolds for Microwave Channelizing Filters," IEEE Transactions on Microwave Theory and Techniques, MTT-18, No. 5, pp. 270-726, May 1970.

23. A. E. Atia, "Computer Aided Design of Waveguide Multiplexers," IEEE Transactions on Microwave Theory and Techniques, MTT-24, No. 3, pp. 332-336, March 1974.

24. W. L. Everitt and G. E. Anner, Communication Engineering, McGraw-Hill, New York, 1956.

25. G. L. Matthaei, "Impedance Matching Structures Having a Tchebsycheff Characteristic," Proceedings of the IEEE, Vol. 52, pp. 939-963, August, 1964.